# Multi-Antenna Systems and Interconnection Strategies for CDMA Wireless Access Networks

by

**Halim Yanıkömeroğlu**

A thesis submitted in conformity with the requirements
for the Degree of Doctor of Philosophy,
Department of Electrical and Computer Engineering,
at the University of Toronto

In the name of God, the Beneficent, the Merciful

(1) Say: "He is the One God:

(2) God the Eternal, the Uncaused Cause of All That Exists.

(3) He begets not, and neither is He begotten;

(4) and there is nothing that could be compared with Him."

The Noble Qur'an, Chapter 112

# Multi-Antenna Systems & Interconnection Strategies for CDMA Wireless Access Networks

**Halim Yanikomeroglu**

**Degree of Doctor of Philosophy**

**Department of Electrical and Computer Engineering**

**University of Toronto**

**1998**

## Abstract

The main objective of this thesis is to utilize antennas in novel ways so as to achieve performance benefits at the system level through spatial interference management. To this end, we study CDMA multi-antenna wireless access networks (where the transmission and reception are through multiple antennas distributed in the service area), and compare their performance with that of the conventional networks where only one central antenna (CA) exists.

We first demonstrate that by using CDMA distributed antenna (DA), the power control dynamic range can be reduced significantly; this yields a notable reduction in the outage.

The DA system simulates a hypothetical optimal CA system; therefore, even though the capacity of a DA system may be considerably higher than that of a CA type, the capacity is still low per antenna element (AE). In order to overcome this shortcoming, we present the sectorized distributed antenna (SDA) system, where each AE is connected to a separate feeder. We further suggest a novel nonlinear power control algorithm which balances the SIR in SDA systems.

We demonstrate analytically and through simulations that in a CDMA SDA system the reverse link capacity increases approximately linearly with increasing numbers of AE's. This increase is still valid, despite the overlapping antenna patterns and non-uniform traffic, due to the joint decoding (enhanced macrodiversity) capability of the SDA system, and also to the effective power control algorithm used. Therefore, the reverse link capacity of an SDA system with $L$ AE's is higher than that of an $L$-cell cluster serving the same region.

In order to achieve maximum performance from the SDA architecture, the interference picked up by an AE for a user should be uncorrelated with those picked up by other AE's. To this end, the conditions, under which the correlated interference occurs, are evaluated, and the effects of the system parameters on the correlation are analyzed.

Finally, AE interconnection strategies are studied in order to determine cost-efficient as well as robust and flexible interconnection architectures, by using results from the theory of minimal networks, especially those on Steiner trees.

*To my wife, Berna Akçakır Yanıkömeroğlu*

# Acknowledgements

All praise is due to God alone, the Sustainer and Cherisher of all the worlds.

I would like to thank my supervisor Prof. Elvino S. Sousa for his invaluable advice, guidance and support. He has always been accessible and very helpful.

Special thanks to my Ph.D. Committee, the external appraiser Norman Secord (Nortel), the internal appraiser Irene Katzela, Alberto Leon-Garcia, Bruce Francis, and Eric Miller (Department of Civil Engineering).

I am thankful to my friends in the Wireless Group for many thought-provoking and stimulating discussions.

Diane Bettencourt Silva's administrative help is also gratefully acknowledged.

During this work, I was assisted by the financial support provided through Canadian Institute for Telecommunications Research under the NCE program of the Government of Canada, the University of Toronto Differential Fee Waiver Scholarship, the University of Toronto Open Fellowship, and the Ontario Graduate Scholarship.

I am deeply grateful to my parents for their neverending care. I also offer deep thanks to my parents-in-law.

Last, but not least, I am indebted to my wife, Berna, for her constant encouragement, endless support and understanding. I am also grateful to her for proofreading this entire manuscript.

# Contents

# List of Figures

# List of Tables

## List of Abbreviations and Acronyms

| | |
|---|---|
| **AE** | antenna element |
| **AMPS** | advanced mobile phone system |
| **ARU** | antenna remote unit |
| **BS** | base station |
| **CA** | central antenna |
| **CDF** | cumulative distribution function |
| **CDMA** | code-division multiple access |
| **CS** | central station |
| **DA** | distributed antenna |
| **DR** | dynamic range |
| **DS** | direct sequence |
| **E/O** | electooptic |
| **FDMA** | frequency-division multiple access |
| **FM** | frequency modulation |
| **FST** | full Steiner tree |
| **GSM** | global system for mobile |
| **LNA** | low noise amplifier |
| **LOS** | line-of-sight |
| **MAI** | multiple access interference |
| **Micro-BS** | microcell base station |
| **MRC** | maximal ratio combining |
| **MST** | minimal spanning tree |
| **MTSO** | mobile telephone switching office |
| **NoI** | number of iteration |
| **NP** | non-polynomial |
| **O/E** | optoelectric |
| **PA** | power amplifier |
| **PBPC** | power-balanced power control |
| **PC** | power control |
| **PDS** | passive double star |
| **PN** | pseudo-noise |
| **PPC** | perfect power control |
| **RBS** | radio base station |
| **RF** | radio frequency |

| | |
|---|---|
| **RX** | receiver |
| **SAW** | surface acoustic wave |
| **SBMPC** | SIR-balanced macro power control |
| **SBPC** | SIR-balanced power control |
| **SCM** | sub-carrier multiplexing |
| **SDA** | sectorized distributed antenna |
| **SIR** | signal-to-interference ratio |
| **SMT** | Steiner minimal tree |
| **ST** | Steiner tree |
| **TDM** | time-division multiplexing |
| **TDMA** | time-division multiple access |
| **TX** | transmitter |
| **WAN** | wireless access network |

## List of Mathematical Terms

| | |
|---|---|
| $L$ | number of antenna elements |
| $K$ | number of users |
| $N$ | spread-spectrum processing gain |
| $D$ | inserted delay in the DA common feeder |
| $p$ | number of sectors in a sectorized antenna |
| $\mathbf{P}$ | received power matrix at the CS |
| $P_{ij}$ | received power for user $i$ from AE $j$ |
| $\tilde{\mathbf{P}}$ | transmit power matrix of users |
| $\tilde{P}_i$ | transmit power of user $i$ |
| $\mathbf{G}$ | link gain matrix |
| $G_{ij}$ | link gain between user $i$ and AE $j$ |
| $\mathbf{\Gamma}$ | SIR vector for users at the CS |
| $\Gamma_i$ | SIR for user $i$ at the CS |
| $\Gamma_{ij}$ | SIR at the $j$th finger of user $i$'s receiver at the CS |
| $\gamma$ | balanced SIR value in SBMPC algorithm |
| $\beta$ | the constant that denotes the effect of intercell interference |
| $w_i$ | wireless user $i$ |
| $\xi_{ij}$ | chi-square random variable characterizing the multipath fading |
| $\mathbf{E}(.)$ | expected value |
| $\mathbf{Z}$ | vector denoting AE locations |
| $Z_j$ | triplet that denotes the coordinates of AE $j$ |
| $\alpha$ | distance-power-law coefficient |
| $\kappa$ | height of the AE's |
| $y$ | square cell side length |
| $d_{ij}$ | distance between user $i$ and AE $j$ |
| $A$ | log-normal random variable characterizing the shadow fading |
| $\epsilon$ | stopping margin in the iterative solution of SBMPC algorithm |
| $\nu$ | iteration step in the iterative solution of SBMPC algorithm |
| $\nu_t$ | iteration step at the termination of the iterative solution algorithm |
| $\Lambda_i$ | error in $i$th user's SIR value after the iterations |
| $\eta$ | NoI's after which the iterations oscillate normally when a type 1 problem occurs |
| $\mu$ | threshold $K/L$ ratio between the loaded and unloaded systems |
| $\mathcal{E}_i$ | $i$th of the $K$ equations used in the iterative solution of SBMPC algorithm |
| $m$ | number of stages in the multi-stage stop criterion |

| | |
|---|---|
| $t_{iI,t}$ | total propagation time from user $i$ to the CS through AE $I$ |
| $t_{1I}$ | propagation time in the air from user $i$ to AE $I$ |
| $t_{I,c}$ | propagation time in the cable from AE $I$ to the CS |
| $t_{12I}$ | difference between $t_{1I,t}$ and $t_{2I,t}$ |
| $\Delta_{12,I-II}$ | difference between $t_{12I}$ and $t_{12II}$ |
| $c_i(t)$ | spreading code of user $i$ |
| $c$ | speed of light |
| $h$ | normalized distance |
| $s$ | distance scaling factor |
| $\vartheta$ | difference between $h_{1I}$ and $h_{1II}$ |
| $\tau$ | spreading code chip duration |
| $R_c$ | chip rate |
| $T$ | information bit duration |
| $\Delta_i$ | spreading code phase of user $i$ (normalized to $\tau$) |
| $\Delta_{ij}$ | difference between the spreading code phases of users $i$ and $j$ (normalized to $\tau$) |
| $f_c$ | carrier frequency |
| $b_i(t)$ | information signal of user $i$ (before spreading) |
| $m_i(t)$ | transmitted signal of user $i$ (after spreading) |
| $\zeta_{iI}$ | interference (noise) component at the $I$th finger of the Rake receiver of user $i$ |
| $\psi_{iI}$ | deterministic component of $\zeta_{iI}$ |
| $n_{iI}$ | random component of $\zeta_{iI}$ |
| $\langle . \rangle$ | inner product |
| $\rho_{12,I-II}$ | correlation coefficient of the random variables $\zeta_{1I}$ and $\zeta_{1II}$ |
| $\mathbf{U}$ | correlation matrix |
| $\phi_i$ | percent correlation for user $i$ |
| $\mathbf{\Psi}$ | set of L points (AE's) in the plane |
| $\Psi_i$ | point $i$ in the plane |
| $a$ | hexagon radius in hexagonal grid |
| $\Omega$ | length of interconnecting network |
| $\chi$ | Steiner ratio |
| $C$ | system capacity |
| $\varphi$ | reduction in capacity |

# Chapter 1

## Introduction

Wireless communications have captured the attention of the public, media and industry [2–6]. Clearly, it is, by any measure, the fastest growing segment of telecommunications.

Only a decade ago, a few business people or wealthy individuals who had bulky and expensive vehicular phones would have had access to mobile communications. Today, the cellular phone has become a widespread consumer product. Also, it is apparent that there is a huge potential market for data communication services with wireless terminals. The demand for wireless data communications includes not only fax and e-mail (which is already available to a limited extent), but also wireless web-browsing and web-based applications. In fact, it is expected that data traffic of wireless networks will exceed voice traffic in the near future.

Given the pace of development in the wireless industry, it is not easy to anticipate future wireless services, for instance, those that will be available in twenty years. However, one can state quite confidently that wireless service providers face many challenges, even in matching the needs of today's wireless users.

As far as the service provider is concerned, more and more capacity is required within the margins of a reasonable infrastructure/deployment cost. From the wireless user's perspective, however, the provision of voice communications comparable to wire-line quality, and the availability of data rates that would comfortably enable web-browsing and web-based applications are required; moreover, these services should be possible with compact and low-cost wireless terminals. Finally, an almost ubiquitous radio coverage is essential.

The current wireless systems are far from capable of fulfilling these requirements, and furthermore, there is no single ideal method of implementing a network with such appealing results. Indeed, there are many different wireless systems, architectures, technologies, and services being planned or proposed.

This thesis is about code division multiple access (CDMA) multi-antenna systems, where the transmission and reception are through multiple antennas distributed in the service area. We try

to demonstrate that multi-antenna systems, combined with effective power control algorithms, yield efficient interference management in CDMA systems.[1] This results in an improved signal-to-interference ratio (SIR), or equivalently, an increased capacity. In a system with many antennas, practical issues of implementation are also of concern. To this end, cost-efficient, robust and flexible antenna interconnection strategies are also discussed in this thesis.

In Sec. 1.1, a brief overview of wireless access networks (WAN's) is presented. In Sec. 1.2, the spatial interference control features of recent CDMA-based WAN's are addressed. An antenna system known as the distributed antenna, which is very effective in interference management, is discussed in Sec. 1.3, and finally, the motivation and outline of this thesis are given in Sec. 1.4.

## 1.1 Wireless Access Networks

WAN is the interface between the wireless users and the fixed network (such as, the public switched telephone network [PSTN] or other broad-band networks), as shown in Fig. 1.1. WAN's

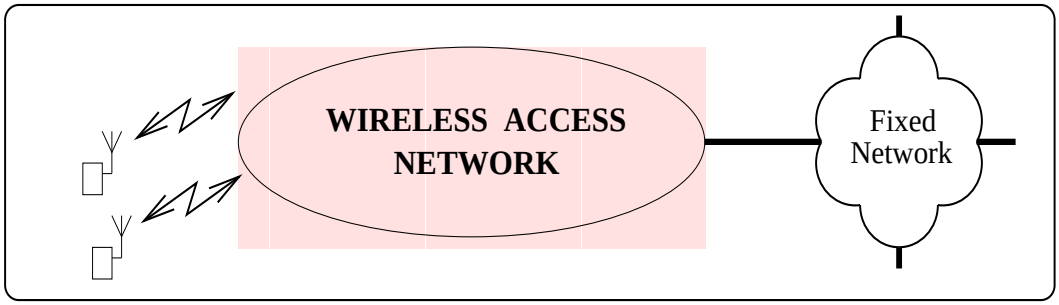


Figure 1.1: The wireless access network.

interact with existing fixed networks to extend information services to wireless terminals.

Our objective in this section is to explore the relationship between the WAN architecture and the multiple access interference (MAI), especially in CDMA systems, in order to develop insight into the techniques that can efficiently reduce the MAI.[2]

### 1.1.1 Main Features of Conventional Wireless Access Networks

We use the word *conventional* to indicate the WAN's that have been deployed in the last two decades for cellular mobile radio communications. Such a WAN is illustrated in Fig. 1.2. The main features of conventional WAN's are discussed below.

[1] In this thesis, CDMA refers to direct sequence (DS) CDMA, unless otherwise stated.

[2] Only a limited number of references are given in this section; for a more thorough discussion, the interested reader can refer to one of the many good books on the subject, such as [7–10] on cellular mobile communications, and [11–13] on CDMA systems.

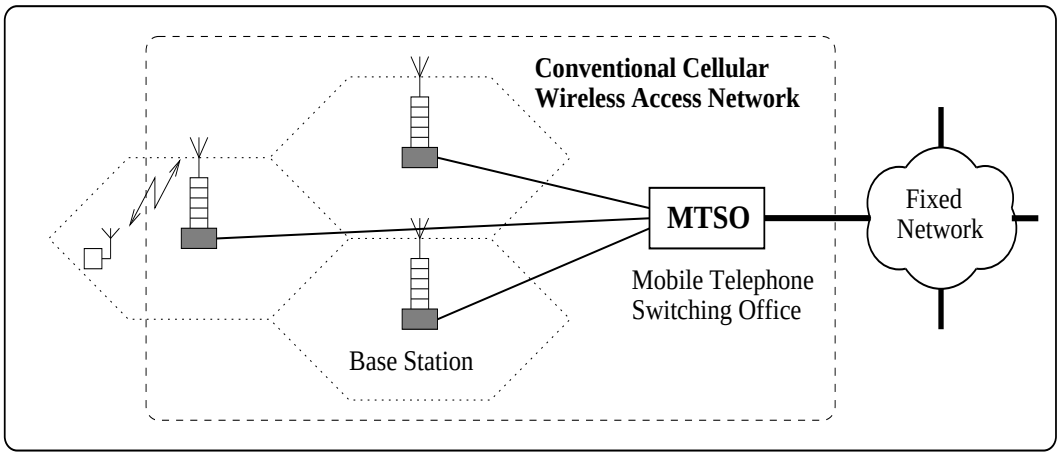


Figure 1.2: Conventional wireless access network.

**(a) Cellular Structure:** One key concept in conventional WAN's is the cellular structure. In order to obtain frequency reuse capability, the service area is divided into cells, and the same set of resources are reused in different cells that are sufficiently apart from one another, so that co-channel interference is within tolerable limits. Each cell is covered by a base station (BS) which is deployed in the center of the cell. The BS antenna is elevated in the order of tens of meters; this results in the cell radii to be in the order of many kilometers.

**(b) Handoff:** When the wireless user moves from the coverage region of one BS to that of another one, the communication is also transferred from one BS to the other one; this process is known as *handoff*. The BS's are connected to a mobile telephone switching office (MTSO) which is the gateway to the fixed network. The main function of the MTSO is link control; that is, the control of the handoff processes.

**(c) Wireless User – BS Relationship:** In conventional WAN's, each wireless user communicates with a particular BS; therefore, there is a many-to-one set relationship between the set

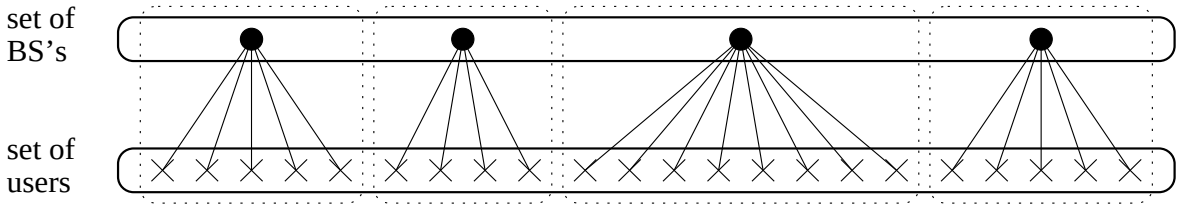


Figure 1.3: Many-to-one set relationship between the set of wireless users and the set of BS's.

of wireless users and the set of BS's, as illustrated in Fig. 1.3. In Fig. 1.3, the solid lines denote the radio links.

**(d) Distributed Processing:** One other main feature of conventional WAN's is that the processing is distributed in the system. In other words, along with the processes performed in

bulk (such as, amplification), all the signal-specific processing (such as, filtering, modulation, and detection) is performed at the BS's. Obviously, this yields expensive BS's.

### 1.1.2 Cellular Air-Interface Standards

Before discussing the interference-related issues in conventional WAN's, we will briefly address the main cellular air-interface standards in North America and Europe.

The first cellular standard in North America, AMPS (advanced mobile phone system), was introduced in 1983. AMPS is a frequency-division multiple access (FDMA) -based analog system which employs frequency modulation (FM). AMPS and similar analog standards are referred to as first generation (1G) systems.

The next widely deployed cellular standard in North America is IS-54 which was introduced in 1990. IS-54 is sometimes referred to as digital-AMPS because of its capability of backward compatibility. Around the same time (in 1991), another standard, GSM (global system for mobile), was introduced in Europe. Both IS-54 and GSM are time-division multiple access (TDMA) -based digital systems.

Finally, in 1993, IS-95 standard was introduced. IS-95 is also a digital system, but based on code-division multiple access (CDMA). The digital IS-54, GSM, and IS-95 standards are referred to as second generation (2G) systems.

Presently, the specifications of the third generation (3G) systems are being discussed. There is strong indication that the 3G systems will employ wideband-CDMA technique, and are expected to be deployed early in the next century.

### 1.1.3 The Nature of Multiple Access Interference in Various Multiple Access Schemes

In multiple access schemes, since more than one user can utilize the same resource (time or frequency), MAI occurs. There are two types of MAI, namely, intracell and intercell interference, and their relative significance differs from one multiple access scheme to another.

TDMA and FDMA are slotted schemes; that is, the resources are allocated to users in a disjointed manner. In TDMA or FDMA systems, since the orthogonality of the time or frequency slots in a cell can easily be maintained, the intracell interference can be eliminated completely. Therefore, in these systems, it is the intercell interference which is the single most important factor preventing the use of the available time or frequency slots in adjacent cells. Consequently, the reduction of interference in TDMA or FDMA systems yields a smaller reuse distance, in other words, a smaller cluster[3] size.

[3] A cluster is a set of cells in which all the available bandwidth is utilized. Therefore, a cluster is the main

Clearly, in TDMA and FDMA systems, the interference is from users in other clusters. In a CDMA system, however, resources are allocated to all simultaneous users (this yields a cluster size of 1). Therefore, each user in the system contributes to the background noise affecting the other users.

The forward[4] link of a cellular system constitutes a one-to-many (broadcast) channel, and the reverse link, a many-to-one (multiple access) type. However, because of the disjoint allocation of channels and the maintenance of orthogonality in FDMA and TDMA systems, both the forward and reverse links are, indeed, composed of many one-to-one channels. Similarly, in the forward link of a CDMA system, through the use of synchronization and orthogonal spreading codes, the orthogonality can be maintained; so the forward link of a CDMA system is also composed of many one-to-one channels. On the other hand, synchronization in the reverse link of a CDMA system is, in general, very difficult. As a result, all the users interfere with one another; in other words, the reverse link of a CDMA system constitutes a truly many-to-one channel.

Interference management is very important in cellular systems regardless of the multiple access scheme used. After all, it is the level of interference that determines the frequency reuse efficiency. However, it should be emphasized that the concept of interference management is fundamentally more important for CDMA systems than for FDMA and TDMA types — this applies especially in the reverse link of an asynchronous CDMA system, because of the many-to-one nature of the multiple access channel, as discussed above. Any reduction in MAI, in a CDMA system, yields a direct increase in the capacity. Interference reduction also yields a capacity increase in FDMA and TDMA systems, but this increase is not as significant as that in CDMA types.

In the next section, spatial processing features of recent WAN's, which yield efficient interference reduction, are discussed.

## 1.2 Spatial Interference Control Features of Current CDMA-Based WAN's

The conventional WAN architecture discussed in the previous section was originally designed for FDMA systems. Later on, when TDMA systems were introduced, they also used the same WAN architecture. In time, when greater capacity and better coverage were required, smaller cells with less elevated antennas have been deployed. The deployment of even smaller cells, which are referred to as microcells, has been discussed in the literature for a significant period [14, 15]. It

building block in constructing the frequency reuse pattern. In FDMA and TDMA systems, cluster sizes of 4 and 7 are commonly used.

[4]The forward link is defined as the radio link from the BS to the wireless users, and the reverse link is that from the wireless users to the BS.

is worth noting, however, that despite the smaller cell size and less elevated BS antennas, the microcellular systems have essentially the same architecture, and thus the same features, as the conventional WAN's discussed in Sec. 1.1.1.

The conventional WAN architecture does not have rigorous spatial processing capability, which is very effective in interference reduction in CDMA systems. Because of this fact, with the standardization of CDMA with IS-95, some modifications were made in the conventional WAN architecture to introduce spatial processing features.[5] Although the scope of these modifications were limited, they resulted in significant capacity enhancements in IS-95 based systems. A summary of the major spatial interference control features of such WAN's are discussed below.

**(a) Sectorized Antennas:** By employing $(360/p)^o$ sectorized antennas ($p$ is a positive integer), MAI can be reduced approximately $p$ times, and thus the capacity can be increased approximately $p$ times.[6] Sectorized antennas are also effective in FDMA and TDMA systems; by employing $120^o$ ($p=3$) sectorized antennas, the cluster size can be reduced from 7 to 4. However, it should be noted that the resulting increase in capacity (1.75 times) is still significantly lower than that (3 times) in a CDMA system.

**(b) Soft Handoff:** In the reverse link of a CDMA system, during the process of handoff,

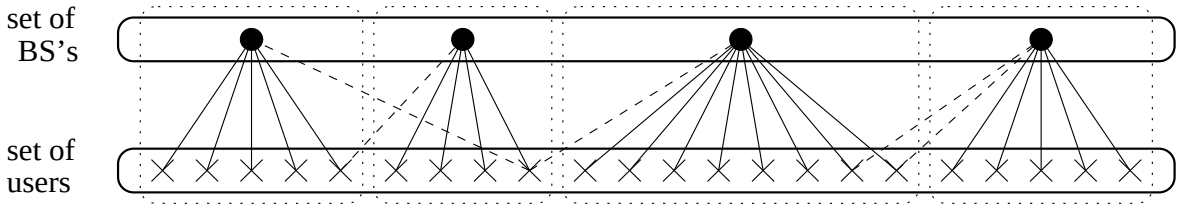


Figure 1.4: Limited many-to-many set relationship between the set of wireless users and the set of BS's, in a cellular system with soft handoff.

the wireless user may communicate with two or more BS's simultaneously; this process is known as *soft handoff*. Soft handoff is a unique capability of CDMA systems; such a concept does not exist in FDMA and TDMA systems. In a system with soft handoff, there is a many-to-many set relationship between the set of wireless users and the set of BS's, as shown in Fig 1.4, unlike the many-to-one type in the conventional WAN's (see Fig 1.3). In Fig 1.4, the solid and broken lines denote the permanent and temporary radio links, respectively.

**(c) Antenna Arrays:** By using an array of collocated antenna elements (AE's), the antenna radiation pattern can be electronically steered, so that the main lobe and the nulls of the radiation

[5] During the course of time, some of these modifications have also been adapted for FDMA- and TDMA-based systems.

[6] The increase in capacity will, however, be less than $p$ times in practice, because of the imperfections in the antenna patterns.

pattern can be directed towards the user of interest and the interferers, respectively. Obviously, this scheme yields substantial enhancements in SIR values [16–18].

**(d) Distributed Antennas:** A distributed antenna (DA) system also employs many AE's, but these AE's are distributed *throughout* the cell, unlike an antenna array where the AE's are located only a few wavelengths apart. The DA structure is radically different than the conventional BS antenna type. Since DA and its derivatives constitute the main topics of this thesis, this antenna structure is discussed in detail in the next section.

Power control algorithms (which are essential in CDMA systems), as well as advanced signal processing techniques, such as multiuser detection, are not included in the above list, since the improvements obtained from these techniques do not result directly from the spatial processing features of the WAN architecture.[7]

## 1.3 Distributed Antenna Systems

In mid-1950's, it was accidentally discovered that an imperfectly shielded wire radiates continuously. This was the origin of *leaky feeder* techniques [shown in Fig. 1.5(a)], which were used

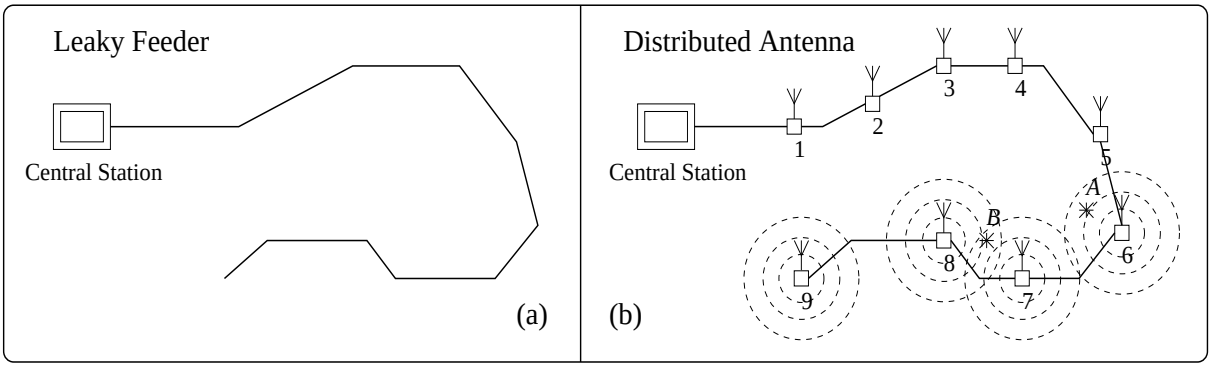


Figure 1.5: (a) Leaky feeder. (b) Distributed antenna.

without being entirely understood for about 20 years [19, 20]. Leaky feeders have found wide usage in subsurface communications, such as in mines and tunnels, in order to achieve simple coverage. Recently, leaky coaxial feeders are being considered for road vehicle communications in intelligent transportation systems [21].

DA is the discrete version of the leaky feeder structure. Because of the significant conceptual differences between the narrowband DA and CDMA DA systems, these two types are discussed separately.

[7] Power control will be discussed in great detail in Ch.s 2 and 4.

### 1.3.1 Narrowband DA Systems

In a DA system, many simple omni-directional AE's are coupled to a common feeder, as shown in Fig. 1.5(b), and the same signal is transmitted from (and received by) all of these AE's. This is generally called simulcasting. There is no signal-specific processing at the AE's; all of the processing is performed at a central station (CS).[8] However, amplification in the feeder and/or AE's would, most likely, be inevitable.[9]

In a DA system, the AE's are *distributed* throughout the cell area; this is in contrast with the situation in conventional cells where the BS antenna is *centralized*; we refer to this latter case as the central antenna (CA) type. Note that the conventional CA system can be thought of as a special case of the DA type with one AE.

The similarity between leaky feeder and DA is as that between integration and summation. One main advantage of DA over leaky feeder is that there is more control on the DA structure, since the radiation is from controlled locations.

Similar to leaky feeder, DA has been employed in environments that are very hostile for radio propagation, such as tunnels [22–29]. In such early systems, the DA structure was used merely for coverage in the environments where user density was relatively low, yet extensive coverage was still required. Saleh et. al.'s paper [30] is, perhaps, the first to analyze the performance of a DA system in the context of cellular mobile communications. It is worth emphasizing that there is no need for handoff as long as a user is in the same DA cell. Since then, other studies on the performance of DA in cellular systems appeared in the literature [31–34], Kerpez's work [34] especially is quite comprehensive.

The main shortcoming of DA is the self-interference due to simulcasting in overlapping regions of the radio coverage. Let us consider the forward link of the DA system shown in Fig. 1.5(b). When a user is at point $A$, it receives signals from AE 6; however, when it moves to point $B$, it receives signals from both AE 7 and AE 8, and this may cause severe interference (the same argument is true also for the reverse link).

In environments where the radio propagation is extremely difficult, such as in subsurface areas, occasional poor performance due to simulcast interference can easily be tolerated, since there are not many other options. After all, in such environments, the performance of DA would be far better than that of a conventional BS anyway. In personal communication systems, however, such performance degradations can hardly be tolerated because of the more stringent quality of service requirements. Therefore, if DA systems are to be used in cellular WAN's, rigorous site-specific

[8] The word *central* does not refer to the geographical center of the service area, but rather to the centralized nature of signal processing. The CS can be located at any convenient place in the service area.

[9] The practical issues related to deployment and implementation are discussed in detail in Ch. 6.

engineering is required to prevent the occurrence of overlapping regions. Obviously, this is not very efficient in mass deployment.

### 1.3.2 CDMA DA Systems

In 1991, Qualcomm researchers Salmasi and Gilhousen developed a bright idea [35]: if CDMA modulation is used in a DA system, the signals coming from multiple AE's can be distinguished by a Rake receiver. This would eliminate the simulcast interference and the related concerns on site-specific planning.

In fact, the presence of radio links between a user and more than one AE is an advantage. Theoretically, the user would receive signals from all of the AE's (although, in practice, only a few of these signals may be strong enough to make use of), and would utilize them by diversity combining (the same is true in the reverse link also). Obviously, this is macro diversity which is

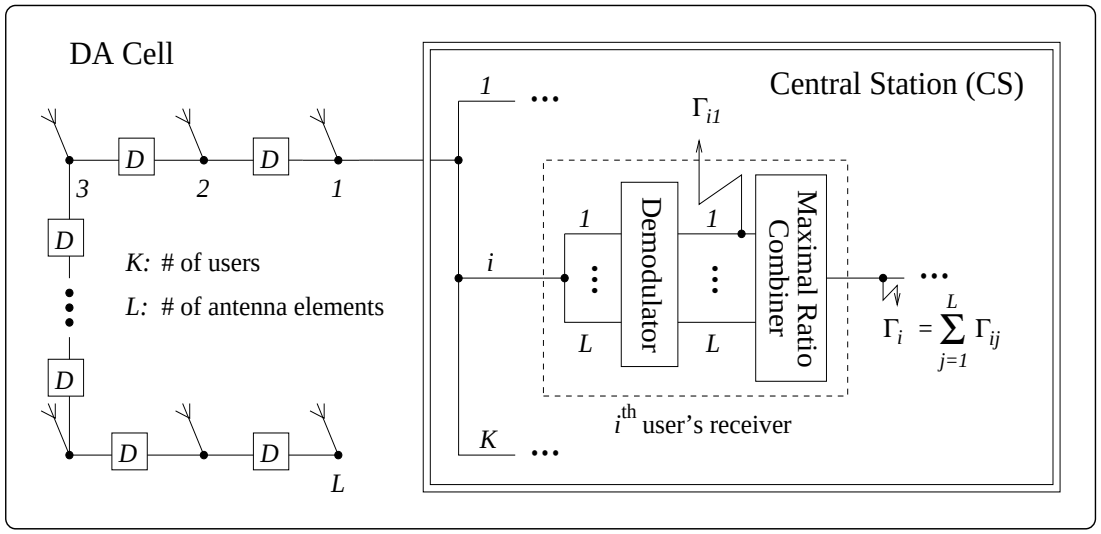


Figure 1.6: CDMA DA system.

effective against not only multipath fading but also shadow fading.[10]

A CDMA DA system is illustrated in Fig. 1.6. In order to differentiate the many replicas of the same signal at the receiver, CDMA modulation is employed, and delay elements are inserted into the feeder in order to make sure that the time difference between the signals received from any two AE's is at least one pseudo-noise (PN) code chip duration. In Fig. 1.6, $D$ indicates the delay element.[11] It should be noted that in order to make sure that the signals received by various AE's are distinguishable, the delays introduced throughout the feeder may need to have different

[10] Note that although the classical antenna diversity, implemented by collocated antennas, has proven to be very effective against multipath fading, it cannot offer a remedy against shadow fading.

[11] One way to realize the delay elements is through the use of surface acoustic wave (SAW) technology [36].

values [37]. Also, it is interesting to note that, depending on the inter-AE distance, the required delays for path resolution may naturally be introduced as a result of the propagation delay in the cable.

### 1.3.3 Main Features of CDMA DA Systems

The salient features of the CDMA DA systems can be discussed under two main categories: coverage and diversity.

**(a) Coverage**: DA is very efficient in attaining coverage [38,39]; this is especially important in environments hostile to propagation. After all, coverage is the very main reason why DA (and

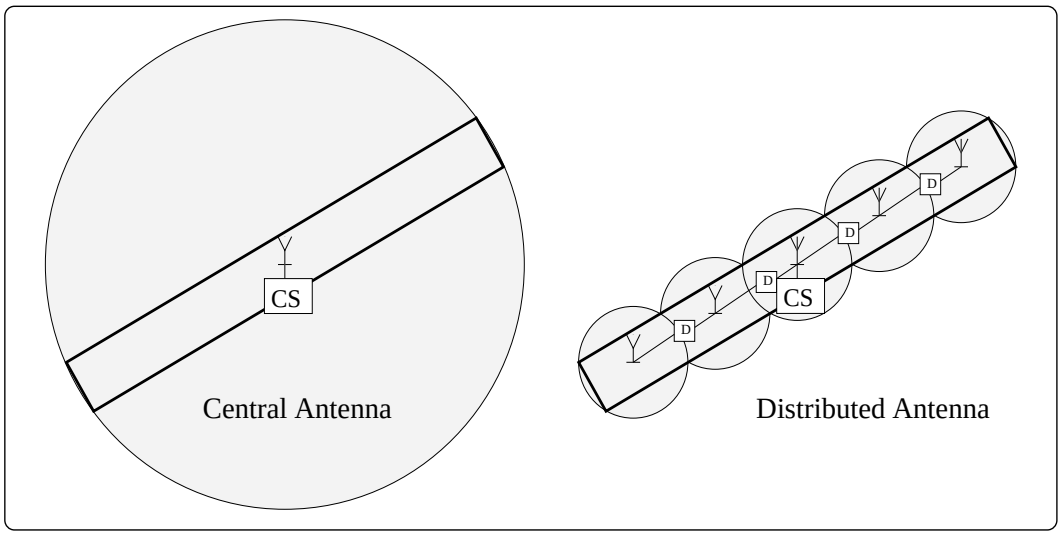


Figure 1.7: Uniform coverage with CDMA DA system.

its precedent, leaky feeder) found widespread applications.

There are other benefits related to efficient coverage. For instance, let us consider a linear area (such as a highway) to be given radio coverage. If a CA is used, there is a significant power waste, as shown in Fig. 1.7. However, if a DA scheme is used, energy is injected only where it is required. The corollary of this statement is that the formation of cells with desirable shapes, even non-contiguous ones, is possible [40]. Efficient use of transmit power yields transmission with relatively low power levels [41, 42]. Power savings are especially important for the wireless terminals, since this results in extended battery recharge times.

Efficient coverage has a very important impact on interference management: by using DA, intercell interference can be reduced significantly. This issue will be discussed in more detail in Ch. 2.

**(b) Diversity**: DA provides not only microdiversity against multipath fading, but also macrodiversity against shadow fading [38,39]. DA's macrodiversity capability is particularly important,

because schemes such as collocated antennas and antenna arrays cannot offer efficient solutions to shadow fading.

It is worth noting that in the literature, CDMA DA has mainly been proposed for indoor wireless communications [35,41]. The outdoor deployments of CDMA DA have been quite limited; one such rare example is San Diego, California, area.[12]

## 1.4 Thesis Motivation and Outline

The following fundamental question is investigated in this thesis: *In a CDMA system, how should the signals be collected from and distributed to the wireless users?* To this end, the main objective of this thesis is to utilize antennas in novel ways so as to achieve performance benefits at the system level.

The importance of finding efficient ways of delivering and receiving signals in wireless multiple access environments is very well known. In this context, leading spatial interference control techniques have been qualitatively discussed in Sec.s 1.1.3 and 1.2. The major part of this thesis is devoted to furthering the understanding of spatial interference control, and the corresponding performance improvements, in multi-antenna CDMA systems.

The thesis outline is presented here. The motivation of the research in each chapter, not the results, will be shown. At the end of each individual chapter, there is a section summarizing the results of that chapter.

**Chapter 2:** Since CDMA DA provides coverage and diversity against both shadow and multipath fading, it is intuitive to expect that this architecture would ease power control (PC), compared to the conventional CA type. The relationship between the number of AE's in a DA system and the resulting improvements in PC are discussed in Ch. 2.

**Chapter 3:** We stated in Sec. 1.2 that with soft handoff, the many-to-one relationship (see Fig. 1.3) between the set of BS's and that of users in conventional WAN's is changed to a many-to-many type (see Fig. 1.4). It should be noted, however, that this many-to-many set relationship

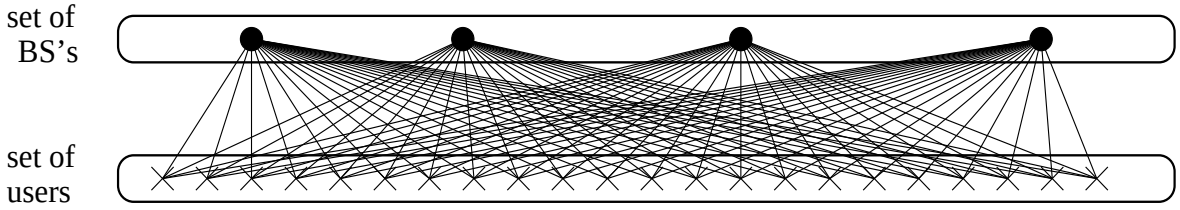


Figure 1.8: Many-to-many relationship between the set of wireless users and the set of BS's, in a system where users are in continuous soft handoff with all BS's.

[12]Personal communication with Ed Tiedemann, Vice-President, Technology, Qualcomm Inc., June 1998.

exists only in a limited sense, since only a few users close to the cell boundaries would temporarily be engaged in soft handoff.

It would be interesting to investigate the logical extent of the soft handoff; that is, the situation in a system where all the users in the system permanently communicate with all the BS's (or AE's). In such a scenario, the set relationship would be a truly many-to-many type, as illustrated in Fig. 1.8. This relationship deserves attention especially in the reverse link of such a system, since the radiated energy from a user naturally reaches many BS's (or AE's) anyway. Obviously, the system that makes use of this energy will outperform the conventional type that treats it as pure interference. This system is called sectorized distributed antenna (SDA)[13], and will be analyzed in Ch. 3.

**Chapter 4:** In the SDA system described in Ch. 3, the concept of PC deserves special attention. Because, the PC algorithms in the literature, developed mainly for conventional WAN architectures (where the set relationship between the BS's and users is a many-to-one type), do not necessarily perform efficiently in an SDA system where the set relationship is many-to-many due to macrodiversity (joint decoding). A new PC algorithm for SDA systems is introduced in Ch. 4.

**Chapter 5:** It is intuitive to expect that in an SDA system placing more AE's would yield a better performance. But, in a given service area to be covered by an SDA cell, is it possible to place as many AE's as we wish without an upper limit, or the law of diminishing returns apply after a certain point? In other words, are the returns of the SDA system scalable? Also, in a service area, are some AE locations *better* than the others? The answers for these and many other related questions on the performance of multi-antenna systems can adequetly be answered only after developing a comprehensive understanding on the issue of correlation between the interference received by different AE's in the system. The analytical framework of the correlated interference analysis, which may eventually enable us to answer many such fundamental questions on multi-antenna systems, is presented in Ch. 5.

**Chapter 6:** In a system which consists of a few BS's and a switching office, it may not matter how the interconnection of these network elements is made. But, if there is an extensive network with thousands of AE's and numerous processors/switches, then it may be crucial to have a strategy or algorithm to achieve the interconnection in an efficient manner, since even modest improvements in the design of the WAN would result in significant savings. In this chapter, antenna interconnection strategies for wireless access networks are studied in order to determine cost-efficient as well as robust and flexible interconnection architectures.

**Chapter 7:** In this chapter, some of the main results of Ch.s 2-6 are reemphasized, by com-

[13]The reason for using the term *sectorized* will be explained in Ch. 3.

paring the multi-antenna systems addressed in this thesis with the conventional cellular systems.

A final note is that in the rest of this thesis, DA and SDA refer to CDMA DA and CDMA SDA systems, respectively, unless otherwise stated.

Parts of this thesis (Ch.s 2, 3, 4, and 6) were published (or are accepted for publication) in [43–49]. The work in Ch. 5 is under preparation for publication.

# Chapter 2

## Reverse Link Power Control and Number of Antenna Elements in CDMA Distributed Antenna Systems

In this chapter the relationship between the number of AE's in a CDMA DA system and the yielding reverse link SIR is investigated by taking PC dynamic range into account.

In environments hostile to propagation, perfect power control[1] may not be realized with a CA, because this would require an impractically high dynamic range. This situation may yield a significant decrease in capacity. In such environments, the DA system is an ideal solution, since as the number of antenna elements increases, the dynamic range of the power control decreases.

### 2.1 System Model

In a CDMA DA system, the resolved signals are individually demodulated and then combined in a maximal ratio combining scheme to attain diversity, as illustrated in Fig. 1.6. In such a case, the output SIR at the CS for any user $i$, $\Gamma_i$, would be

$$\Gamma_i = \sum_{j=1}^{L} \Gamma_{ij}, \qquad i \in \{1, \ldots, K\}, \tag{2.1}$$

where $K$ is the number of users, $L$ is the number of AE's, and $\Gamma_{ij}$ is the SIR at the $j$th finger of the receiver corresponding to user $i$.

Throughout this thesis, a flat fading channel is considered. For small cell sizes with IS-95 type chips rates (around 1 Mcps), the flat fading assumption would be a realistic one. In such a case, there is assumed to be only one path between a user and an AE.[2] Then, a total of $L$ distinguishable signals would be received at the CS from each user. Since the signals picked up

[1] Perfect power control will be defined in Sec. 2.2.1.

[2] Due to higher bandwidths and/or smaller cell sizes used, multipath fading may become frequency selective. A DA system which receives a total of $\mathcal{L}$ paths from $L$ AE's ($\mathcal{L} \geq L$) is, in essence, similar to the one with $\mathcal{L}$ AE's where there exists only one path per AE. However, it should be noted that as a consequence of the distributed nature of the AE's, a DA system can mitigate against shadow fading as well as multipath fading; on the other

by all the AE's accumulate in the feeder, there are a total of $LK$ signals delivered to the CS. In a particular user's receiver, each finger of the Rake locks onto that user's signal received by one of the AE's, and all the remaining $LK-1$ signals are treated as interference, including the user-of-interest's signals received by the other AE's. The powers of the received signals at the CS

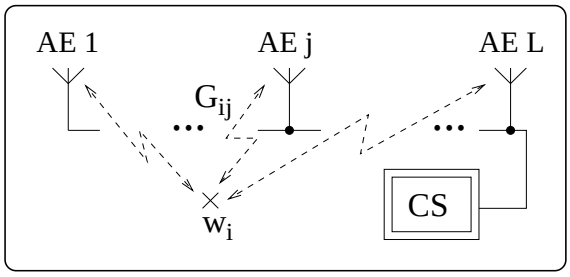


Figure 2.1: The link gain model in a DA cell.

are represented by a $K \times L$ matrix $\mathbf{P} = \{P_{ij}\}$ such that

$$P_{ij} = G_{ij}\tilde{P}_i, \tag{2.2}$$

where $\tilde{P}_i$ is the $i$th user's transmit power, and $G_{ij}$ is the link gain between user $i$ and AE $j$, as shown in Fig. 2.1.

In a DA system, the intercell interference is expected to be much less significant compared to a system with a CA.[3] Therefore, along with the background noise, the intercell interference is also omitted in our analysis. Based on these assumptions, a user's SIR at a finger of the corresponding Rake receiver would be the ratio of the signal power at that finger to that of the intracell interference. The total interference power is modeled as the sum of the powers of the individual active (intracell) interferers. Then, if factors such as the voice activity and frequency reuse efficiency are omitted, SIR for a user $i$ would be

$$\Gamma_{i,\mathrm{DA}} = \sum_{j=1}^{L} \Gamma_{ij} = N \sum_{j=1}^{L} \frac{P_{ij}}{(\sum_{k=1}^{K}\sum_{l=1}^{L} P_{kl}) - P_{ij}}. \tag{2.3}$$

In the above, $N$ denotes the CDMA processing gain.

hand, path diversity (obtained as a result of frequency selective fading) is effective only against multipath fading. Therefore, even if an environment requiring service is highly frequency selective, more than one AE should be utilized if there are coverage problems.

[3]This is due to the fact that in a DA system, as the number of AE's increases, the required transmit power level for each AE will decrease, and the coverage will become more of a uniform type. Subsequently, the intercell interference caused by these low power AE's will be less compared to that resulting from a high power CA. The reduction in the intercell interference will become more apparent after the results presented in Sec. 2.3.2, especially those summarized in Eqn.s 2.21 and 2.22.

If the intercell interference is required to be included in the analysis, then the effective number of users in a DA cell can be assumed to be $K_o = K/(1+\beta)$, where $\beta$ is a constant that denotes the effect of intercell interference as a fraction of the intracell type, with $\beta \geq 0$. We anticipate that as $L$ increases, $\beta$ would become closer to 0.

## 2.2 DA and Perfect Power Control

In the absence of PC, every user in a cell would transmit at the same power level. Then, in a CA system, the signals of the users which are close to the CA would be received much more strongly than those of distant users; this would be detrimental in the reverse link of a CDMA system — a phenomenon known as the near-far problem. In addition, shadow and multipath fading occurs. Therefore, it is essential to employ PC to eliminate the potential excessive differences in the powers of the received signals corresponding to different users.

### 2.2.1 Power-Balanced Power Control Algorithm

We consider a power-balanced PC (PBPC) algorithm similar to that of IS-95; i.e., the total received power for every user is kept at a constant level.[4] The PBPC problem in a DA system can be defined as follows:

$$\text{find } \tilde{P}_i, \text{ subject to } \sum_{j=1}^{L} P_{ij} = \sum_{j=1}^{L} G_{ij}\tilde{P}_i = 1, \quad \forall i. \tag{2.4}$$

Obviously,

$$\tilde{P}_i = \left( \sum_{j=1}^{L} G_{ij} \right)^{-1}, \quad \forall i. \tag{2.5}$$

Therefore, if the link gains are known, PBPC is computationally very simple.

If PC can *always* be maintained despite distance, and shadow & multipath fading, then we refer such a case as the perfect PC (PPC) type. In other words, if there is no upper or lower limit imposed on the dynamic range (DR), or the required $\tilde{P}_i$ always turns out to be between these limits anyway, this is a PPC case.[5] On the other hand, the case where these limits do exist due to the practical limitations and thus $\tilde{P}_i$ is at least occasionally hard-limited, is referred to as the *limited dynamic range* type.

[4] The actual value of this constant does not affect the SIR value, because the SIR will be the ratio of the signal and interference powers (when the background noise is omitted). Without loss of generality, we will assume that this constant is 1.

[5] In the PPC case, the power adjustments are assumed to be performed instantaneously with the required step size.

In the definition of PPC, we followed the convention in the literature. It is worth noting, however, that perfectness in this context does not necessarily mean optimality. That is, a PC algorithm may be *perfect* but suboptimal, such as the PBPC algorithm in a DA case. We will discuss the optimal SIR-balanced PC algorithm in Ch. 4.

### 2.2.2 Single-Cell Systems

Let us consider a single-cell system with a CA and $K$ users. If PPC is possible, then, by substi-

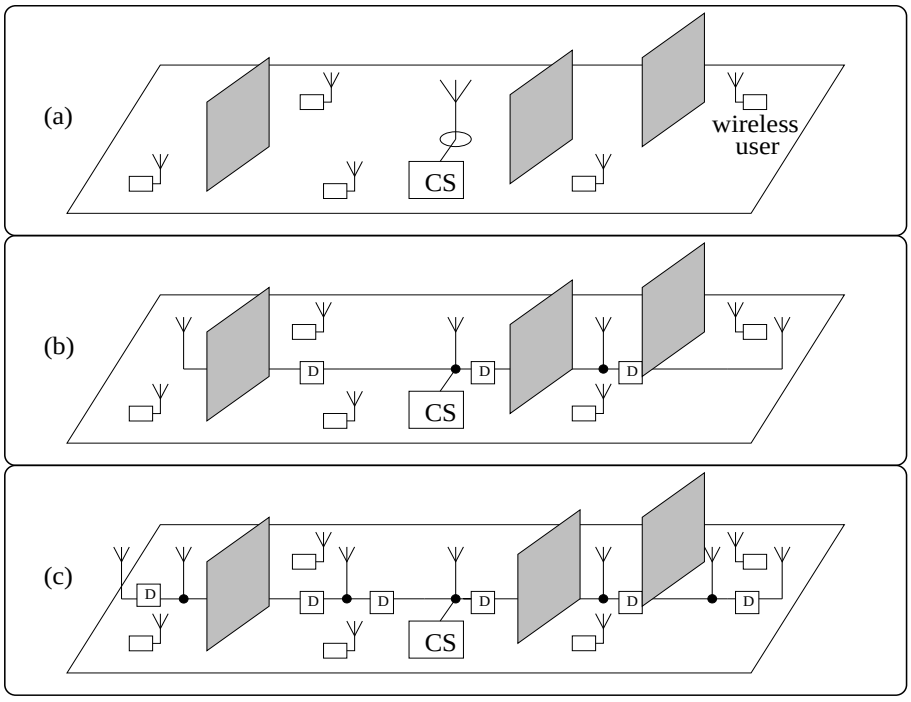


Figure 2.2: Coverage in a harsh environment: (a) with a CA, (b) with a DA with few AE's, and (c) with many AE's.

tuting $L=1$ in Eqn. 2.3, the SIR can simply be calculated as

$$\Gamma_i = \frac{N}{K-1}, \quad \forall i. \tag{2.6}$$

This is the best value achievable for such a scenario, therefore there is no need for DA in this case.

However, in environments with shadow and multipath fading, as the one depicted in Fig 2.2(a), to maintain PPC continuously is often impossible. When a user's signal is in a deep fade, especially because of blockage, a very high level of power would need to be sent for relatively long periods, and this would require an impractically large DR. It is worth noting that if PPC were possible, then the SIR would still be the expression given in Eqn. 2.6.

The unrealistic requirements on the DR of PC, due to the blockage and shadow fading problems, can be alleviated by using a DA [Fig 2.2(b)]. In a DA cell, no user is almost ever significantly affected from shadow fading; therefore, the SIR is close to that of an ideal CA case as given in Eqn. 2.6, where PPC is possible.

If the DR of PC is still high due to multipath fading, additional AE's can be used as illustrated in Fig. 2.2(c).

### 2.2.3 Multi-Cell Systems

The situation is quite different in a multi-cell system because of the intercell interference. As stated earlier, if a user's signal is in a deep fade or if blockage occurs between the user and the corresponding CA, then this user must transmit at a very high power level in order to maintain PPC. Since the multipath fading (and also to some extent the shadow fading) between a user and the neighboring CA's is independent of that between the user and the corresponding CA, high levels of interference occur for those neighboring CA's during the maintenance of PPC.[6] Therefore, continuous maintenance of PPC, which yields optimal results in a single-cell system, may yield a considerable decrease in SIR (and thus, in capacity) in a multi-cell system employing CA's [50]. In fact, it is shown in [50] that limiting the maximum transmitted power level in situations requiring the transmission of very high levels of power, is a good compromise that increases the SIR (and thus, the capacity) by reducing the excessive intercell interference.

In a DA system, on the other hand, such situations requiring the transmission of very high levels of power are almost eliminated, even in systems with a moderate number of AE's. Therefore, in a multi-cell environment even if maintaining PPC is possible with a CA, a DA system should be preferred; because, by this way interference to adjacent cells is kept at a minimal level and thus the system capacity is increased.

In the rest of this chapter, the benefits of using the DA in a single-cell system is demonstrated; it is worth noting that the returns are even more when the DA is employed in a multi-cell system.

## 2.3 Analysis and Simulation Results

Simulations with and without multipath fading have been run. For these cases, $G_{ij}$'s are simply taken to be

$$G_{ij,\text{no-fading}} = \frac{1}{d_{ij}^4}, \quad G_{ij,\text{multipath-fading}} = \frac{\xi_{ij}}{d_{ij}^4}. \tag{2.7}$$

[6] The same reasoning is valid even if the required power level for maintaining PPC is beyond practical limits and thus the wireless user transmits at the maximum power level available instead.

In the above, $d_{ij}$ is the distance between user $i$ and AE $j$, and $\xi_{ij}$'s are independent chi-square random variables with two degrees of freedom, with $\mathbf{E}(\xi_{ij}) = 1,\ \forall i, j$ ($\mathbf{E}(.)$ denotes the expected value). As it is well known, the square of a Rayleigh distributed random variable is chi-square distributed.

Simulations have been run for various values of $L$ which are chosen such that $\sqrt{L}$'s are integers; namely, $L = 1$, 4, 16, and 100. $L = 1$ corresponds to the CA, and $L = 100$ is considered to give an example of a case where $L$ is very large. The AE's are assumed to be uniformly placed on a square cell with side length $y$ meters. It is further assumed that the AE's are $\kappa$ meters above the users, so the minimum value of $d_{ij}$ is $\kappa$. Based on these assumptions, the AE locations can be represented by the vector $\mathbf{Z} = \{Z_j\}_{j=1}^{L}$, where $Z_j$ is the triplet entry that denotes the coordinates of AE $j$:

$$Z_j = \left( \frac{2[(j-1) \bmod \sqrt{L}] + 1}{2\sqrt{L}}\, y,\ (1 - \frac{2\lceil j/\sqrt{L} \rceil - 1}{2\sqrt{L}})\, y,\ \kappa \right). \tag{2.8}$$

In the above, $\lceil . \rceil$ denotes the ceiling function. AE locations for the case of $L = 16$ is depicted in

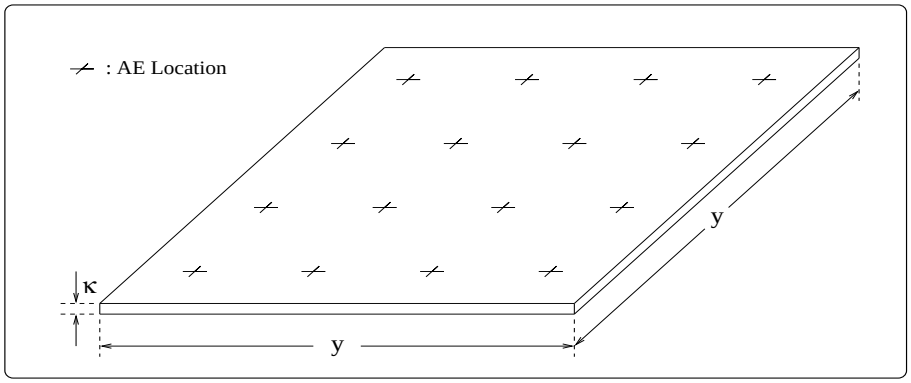


Figure 2.3: AE locations for the case of $L = 16$.

Fig. 2.3. In the simulations $\kappa$ is taken to be $0.02\, y$.

The first two coordinates of the user locations are determined by two independent uniform random variables in the range $[0,\ y]$, and the third coordinate is always kept at zero. Finally, the following values are chosen for the processing gain and the number of users: $N = 128$, $K = 50$.

For a certain set of user locations, the SIR's for all the users are calculated, and this process is repeated 200 times yielding a collection of 10,000 points to plot the CDF's (cumulative distribution functions) accurately.

### 2.3.1 Range of SIR for the Case of PPC

For the case of PPC, the lower and upper limits of the SIR can be calculated. It is worth noting that, in general, $\Gamma_{i_m} \neq \Gamma_{i_n}$, for $\{i_m, i_n\} \in \{1, ..., K\}$ and $i_m \neq i_n$ (see Eqn. 2.3).

A user $i_m$ will have the lowest possible SIR if the signals from this user have equal strengths at each AE; i.e., $P_{i_m j} = 1/L$, $\forall j$ (see Eqn. 2.4), as shown in Fig. 2.4(a). If there is no fading, this will occur when the user is at a point which is equidistant from all the AE's in the cell;[7] i.e., if $G_{i_m j}$ is the same for $\forall j$. From Eqn. 2.3, the SIR at a finger of the Rake receiver of this user is

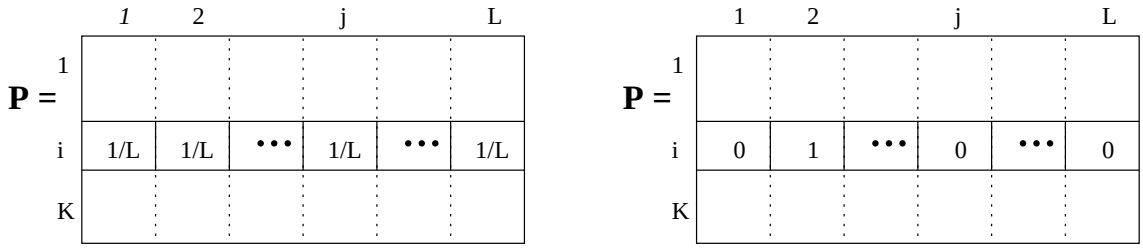


(a) The Worst Case (b) The Best Case

Figure 2.4: The **P** matrices corresponding to (a) $\Gamma_{\mathrm{DA,PBPC,LL}}$ and (b) $\Gamma_{\mathrm{DA,PBPC,UL}}$ cases.

calculated as

$$\Gamma_{i_m j} = N\frac{1/L}{K - 1/L} = \frac{N}{LK-1}, \ \forall j. \tag{2.9}$$

After combining, the lower limit of SIR in a DA system with PBPC, $\Gamma_{\mathrm{DA,PBPC,LL}}$, is found as

$$\Gamma_{\mathrm{DA,PBPC,LL}} = L \times \Gamma_{i_m j} = \frac{NL}{LK-1}. \tag{2.10}$$

On the contrary, a user $i_n$ will have the highest possible SIR, if only one of the entries in the $i_n$th row of **P** is 1, and all the rest are 0; i.e., if

$$P_{i_n j} = \begin{cases} 1 & \text{if } j = j_n, \\ 0 & \text{otherwise,} \end{cases} \tag{2.11}$$

as shown in Fig. 2.4(b). For the case of no fading, this will occur when the user $i_n$ is very close to an AE $j_n$, thus its signal is received practically by only this AE. In this case, there is no need for diversity combining, since $\Gamma_{i_n j} = 0$, for $j \neq j_n$. The upper limit of SIR, $\Gamma_{\mathrm{DA,PBPC,UL}}$, is then the SIR at the $j_n$th finger since there is no contribution from the other fingers of the Rake:

$$\Gamma_{\mathrm{DA,PBPC,UL}} = \frac{N}{K-1}. \tag{2.12}$$

Note that the SIR expressions given in Eqn.s 2.6 and 2.12 are identical. Therefore, if the above described scenario for the upper limit of SIR is true for all the users, i.e., $\Gamma_i = \Gamma_{\mathrm{DA,PBPC,UL}}$, $\forall i$, this means that the DA is behaving like a CA with PPC, which is the ideal case.

[7] This is possible if all the AE's can be placed on a circle which has the user $i_m$ in its center. Based on the AE locations considered in this thesis (see Eqn. 2.3), such a situation would only be possible for the $L=4$ case, along with the trivial $L=1$ case.

For an arbitrary set of user locations, the SIR's will be between the above limits depending on the locations of the AE's and the users in the cell:

$$\left(\frac{N}{K} <\right) \frac{LN}{LK-1} \leq \Gamma_i \leq \frac{N}{K-1}, \quad \forall i. \tag{2.13}$$

Note that in the above, the upper limit corresponds to the case of $L=1$ when there is PPC, while the lower one corresponds to the general case of $L$ AE's with the limiting case of $L \to \infty$ given in parenthesis in Eqn. 2.13. Therefore, in a single-cell system, once PPC is achieved with a certain number of AE's, adding more of them would not improve the performance. In fact, the SIR would deteriorate, but only slightly, since the upper and lower limits are very close to each other.

One may find this result counter-intuitive, because a greater $L$ corresponds to a Rake receiver with a greater number of fingers, which, in turn, corresponds to more diversity branches. However, it should be remembered that in the reverse link of a DA system, since all the received signals accumulate in the feeder, with an increasing number of AE's the MAI also increases. This is a case where the Rake receiver has more fingers with poorer SIR values, which, in the end, yields no further gain (once again, this is true as long as PPC is maintained).

In a multi-cell system, on the other hand, a greater $L$ would yield a lower level of intercell interference, which would correspond to a greater SIR value; however, the returns would diminish gradually. Taking the increasing complexity and processing in the system into account, adding more AE's would not be worth it after a point.

The CDF's of the SIR's for various number of AE's, with and without multipath fading, is plotted in Fig. 2.5. It is observed from this figure that the range of SIR is

$$\frac{N}{K} = 4.08 \text{ dB} \leq \frac{NL}{LK-1} < \Gamma \leq \frac{N}{K-1} = 4.17 \text{ dB}, \tag{2.14}$$

in agreement with Eqn. 2.13.

### 2.3.2 Number of AE's and PPC Dynamic Range

As stated before, PC is essential to mitigate the near-far problem. As the number of AE's increases, the near-far problem becomes less significant. Therefore, higher $L$ values translate into smaller PC DR's.

For the case where there is no fading, the maximum and minimum values of the transmit power $\tilde{P}$, namely, $\tilde{P}_{\max}$ and $\tilde{P}_{\min}$, can be calculated, and then by taking their ratio, the PC DR can be found. The calculations for $L=1$ and $L=4$ cases are given below; those for $L=16$ and $L=100$ cases are more tedious but can be carried out in a similar way.

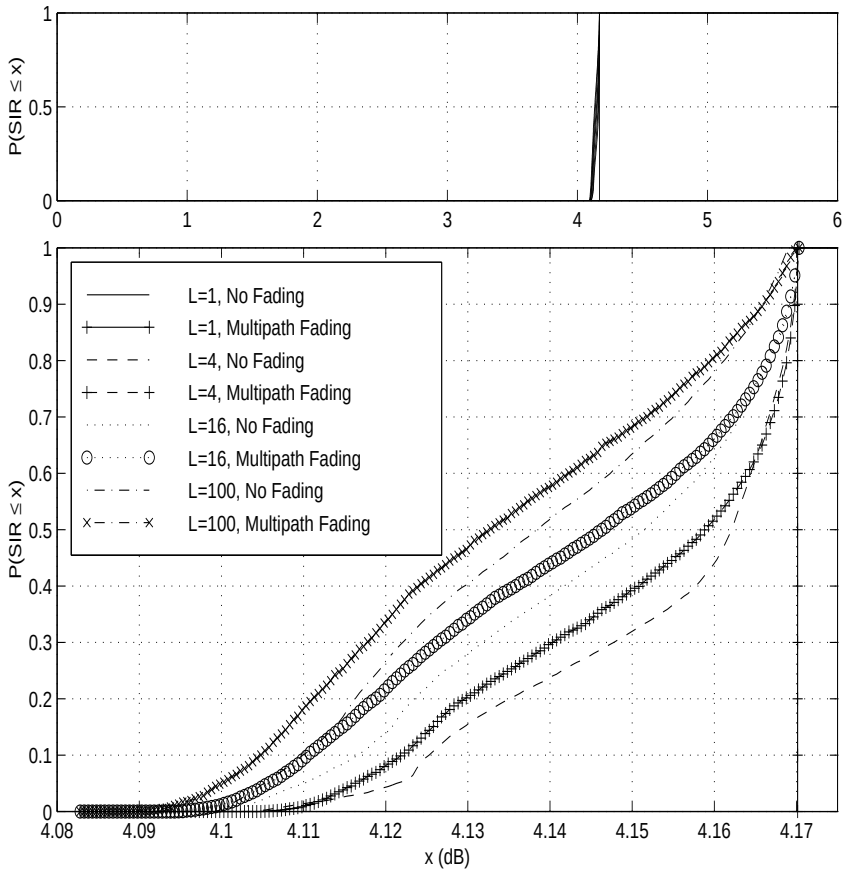


Figure 2.5: SIR statistics for varying numbers of AE's in a single-cell system, for the case of PPC, with and without multipath fading, drawn in regular and enlarged scales.

$\underline{L = 1:}$ First, the following observation is made from Eqn.s 2.5 and 2.7: for the special case of $L=1$, $\tilde{P}_i$ reduces to $\tilde{P}_i = d_{i1}^4$, $\forall i$.

A user $i_m$ will have to transmit at the maximum power level if it is at the farthest location from the single AE, which corresponds to the corners of the cell: $\{(0, y, 0)$, $(y, y, 0)$, $(0, 0, 0)$, $(y, 0, 0)\}$. Since $\mathbf{Z} = \{(0.5y, 0.5y, 0.02y)\}$,

$$\tilde{P}_{\max} = d_{i_m 1}^4 = (0.5^2 + 0.5^2 + 0.02^2)^2 y^4 = 0.25y^4. \tag{2.15}$$

On the other hand, a user $i_n$ will have to transmit at the minimum power level if it is at the point (0.5y, 0.5y, 0), which is the closest location to the AE. So,

$$\tilde{P}_{\min} = d_{i_n 1}^4 = (0.02y)^4 = 1.6 \times 10^{-7} y^4. \tag{2.16}$$

Now, the DR can be obtained from Eqn.s 2.15 and 2.16 as

$$\text{Dynamic Range} = \tilde{P}_{\max}/\tilde{P}_{\min} = 62 \text{ dB}. \tag{2.17}$$

| Dynamic Range (dB) | | | | |
|---|---|---|---|---|
| $L$ | 1 | 4 | 16 | 100 |
| No Fading | 58.6 | 49.4 | 36.1 | 20.8 |
| Rayleigh Fading | 99.7 | 66.5 | 53.8 | 35.3 |

Table 2.1: Dynamic range comparison for no fading and Rayleigh fading cases.

$\underline{L = 4}$: Similar to the $L=1$ case, a user $i_m$ will have to transmit at the maximum power level if it is at one of the corners of the cell; say, at the point $(0, y, 0)$. The corresponding link gains are calculated from Eqn. 2.7 as $G_{i_m} = \{63.59, 2.56, 2.56, 0.79\} \times y^{-4}$, where $G_{i_m}$ is the $i_m$th row of the link gain matrix, $\mathbf{G}$. Then, $\tilde{P}_{\max}$ is obtained as

$$\tilde{P}_{\max} = 1.44 \times 10^{-2} y^4. \tag{2.18}$$

A user $i_n$ will have to transmit at the minimum power level when it is at the closest location to an AE, which corresponds to one of the following points: $\{(0.25y, 0.75y, 0), (0.75y, 0.75y, 0), (0.25y, 0.25y, 0), (0.75y, 0.25y, 0)\}$; for instance, the point $(0.25y, 0.75y, 0)$. Then, $G_{i_n} = \{6.25 \times 10^6, 15.95, 15.95, 3.99\} \times y^{-4}$, and

$$\tilde{P}_{\min} = 1.60 \times 10^{-7}. \tag{2.19}$$

Finally, from Eqn.s 2.18 and 2.19, the DR is calculated as

$$\text{Dynamic Range} = \tilde{P}_{\max}/\tilde{P}_{\min} = 49.5 \text{ dB}. \tag{2.20}$$

For comparison, the DR's obtained from the simulations are also given in the following table:

The CDF's of the DR's are plotted in Fig. 2.6, for the cases where there is no fading and where there is multipath fading. It is obvious from this figure and from Table 2.1 that as $L$ increases, the DR decreases. Also, note that for the case where there is multipath fading, the reduction in the DR is most significant (more than 33 dB) when $L$ is increased from 1 to 4.

It is further observed from Fig. 2.6 and Table 2.1 that the DR is considerably higher for the cases where there is multipath fading; this is even more significant for smaller $L$ values.

In the limiting case, a 2-dimensional leaky feeder can be imagined; this would correspond to the case where $L \to \infty$. In such a case, there would not be any near-far problem, and thus, there would not be any need for PC:

$$\begin{aligned} L = 1 \quad &\Rightarrow \quad \text{Dynamic Range: Very high (may} \to \infty) \\ L \to \infty \quad &\Rightarrow \quad \text{Dynamic Range} = 0 \text{ dB}. \end{aligned} \tag{2.21}$$

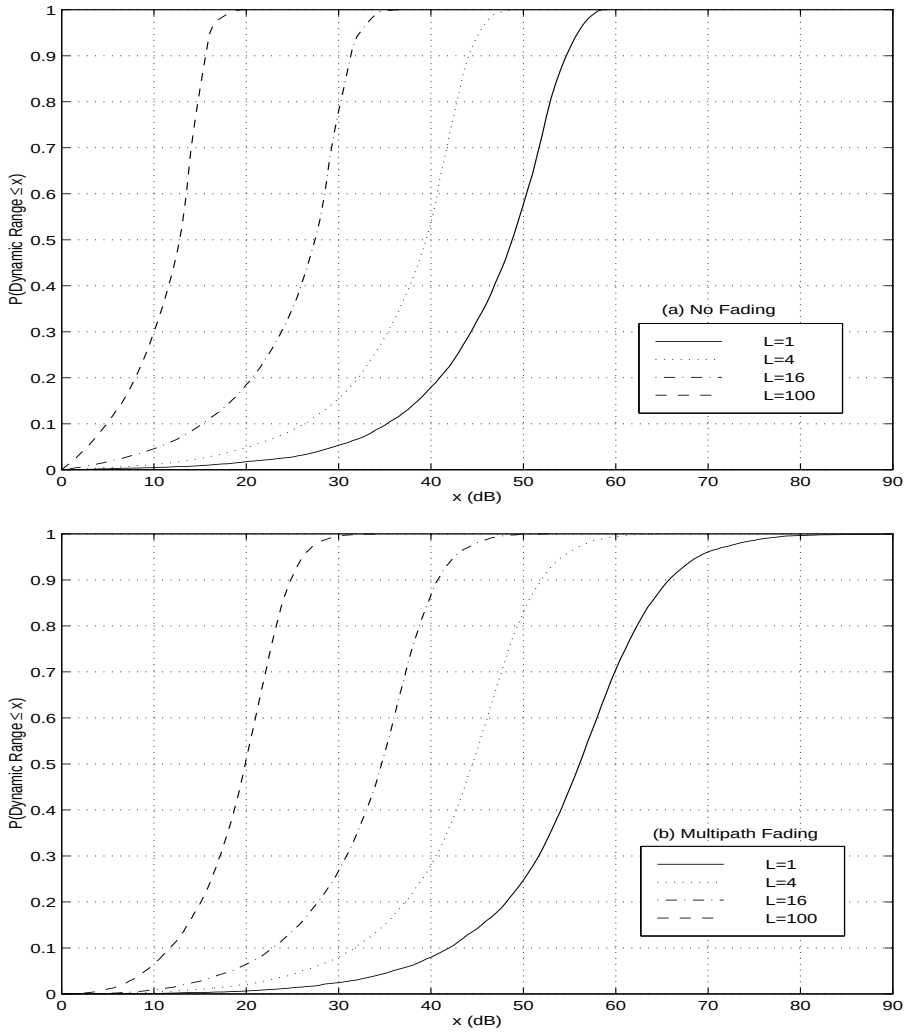


Figure 2.6: PPC dynamic range statistics in a single-cell system for varying numbers of AE's: (a) no fading, and (b) multipath fading cases.

Eqn. 2.21 implies that in the limiting case of $L \to \infty$, a coverage rule other than $d^{-\alpha}$ type, where $\alpha$ is the distance-power-law coefficient, is attained:

$$\begin{aligned} L = 1 \quad &\Rightarrow \quad d^{-\alpha} \\ L \to \infty \quad &\Rightarrow \quad \begin{cases} d^0, & \text{inside the DA cell} \\ 0, & \text{outside the DA cell.} \end{cases} \end{aligned} \tag{2.22}$$

This would yield perfectly uniform coverage with no intercell interference.

However, it is worth noting that as $L$ increases, so does the complexity and processing in the system; the case where $L \to \infty$ would require a Rake receiver with an infinite number of fingers!

A final note is that the SIR's corresponding to the cases addressed in this section will be similar to those plotted in Fig. 2.5, where, due to PPC, the maximum and minimum values are

between the limits given in Eqn. 2.13.

### 2.3.3 SIR Statistics for the Case of no PC

Since the need for PC becomes less significant as $L$ increases, it is worth investigating the statistics of SIR for the case where there is no PC at all. Fig. 2.7 shows the corresponding CDF's for varying

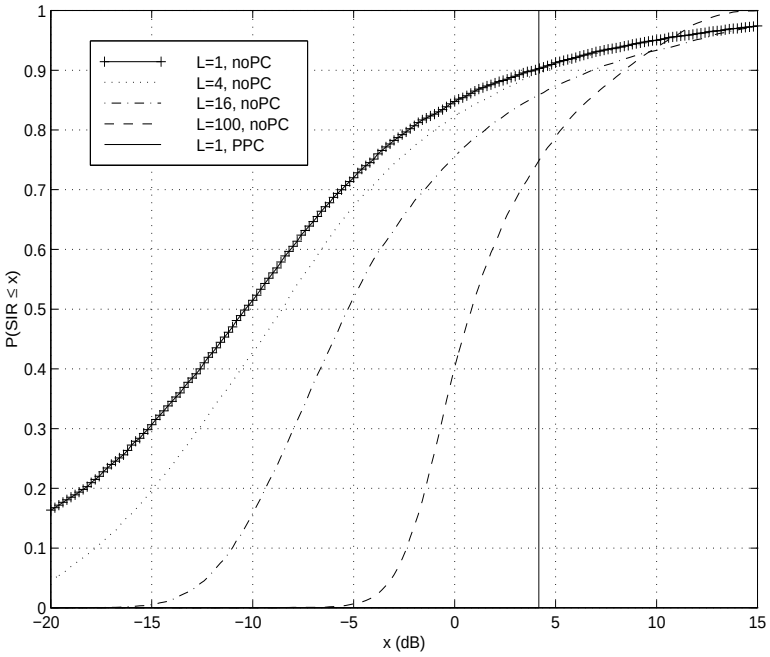


Figure 2.7: SIR statistics in a single-cell system, for varying numbers of AE's, when there is no PC, also for the CA when there is PPC — all for the case when there is no fading, with $K=50$ and $N=128$.

numbers of AE's, when there is no fading. For comparison purposes, the CDF of SIR for the case of $L=1$ with PPC, i.e., the ideal case, is also shown in the same figure.

It is observed from Fig. 2.7 that as $L$ increases, the SIR statistics approach that of the CA with PPC; however, even for very large $L$ values (such as 100), PC is still essential, but the corresponding DR would be much smaller as discussed in the previous section.

Note that when there is multipath fading, the discrepancy between the cases where there is no PC, and the CA case with PPC, would be even greater.

### 2.3.4 SIR Statistics for the Case of PC with Limited DR

So far, a DR without any limits is considered for the PC, which is referred to as the PPC. In this section, the SIR statistics for the case of a limited PC DR, in the presence of multipath fading, is investigated.

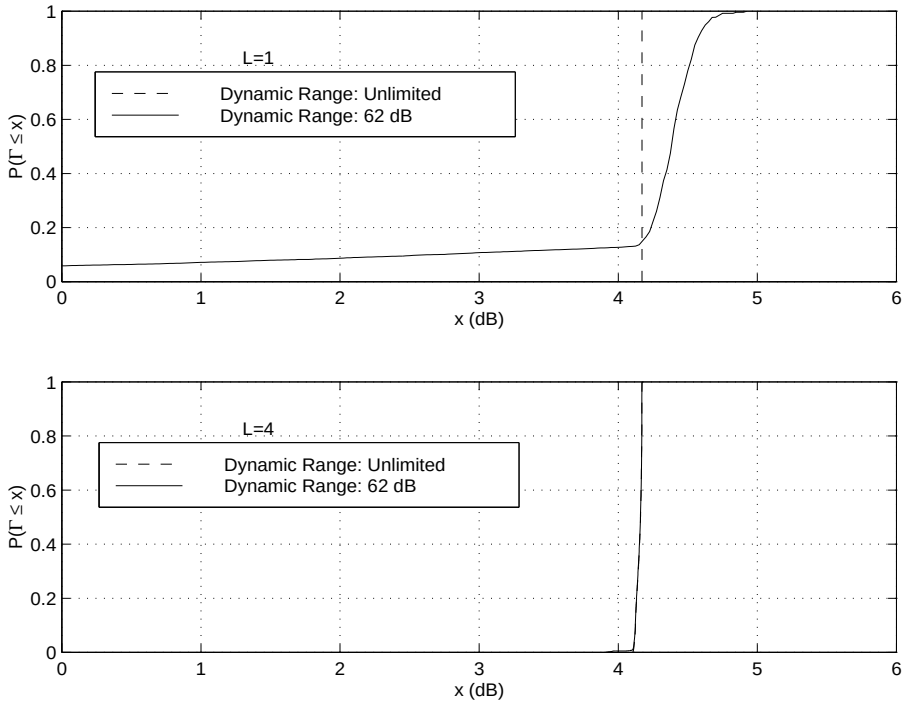


Figure 2.8: SIR statistics in a single-cell system for the case where there is multipath fading with limited and unlimited DR ($K=50$ and $N=128$).

In order to set a realistic range for the DR, it is assumed that if there were no multipath fading, PPC should have been maintained by one AE (i.e., the CA), therefore, the DR is set to 62 dB, the value given in Eqn. 2.17. If the required power level for any user $i$, $\tilde{P}_{i,\text{required}}$, is greater than the value given in Eqn. 2.15, or less than the one given in Eqn. 2.16, $\tilde{P}_i$ is hard limited to these values, respectively; that is,

$$\tilde{P}_i = \begin{cases} 1.6 \times 10^{-7} & \text{if } \tilde{P}_{i,\text{required}} < 1.6 \times 10^{-7} \\ \tilde{P}_{i,\text{required}} & \text{if } 1.6 \times 10^{-7} \leq \tilde{P}_{i,\text{required}} \leq 0.25 \\ 0.25 & \text{if } 0.25 < \tilde{P}_{i,\text{required}} \end{cases} , \forall i. \tag{2.23}$$

The effect of this hard-limiting is shown in Fig. 2.8, for the cases of $L = 1$ and $L = 4$. It is observed from these figures that limiting the DR has a detrimental effect for the $L = 1$ case; around 13% of the users have SIR values less than 4.08 dB given in Eqn. 2.14, which is assumed to be the minimum acceptable level. However, the effect is almost insignificant for the $L=4$ case, since the outage is only 0.7%. In other words, using a DA with $L=4$, instead of a CA type, the outage is reduced from 13% to 0.7%. For the limited DR case, the statistics of SIR is plotted in Fig. 2.9, for $L=1$ and $L=4$.

The conclusion is that if the DR is limited, then, for the parameters chosen in this study, a

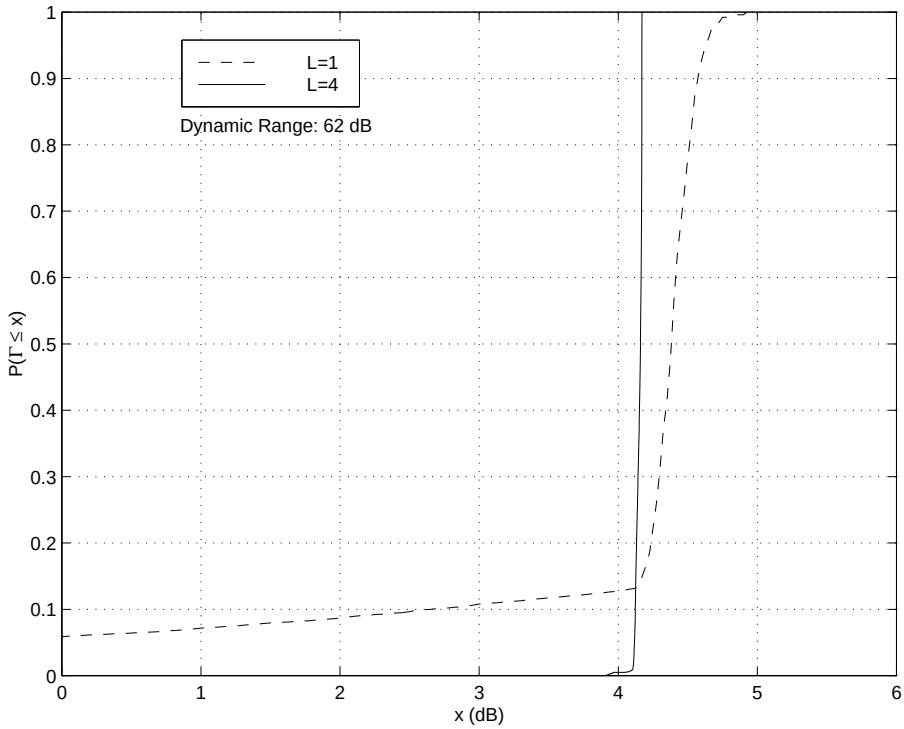


Figure 2.9: SIR statistics in a single-cell system for the case where there is multipath fading and the DR is limited to 62 dB, $L = 1, 4$, ($K = 50$ and $N = 128$).

CA system does not perform satisfactorily; however, the performance can be improved almost to that of an ideal CA by using a DA with $L = 4$.

## 2.4 Chapter Summary and Remarks

In environments where the radio coverage is difficult, achieving PPC may not be possible by using a CA, because this would require an impractically large DR. This situation may yield a significant decrease in the capacity of the system. In such situations, the DA system is an ideal solution, since as the number of AE's in a DA system increases, the DR of the PC decreases. It is demonstrated that by using a DA system with as small as 4 AE's, instead of the CA type, the outage can be reduced from 13% to 0.7%. It should be noted, however, that PC is essential even for DA systems with very large numbers of AE's.

However, in a single-cell system (where intercell interference is not an issue), once the DR of PC is between practical limits, adding more AE's to a DA does not improve the SIR. Yet, as $L$ increases, so does the complexity and processing in the system. Therefore, the optimal strategy for a single-cell system can be stated as to put as many AE's as necessary to achieve PPC, but not to exceed this number.

It is worth noting that in a single-cell system, even if all the energy in the air were to be collected by a DA with infinitely many AE's, the performance would not surpass that of an optimal CA, which would most likely be a hypothetical one however, where signal fluctuations can be compensated for, in all fading conditions by a perfect PC scheme. So, the only extra benefit would be the reduction in PC DR, at the expense of increased complexity. In fact, if such a system were possible, then, from solely an SIR point of view, there would be no need to introduce a DA system.[8]

In a multi-cell system, on the other hand, the DA system has the additional advantage of reducing the intercell interference (compared to the CA type) with increasing number of AE's, which would yield even higher SIR values. Therefore, the higher the $L$ is the better the system performs; however, even in this case, the returns would diminish gradually. Moreover, the increasing complexity and processing in the system further imposes a limit on the number of AE's.

## 2.5 Future Research Directions

In the simulations, a Rayleigh fading channel model, which corresponds to the worst case, is considered. However, in a DA system with many AE's, there will, most likely, be line-of-sight between a wireless user and one or more AE's. Furthermore, in such cases, the distance-power-law coefficient, $\alpha$, may be around 2 rather than 4. In that case, the PC DR will further decrease by using a DA structure.

On the other hand, in the analysis in this chapter, the loss (attenuation) in the cable is omitted;[9] if the cable loss were incurred, the reduction in PC DR would have been more modest.

It would be interesting to perform a more realistic PC DR analysis by including the above mentioned two points. In such an analysis, (a) a Rician channel, with $d^{-2}$ type signal attenuation in the air, should be assumed between a user and the few closest AE's – the channel between the rest of the AE's should still be of Rayleigh type with $d^{-4}$ type attenuation; (b) the cable loss should be incurred.

It is possible that these two effects may balance each other, and therefore, the figures that we give in this chapter may, indeed, be not too far away from the real ones.

[8] It should be emphasized, however, that even in such a case DA has still other benefits, as discussed in Sec. 1.3.3. For instance, both the average and peak transmit power levels are considerably less in a DA system compared to that which employs a CA. This translates into compactness and/or extended battery life for wireless terminals, which might be quite an important factor.

[9] We will briefly discuss the cable loss in Sec. 6.1.2 from the implementation point of view.

# Chapter 3

## CDMA Sectorized Distributed Antenna System

Although the simple structure of the DA system is quite attractive, it possesses an inherent limitation: since all the AE's are coupled to a common feeder and there is no signal-specific processing at the AE's, the MAI is accumulated in the feeder. This imposes a direct limit on the capacity since CDMA systems are interference limited.

In summary, in a DA system, the "SIR", or equivalently, the "capacity", versus "number of AE's ($L$)" curve would plateau with increasing values of $L$ due to MAI, as depicted in Fig. 3.1. It is worth noting that although the capacity of a DA system may be considerably higher than

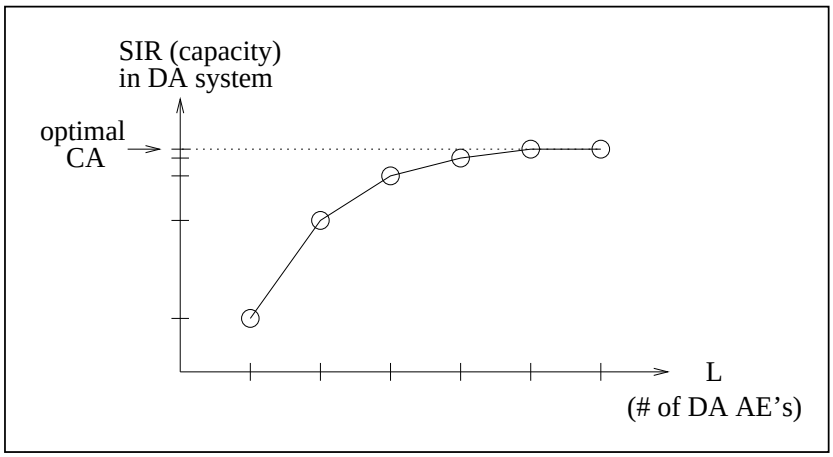


Figure 3.1: Saturation of the capacity increase (with respect to the number of AE's) in a CDMA distributed antenna system.

that which employs a CA (due to diversity, maintenance of perfect PC, minimization of intercell interference, and so on), the resultant increments in the capacity are nevertheless due to indirect effects. Therefore, the capacity is still low per AE, especially for high $L$ values. Indeed, this is the main limitation of a DA system.

## 3.1 The Concept of Sectorizing in a Distributed Antenna Structure

The accumulation of MAI is a consequence of the simple architecture of the DA system. It would

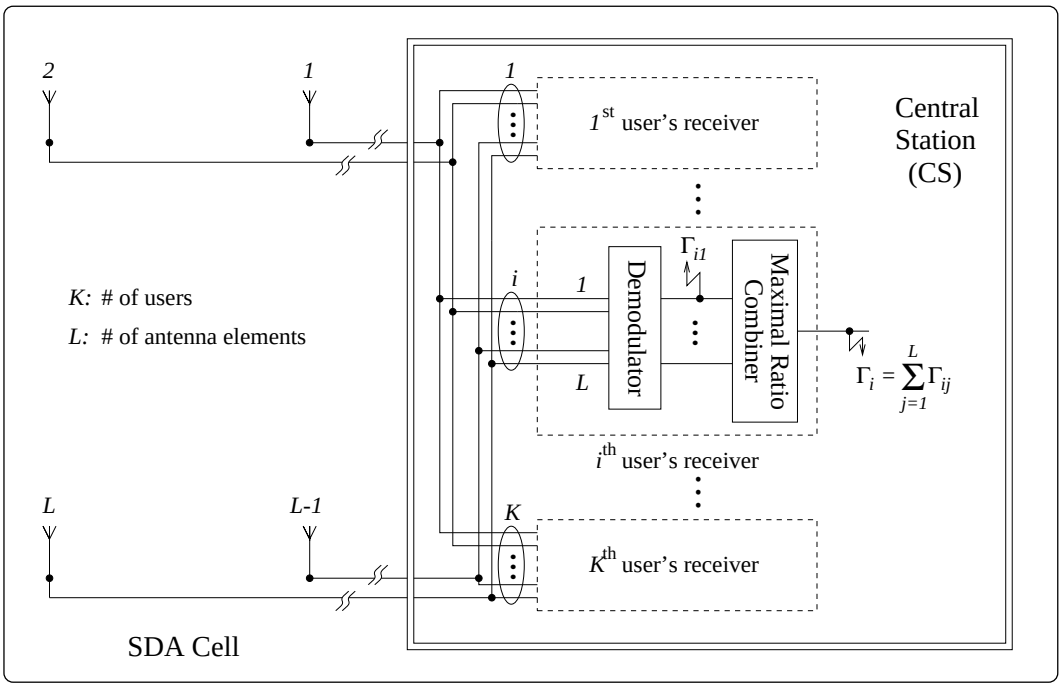


Figure 3.2: CDMA sectorized distributed antenna system.

be most desirable if an architectural change yielding substantial reductions in the MAI were possible without significantly complicating the structure of the system.

In fact, such a change can be realized simply by connecting the AE's with separate feeders to the CS as illustrated in Fig. 3.2. In this thesis, the limiting case of one AE per sector is investigated. In such a case, a wireless user's signal can be picked up by all the AE's in a cell, and then, can be optimally combined at the CS to enhance the performance. We call this novel antenna architecture *sectorized distributed antenna, SDA*. In the reverse link of an SDA system, MAI can be reduced by approximately a factor of $L$, and therefore, the SIR can be increased approximately $L$ times[1]. The rest of the discussion regarding SDA will be on the reverse link, and in Sec. 3.4 we will address the possibilities in the forward link.

It is worth noting that an SDA system with $L$ AE's is conceptually different from the conven-

[1]This increase in SIR would be valid when there exists no correlation between the interference received by different AE's. If such a correlation does exist, then the performance can deteriorate significantly. In this chapter, we will assume that the effect of correlated interference is negligible (unless otherwise stated); the concept of correlated interference will be analyzed in detail in Ch. 5.

tional $L$-branch antenna diversity type, since, in the SDA system, the AE's are not collocated, but rather distributed in the service region. The distributing of the AE's makes the most use of the spatial dimension.[2] It is also important to note that the SDA system offers more returns compared to the conventional macrodiversity and soft-handoff schemes addressed in the literature; because, in those schemes, post-detection combining is employed, which is mainly based on selection combining or on application of majority-logic [11]. In the SDA system, on the other hand, by the placement of more AE's, more signal, or energy (which is already in the air), is collected, and by jointly decoding the collected signals at the CS, all of this energy is utilized.

The SDA system is, in essence, still of a DA type, since all the salient characteristics of the DA are preserved, such as the reception of the same signal by all the AE's, and the performance of all the signal-specific processing at the CS. The AE's are also omnidirectional — the term *sectorized* is used for this system because of the conceptual parallelism with sectorization in the conventional cellular systems.

Along with possession of all the appealing features of the DA system, such as diversity and reduction of intercell interference, the SDA system has one additional feature: the capacity limitation in the DA system is eliminated. The increase in capacity will be demonstrated quantitatively in Sections 3.2 and 3.3; nevertheless, for the sake of illustration, we give the following example to compare the SIR's corresponding to DA and SDA systems.

Consider a hypothetical situation where each user's signal is received at approximately the same power level at each AE. If this system is a DA type, then there would be a total of $LK$ signals accumulated in the feeder, from which only one would be utilized at any branch of the combiner. Thus, the SIR for a user $i$ can be calculated by using Eqn. 2.3 as

$$\Gamma_{i,\mathrm{DA}} = \frac{NL}{LK-1}. \tag{3.1}$$

In the case of the SDA system, however, there would only be $K$ signals accumulated in each of the separate feeders. Therefore,

$$\Gamma_{i,\mathrm{SDA}} = \frac{NL}{K-1}. \tag{3.2}$$

Now, the ratio of $\Gamma_{i,\mathrm{SDA}}$ to $\Gamma_{i,\mathrm{DA}}$ can easily be found as

$$\Gamma_{i,\mathrm{SDA}}/\Gamma_{i,\mathrm{DA}} \;=\; \frac{LK-1}{K-1} \;\approx\; L, \tag{3.3}$$

which maps to an approximately $L$-fold increase in capacity.

In an SDA system, certain system parameters, such as the cell geometry, location of AE's and propagation conditions, can be such that a user's signal may efficiently be received by only $L_o \leq L$ AE's. Let us consider a system in which each user's signal is received by only $L_o$ AE's at

[2] It will become apparent in Ch. 5 that, in fact, the more apart the AE's are, the higher the capacity is!

the same power level, and the remaining $L-L_o$ AE's do not receive any signal from that particular user. If we assume that the users and AE's are distributed uniformly throughout the SDA cell, then, there would be a total of $L_oK/L$ signals in each feeder. Therefore,

$$\Gamma_{i,\mathrm{SDA}|_{L_o}} \approx \frac{NL_o}{(L_oK/L)-1} = \frac{NL}{K-(L/L_o)} \approx \frac{NL}{K-1}. \tag{3.4}$$

The last approximation in Eqn. 3.4 holds especially when $K$ is large (which will be the case in loaded systems). From Eqn.s 3.2 and 3.4 we conclude that even for the case of $L_o \leq L$ significant signals, the almost-linear increase in SIR is preserved. In the rest of this thesis, however, we assume that $L_o = L$, unless otherwise stated.

In Ch. 2, a power-balanced PC algorithm is used. It will be demonstrated in Ch. 4 that, although PBPC works very well in DA systems, it yields great variations among the SIR values of different users in the SDA system.

In order to fix this problem, we propose a PC algorithm which keeps the SIR for all users at the same constant level, say $\gamma$, as follows: find $\tilde{P}_i$ subject to

$$\Gamma_i = N\sum_{j=1}^{L} \frac{G_{ij}\tilde{P}_i}{\left(\sum_{k=1}^{K} G_{kj}\tilde{P}_k\right) - G_{ij}\tilde{P}_i} = \gamma, \ \ \forall i. \tag{3.5}$$

We refer to the above PC scheme as SIR-balanced macro power control (SBMPC). The details of the SBMPC algorithm, its iterative solution, and the convergence characteristics of these iterations will be analyzed in Ch. 4.

## 3.2 Lower and Upper Limits of SIR in an SDA System with SBMPC

The lower and upper limits of SIR in a DA system with PBPC, $\Gamma_{\mathrm{DA,PBPC,LL}}$ and $\Gamma_{\mathrm{DA,PBPC,UL}}$, are given by Eqn.s 2.10 and 2.12. Similarly, we will compute the lower and upper limits of SIR in an SDA system with SBMPC, namely, $\Gamma_{\mathrm{SDA,SBMCP,LL}}$ and $\Gamma_{\mathrm{SDA,SBMPC,UL}}$. It should be borne in mind that, in general, $\Gamma_{i_k,\mathrm{DA,PBPC}} \neq \Gamma_{i_l,\mathrm{DA,PBPC}}$ for $i_k \neq i_l$; however, $\Gamma_{i_k,\mathrm{SDA,SBMPC}} = \Gamma_{i_l,\mathrm{SDA,SBMPC}}$ for $\forall i_k, i_l$.

In an SDA system, the users will experience the lowest possible SIR value if, at each AE, the received signals from all the users are at the same power level; that is, $P_{ij} = m_j$, $\forall i, j$. In the above, $m_j$ is a constant. In general, $m_{j_k} \neq m_{j_l}$ for $j_k \neq j_l$, where $j_k, j_l \in \{1, \ldots, L\}$ . In this case, at each branch of the combiner, there would be $K$ signals of equal power (one of them is the signal of interest and the remaining $K-1$ are the interfering signals), and the contribution to

SIR from each branch would be the same. Based on these facts, $\Gamma_{\mathrm{SDA,SBMPC,LL}}$ can be computed as[3]

$$\Gamma_{\mathrm{SDA,SBMPC,LL}} = \frac{NL}{K-1}. \tag{3.7}$$

On the contrary, the users will experience the highest possible SIR, if only one of the entries in each row of $\boldsymbol{P}$ is nonzero, and in each column there are $K/L$ (assuming $K/L$ is an integer) nonzero entries with the same value; i.e., $(P_{ij}=(n_j \vee 0)) \wedge (\sum_{j=1}^{L} P_{ij}=n_j) \wedge (\sum_{i=1}^{K} P_{ij}=n_j K/L)$, where $n_j$ is a constant, and $\wedge$ and $\vee$ denote the logical "and" and "or" operation, respectively. In general, $n_{j_k} \neq n_{j_l}$ for $j_k \neq j_l$, where $j_k, j_l \in \{1,\ldots,L\}$. In this case, there is no need for diversity combining, and[4]

$$\Gamma_{\mathrm{SDA,SBMPC,UL}} = \frac{N}{K/L-1} = \frac{NL}{K-L}. \tag{3.8}$$

The above expression is valid for the cases where $L < K$. If, however, $L \geq K$, then $\Gamma_{\mathrm{SDA,SBMPC,UL}}$ may approach infinity according to our modelling. We note that in practical cases, almost always $L < K$. Even in the exceptional cases where $L \geq K$, SIR will never approach $\infty$, because of the background noise that we are omitting.

Now, using Eqn.s 2.10, 2.12, 3.7, and 3.8, we obtain

$$\frac{\Gamma_{\mathrm{SDA,SBMPC,LL}}}{\Gamma_{\mathrm{DA,PBPC,LL}}} = \frac{LK-1}{K-1} \approx L, \tag{3.9}$$

$$\frac{\Gamma_{\mathrm{SDA,SBMPC,UL}}}{\Gamma_{\mathrm{DA,PBPC,UL}}} = L\frac{K-1}{K-L} \approx L. \tag{3.10}$$

The results shown in Eqn.s 3.9 and 3.10 translate into an approximately $L$-fold increase in capacity.

Finally, we calculate the ratio of $\Gamma_{\mathrm{SDA,SBMPC,UL}}$ to $\Gamma_{\mathrm{SDA,SBMPC,LL}}$, using Eqn.s 3.7 and 3.8, as

$$\frac{\Gamma_{\mathrm{SDA,SBMPC,UL}}}{\Gamma_{\mathrm{SDA,SBMPC,LL}}} = \frac{K-1}{K-L}. \tag{3.11}$$

[3] The situation described by the received power matrix

$$P_{ij} = m_j, \ \forall i,j \tag{3.6}$$

can correspond to the case where all the users are at the same location (or, at some symmetric locations such that Eqn. 3.6 holds) in the service region. If this is the case, then there is, indeed, a catastrophic situation, since this will yield identical interference components at the combiner branches, and such a system will be similar to the one which has only a single AE. Therefore, $\Gamma_{\mathrm{SDA,SBMPC,LL}}$ will be equal to $N/(K-1)$, rather than the expression given in Eqn. 3.7. Obviously, the possibility of occurrence of such an event is very low. It is worth noting that the case where all the AE's are installed at the same location also yields a similar catastrophic outcome. Finally, it is interesting to note that Eqn. 3.6 may still hold even if the users are not at the same location, due to the propagation conditions and power control (however, this is, perhaps, even a less likely scenario). Such a case would not be a catastrophic type, and if the effects of correlated interference is not significant, Eqn. 3.7 will be valid.

[4] Once again, we do not take the effect of correlated interference into account.

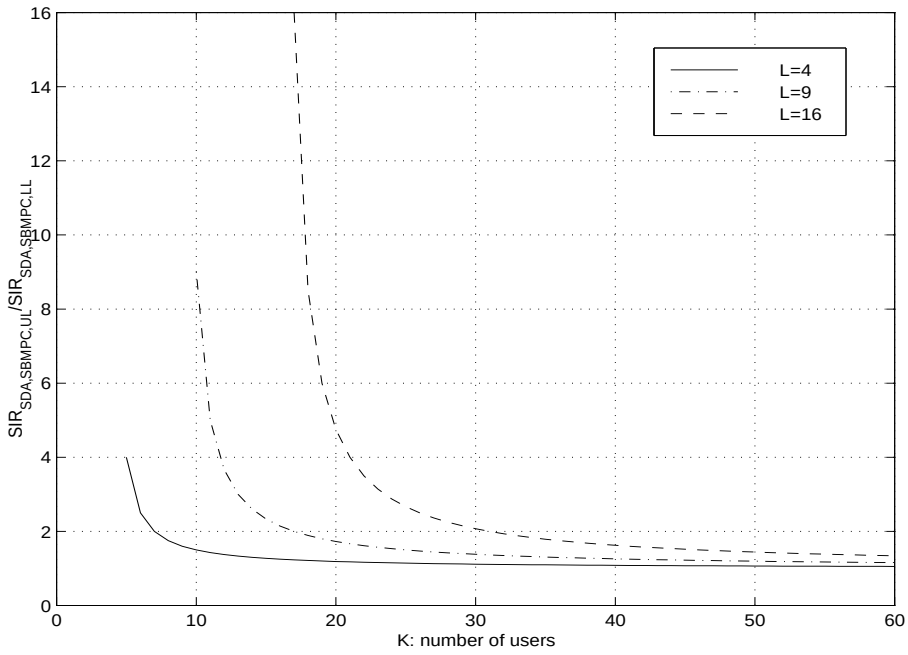


Figure 3.3: Comparison of the ratio of the upper and lower limits of SIR, for various values of $L$, in an SDA system with SBMPC.

The above expression is plotted in Fig. 3.3 as a function of $K$ for various values of $L$, with $K > L$. It is observed that for loaded systems (where $K/L \gg 1$), the ratio given in Eqn. 3.11 is close to unity; however, it may assume much greater values for unloaded systems (where $K$ is in the order of $L$). The reason for this is that when $K$ is in the order of $L$, the relative positions of the users and the AE's have a greater impact on the SIR expression. Because, in an unloaded system, it is possible to have a user distribution such that each user (or group of few users) is close to a different AE. For the cases where $K/L \gg 1$, on the other hand, there would almost always be many users around each AE.

## 3.3 Simulation Results

For simulations, a single SDA cell with $L$ AE's and $K$ users is considered. The same assumptions on the user distribution and AE locations (see Eqn. 2.8 and Fig. 2.3) are made. In this chapter, $L=4$ and $L=16$ cases are considered with $\kappa=0.02\,y$ and $N=128$.

The intercell interference and the possible effects of correlated interference are omitted in our analysis. It is also assumed that the multipath fading is averaged out; in this case, the performance of the system will only depend on the local average received power. Based on these assumptions, the link gains are modeled as $G_{ij} = A_{ij}/d_{ij}^{\alpha}$, where $A_{ij}$ is a random quantity that

models the power variation due to shadowing. $A_{ij}$'s are assumed to be independent, identically distributed log-normal random variables with 0 dB expectation and 8 dB standard deviation. Also, $\alpha = 4$ is used in the simulations.

In the simulations, for a certain set of random user locations, first, the $\boldsymbol{G}$ matrix is formed, and then the balanced SIR value is calculated through the iterative solution of the SBMPC algorithm. This process is repeated for 10,000 different user location sets in order to collect enough data to plot the CDF's accurately.

The SIR CDF's for various SDA systems with varying $K$ and $L$ values are shown in Fig. 3.4(a), (b), and (c). In these figures, the number of users is kept fixed ($K = 20$, 80, and 400, respectively),

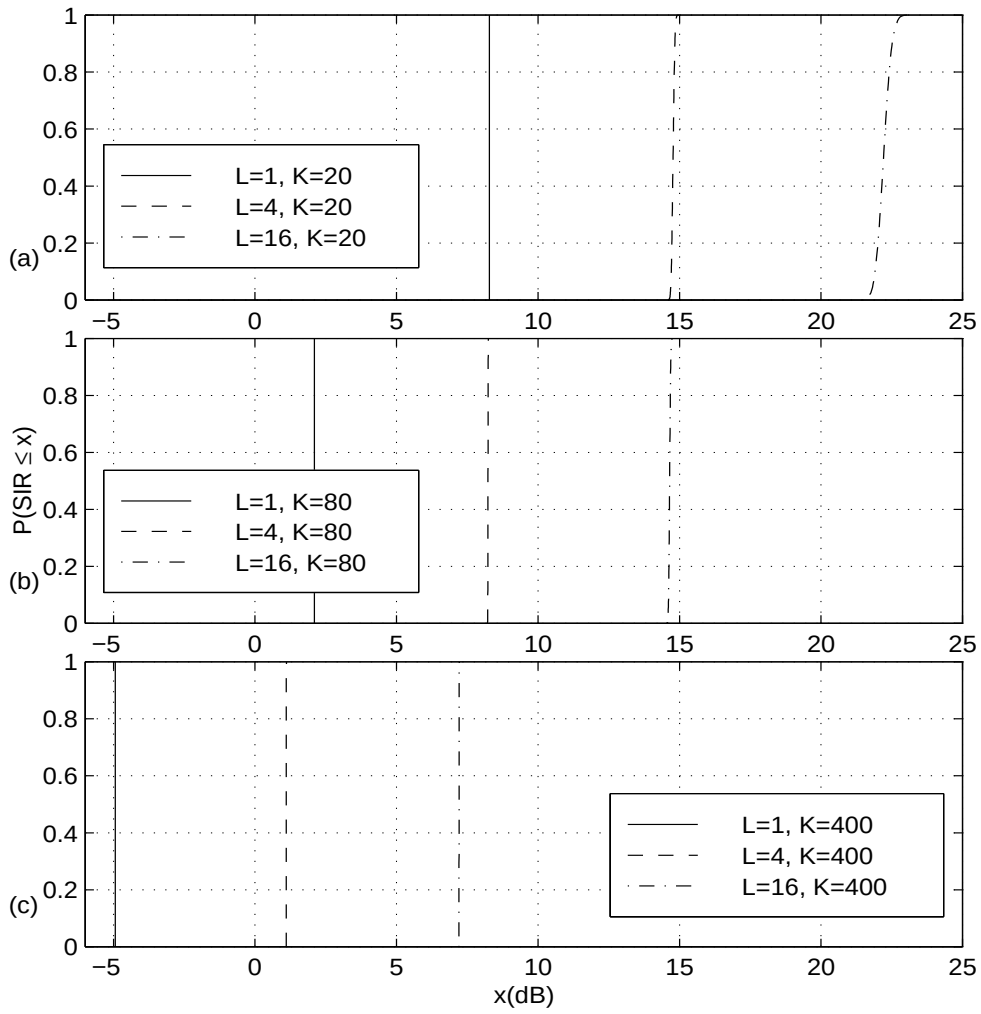


Figure 3.4: Comparison of SIR CDF's for SDA systems (employing SBMPC) for (a) $K = 20$, $L = 4$, and 16, (b) $K = 80$, $L = 4$, and 16, (c) $K = 400$, $L = 4$, and 16.

but the number of AE's is increased from 1 to 4 to 16. It is observed that when $L$ increases from 1 to 4, there is a gain of 6.5, 6.1 and 6.0 dB in the median values of the SIR's corresponding to

$K = 20$, 80, and 400 cases, respectively; when $L$ increases from 4 to 16, the corresponding gains are 7.4, 6.4, and 6.1 dB, respectively. This variation in gain is a result of the difference between

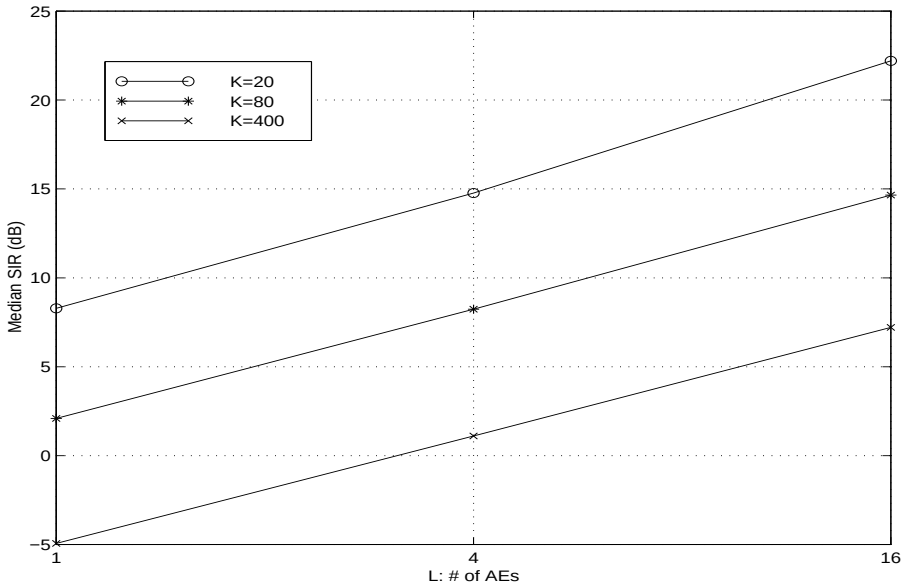


Figure 3.5: Median SIR value (dB) with respect to $L$.

the loaded and unloaded systems discussed in the last paragraph of the previous section. In Fig. 3.5, the median SIR values corresponding to the curves given in Fig. 3.4 are plotted against $L$, for various values of $K$ — the approximately linear increase in SIR is obvious.

In Fig. 3.6, the number of AE's is kept fixed ($L = 4$), and the number of users is varied from 5 to 400. As expected, SIR improves as $K$ decreases. When $K$ is decreased from 20 to 5, the increase in the median value of SIR is 8.22 dB, while when it is decreased from 400 to 100 (still, $\times 4$), this increase is only 6.12 dB. Once again, this variation is due to the difference between the loaded and unloaded systems.

Finally, we consider an SDA system with $L = L_o$ and $K = K_o$. We are interested in determining whether the system can support $fK_o$ users, if $fL_o$ AE's are installed in the same coverage region, where $f$ is a positive integer. If it can, then the $L = L_o$, $K = K_o$, and $L = fL_o$, $K = fK_o$ cases should have identical, or very similar, CDF's. Two types of systems are investigated in the simulations: an unloaded system of $L_o = 1$, $K_o = 5$ with $f = 4$, and 16, and a loaded system of $L_o = 1$, $K_o = 25$, again with $f = 4$, and 16. The corresponding CDF's are shown in Fig. 3.7. It is observed that although the CDF's for various $f$ values are not identical, they are very similar (note that the range of $x$-axis, in Fig. 3.7, is very small). It is also observed that when $f$ becomes larger, there is a slight deterioration in the system performance. This is due to the fact that in such systems the possibility of occurrence of cases which would yield $\Gamma_{\mathrm{SDA,SBMPC,UL}}$ (refer to

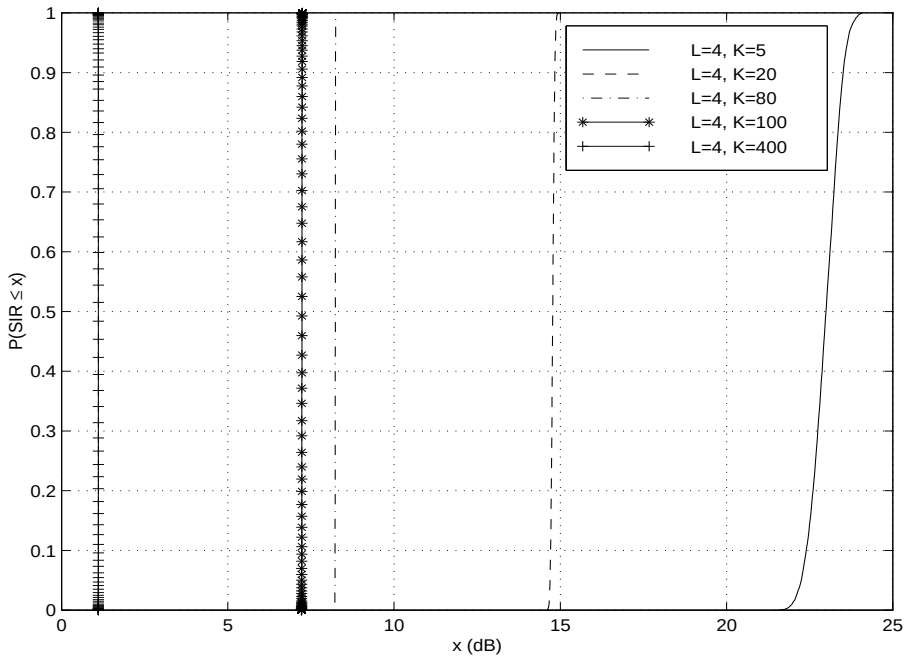


Figure 3.6: Comparison of SIR CDF's for SDA systems (employing SBMPC) which have $L = 4$ AE's, with $K = 5$, 20, 80, 100, and 400.

Eqn. 3.8) becomes statistically less likely, as addressed before. It is observed from Fig. 3.7 that the corresponding deterioration is even less significant in the loaded systems.

The overall conclusion from Fig.s 3.4-3.7 is that the SDA system is scalable. In other words, the SIR increases approximately at the same rate with the increasing number of AE's.

## 3.4 Features of the SDA System

One very important characteristic of the SDA system is the many-to-many relationship established between the users and AE's, which yields an enhanced macrodiversity capability. This feature will become even more important with the increasing interest in wireless systems operating at higher frequency bands where the line of sight (LOS) communications may be essential. Since a user will almost always be in the close vicinity of an AE in an SDA system, maintaining LOS would not be difficult. Therefore, SDA may be a very suitable antenna architecture for systems operating at, for example, 10 GHz and higher frequencies.

It is reported in the literature that by using antenna arrays, a reverse link capacity increase in the order of the number of AE's in the array is achievable [17]. However, as it has already been discussed in Sec. 1.3.3(d), the antenna arrays do not have macrodiversity capability. Hence, when a blockage occurs in the radio link, an antenna array cannot provide an efficient solution! Thus,

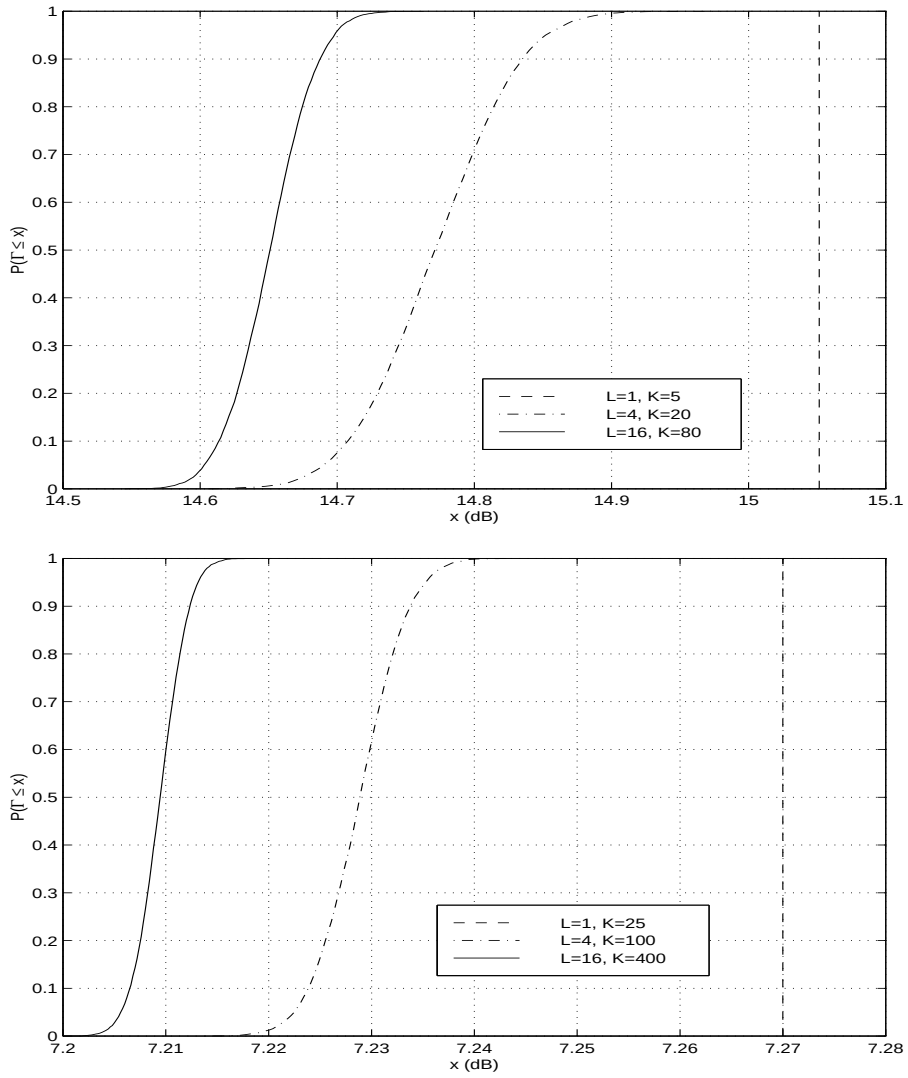


Figure 3.7: Demonstration of the scalable nature of the SDA systems: (a) unloaded system, (b) loaded system.

an antenna array cannot offer the immunity against shadowing effects that an SDA architecture can.

In microcellular systems, intercell interference is a nuisance that must be managed; therefore, in cellular design, the propagation characteristics should be taken into account in order to find appropriate base station locations that would minimize the overlapping of the antenna radiation patterns, and thus the intercell interference. However, intercell interference cannot be entirely eliminated, and this inevitably introduces degradation in system performance. In an SDA system, on the other hand, overlapping of the AE radiation patterns is not a problem; in fact, this may yield an even better result due to diversity reception.

One other important point to note is that in the capacity calculations of microcellular systems,

the assumption of homogeneous user distribution throughout the service area is generally made. In practise, however, this is usually not the case. As an example, let us consider a microcellular system with 4 cells. If the capacity per cell is $K$ users, then the system capacity is said to be $4K$. However, if these $4K$ users are in fact distributed as, say, $2K/3$, $2K/3$, $2K/3$, and $2K$ users, among the 4 cells in the system, then the system would be able to support only $3K$ users, not $4K$! The inhomogeneous user distribution is, in general, not a significant problem in an SDA system.

The idea of sectorization in the context of DA was first introduced in [40] in a qualitative manner. In that conceptual study, a few AE's are placed in each DA sector, and mobile-transparent handoff is performed among the sectors. The SDA architecture presented here corresponds to the limiting case of one AE per sector. However, there is still a major difference between the system discussed in [40] and the SDA architecture presented here, and that is the enhanced macrodiversity feature of the SDA system in the reverse link. Because of this feature of the SDA system, the signals received by all the AE's (sectors) are collectively decoded at the CS.

The discussions presented so far have been on the reverse link of SDA systems. As mentioned in Section 3.1, in the reverse link of an SDA system, although a user's signal is picked up by all the AE's, having separate feeders for each AE prevents the accumulation of MAI. This is not the case, however, for the forward link. If, in the forward link, a user's signal is transmitted by all the AE's, then the system will operate as a conventional DA type. Clearly, this would result in quite a large difference in the forward and reverse link capacities. As a remedy for this situation we propose the following solution: in the forward link, the signal for a particular user could be transmitted through the AE which has the highest SIR in the reverse link for that particular user.[5] Therefore, there would be selection diversity in the forward link, and thus, the benefits of the macro diversity would still be valid. In this SDA system, the reverse link would still outperform the forward one. Yet, it should be noted that higher capacity in the reverse link is never a "problem"; in order to equalize the capacities in both links, more resources (such as bandwidth), from the given pool, can be allocated for the forward link.

The CDMA SDA system may have quite diverse applications with a wide range of cell sizes and number of AE's. For example, an SDA cell may be as small as a microcell (or even a picocell) with only a few AE's (even 2), or it may cover many square kilometers with many AE's. The SDA structure may be utilized both indoors and outdoors, including linear service areas, such as highways.

One other issue is related to the cost of the SDA system: since the SDA architecture has a

[5] Alternatively, a few AE's can be utilized; in this case, the system will work similar to that described in [40] in the forward link.

logical star topology (that is, each AE requires a separate link to the CS), in an SDA system with a large number of AE's, the deployment cost of the wired-network infrastructure may be of concern. Robust, flexible, and cost efficient AE interconnection strategies will be discussed in Ch. 7.

In [1], the ultimate reverse link capacity of a CDMA network is investigated. Although the terminology and modeling in [1] is different from those used here (our work was done independently from that in [1]), the two systems are conceptually similar. Yet, the entirely different motivation, approach, and emphasis in this thesis make it a different study than that of [1]. In Sec.s 4.6 and 5.10, we will make comparisons between the results of this chapter & the next one and those in [1].

## 3.5 Chapter Summary and Remarks

Despite possessing many appealing features, CDMA DA systems suffer from low capacity per AE as a result of the MAI accumulated in the common feeder. To overcome this capacity limitation, we propose an antenna architecture called CDMA sectorized distributed antenna (SDA). In an SDA system, a cell has many sectors in which separate feeders run, so MAI in the reverse link is reduced accordingly. In this chapter, the limiting case of one AE per sector is investigated. In such a case, a wireless user's signal can be picked up by all the AE's in an SDA cell, and then, can be jointly decoded at a central station.

We have demonstrated analytically and through simulations that in a CDMA SDA system with $L$ AE's, the reverse link SIR increases approximately $L$ times. This increase in SIR can be mapped into an equivalent increase in the capacity. If there is not enough demand for all of the potential capacity offered by an SDA system, the increase in SIR can always be partly transformed into higher transmission rates for the existing users.

The conventional diversity techniques (such as antenna, time, and frequency diversity) are mainly used to mitigate fast (multipath) fading. This is achieved by smoothing out the fast fading through the combination of many independently fading channel outputs. As a result, as the order of diversity increases, the combiner output looks increasingly similar to that of a non-fading communication channel. The major diversity gain is achieved when the order of diversity is increased from 1 (no diversity) to 2, and the returns diminish as the order of diversity further increases. We have shown in the previous chapter that the CDMA DA system mitigates also shadow fading, and by the increasing number of AE's, the performance of a CDMA DA system approaches that of a hypothetical optimal CA which is not affected by multipath and shadow fading.

In the SDA scheme, on the other hand, there is also a gain over the MAI, unlike the conventional diversity schemes — the total interference experienced at the CS is reduced approximately by the number of AE's. Therefore, an $L$-element SDA scheme should be compared with a set of $L$ CA's serving the same region, not with an $L$-branch diversity. This gain of the SDA system over the conventional diversity schemes is achieved through the exploitation of the space dimension (i.e., through the distributed nature of the AE's).

An SDA system with $L$ AE's still has two main advantages over a cellular cluster with $L$ CA's, as a result of the joint decoding (enhanced macrodiversity) capability of the SDA system, combined with the SBMPC algorithm: the increase in capacity in an SDA system is still valid (unlike in a cellular type), even if (a) the antenna patterns of the AE's overlap, and (b) the users are not distributed homogeneously throughout the service area (non-uniform traffic). Therefore, sectorization in the context of DA is more efficient than cell-splitting in the conventional cellular systems.

There still remains a fundamental question: in a given service area that is to be covered by an SDA cell, can we put as many AE's as we wish without an upper limit? In an SDA system, putting more AE's would always yield better performance (this is analogous to a dish antenna: the greater the diameter, the better the performance). However, the returns in SIR may diminish gradually as $L$ increases, since signals received by different AE's would start being correlated. This is an immediate consequence of the fact that when $L$ increases, the AE's become closer together. Taking the increasing complexity and processing in the system into account, adding more AE's may not be worthwhile after a point, which may put an upper limit on the number of AE's (sectors). The concept of correlated interference will be discussed in Ch. 5.

# Chapter 4

## SIR-Balanced Macro Power Control for the Reverse Link of CDMA Sectorized Distributed Antenna Systems

Power control is a scheme by which the transmit power levels of the users in a system are controlled and adjusted according to some criteria. The main purpose in employing PC is to keep the SIR level (at the receiver) for all the users above a certain threshold. By employing PC, the possible extensive disparities in users' signals (due to distance, multipath and shadow fading) are compensated for, and at the same time, the injection of excessive energy into the system is prevented. Since each user is a potential source of interference to other users in the system, any reduction in the transmit power of a user also yields a reduction in MAI which affects all of the other users. However, the transmit power of a user should not be reduced in an unregulated manner, since this may cause the SIR level at the receiver (for that user) to drop to unacceptably low levels. It should be obvious even from this short discussion that finding a *good* PC scheme is not a trivial problem.

Since the major benefit of the SDA system is in the reverse link, only reverse link power control is considered in this chapter.

## 4.1 Power Balanced Power Control in CDMA Systems

Many different PC algorithms have been suggested and examined in the literature. A commonly used type in practice (such as in IS-95), due to its computational simplicity and satisfactory performance, is the power-balanced power control (PBPC) algorithm discussed in Sec. 2.2.1. In PBPC, each row of the received power vector, $\mathbf{P}$, sums to a constant; that is, for each user, the total received signal power from all the AE's is the same.

Although PBPC algorithm *balances* the signal power, it does not guarantee the same interference for all users. Therefore, when PBPC is employed, in general, $\Gamma_{i_k} \neq \Gamma_{i_l}$, for $i_k, i_l \in \{1, 2, \ldots, K\}$ and $i_k \neq i_l$.

### 4.1.1 CA Systems

The CA case has already been examined in Sec. 2.2.2. For the sake of completeness, we revisit this case in this section.

Substituting $L=1$ in Eqn. 2.3, the SIR for a user $i$ is obtained as

$$\Gamma_{i,\mathrm{CA}} = N\frac{G_{i1}\tilde{P}_i}{\left(\sum_{k=1}^{K} G_{k1}\tilde{P}_k\right) - G_{i1}\tilde{P}_i}. \tag{4.1}$$

When PBPC is used, the user transmit powers can be calculated from Eqn. 2.5 as $\tilde{P}_i = 1/G_{i1}$. Then,

$$\Gamma_{i,\mathrm{CA,PBPC}} = \frac{N}{K-1}. \tag{4.2}$$

The above expression is independent of the user index $i$. So, in a CA system, PBPC yields the same SIR value for all the users.

In the derivation of Eqn. 4.2, an ideal case with unlimited PC dynamic range is assumed. In a practical system where there are severe propagation anomalies, to transmit at the required power level may, at least time to time, not be possible. In those cases, SIR for different users would be different and the performance would deteriorate, as discussed in Ch. 2.

### 4.1.2 DA Systems

In DA systems the PC dynamic range is much smaller compared to CA types. However, PC is still essential in a DA system, even in a system with a very large number of AE's (refer to Sec. 2.3.3).

We obtain the SIR expression for a user $i$ by substituting Eqn. 2.2 in Eqn. 2.3 as

$$\Gamma_{i,\mathrm{DA}} = \sum_{j=1}^{L}\Gamma_{ij} = N\sum_{j=1}^{L}\frac{G_{ij}\tilde{P}_i}{\left(\sum_{k=1}^{K}\sum_{l=1}^{L} G_{kl}\tilde{P}_k\right) - G_{ij}\tilde{P}_i}. \tag{4.3}$$

If PBPC is employed, the following approximation holds

$$\left(\sum_{k=1}^{K}\sum_{l=1}^{L} G_{kl}\tilde{P}_k\right) - G_{ij}\tilde{P}_i \approx \sum_{k=1}^{K}\sum_{l=1}^{L} G_{kl}\tilde{P}_k = K, \tag{4.4}$$

especially for large $K$ values. Then, the SIR can be calculated from Eqn.s 4.3 and 4.4 as

$$\Gamma_{i,\mathrm{DA,PBPC}} \approx N\sum_{j=1}^{L}\frac{G_{ij}\tilde{P}_i}{K} = \frac{N}{K}. \tag{4.5}$$

Hence, every user has approximately the same SIR value. This is shown to be true by extensive simulations in Sec. 2.3.1 (see Fig. 2.5).

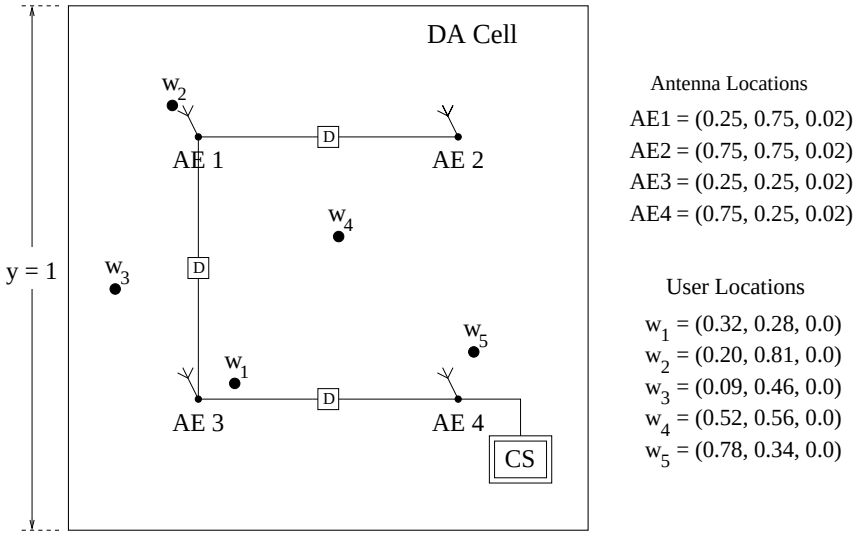


Figure 4.1: An exemplary DA cell with $L=4$ and $K=5$.

In order to develop a better insight into the relation between the MAI and PC in a DA system, we consider a simple case with $L=4$ and $K=5$ as illustrated in Fig. 4.1. We assume that the 5th user, $w_5$, is the user of interest. As it is seen from Fig. 4.1, $w_5$ is the closest user to AE4, and moreover, there are no other users in the vicinity of AE4. However, in the same DA cell there are other users that are closer to some other AE's, such as the pairs $w_1$ – AE3, and $w_2$ – AE1.

The approximate equivalent configurations sensed at the CS, at each finger of the Rake receiver corresponding to $w_5$, are depicted in Fig. 4.2[1]; that is, as long as interference alone is considered, Fig. 4.2 illustrates the approximation of each AE of the DA cell by a CA. In order to simplify the illustration, it is assumed in Fig. 4.2 that a user's signal is picked up by only the closest AE.

The situation at the 4th finger of the Rake receiver is particularly important, because it can easily be anticipated that the most significant contribution to the final SIR value would be from this finger. Although this expectation is true, it is observed from Fig. 4.2(d) that the equivalent configuration sensed at this finger is as if the distant users, which are in the vicinity of some other AE's (that is, $w_1$ and $w_2$), were actually very close to AE4, which is the one near the user of interest. Therefore, due to MAI, one would not be surprised to find that even $\Gamma_{54}$ will not be very high.

The $\Gamma_{ij}/N$ and $\Gamma_i/N$ values for all users, in dB, without power control (noPC) and with PBPC, are given in Table 4.1. In order to have a predictable (deterministic) case, the link gains are modelled as $G_{ij} = d_{ij}^{-4}$.[2] When there is no power control, $P_i$'s are taken to be constant, and for the case of PBPC, they are calculated according to Eqn. 4.3.

[1] The delay elements inserted into the feeder are not shown in Fig. 4.2.

[2] In the simulations presented in Sec. 4.4, a more realistic channel model with fading is considered.

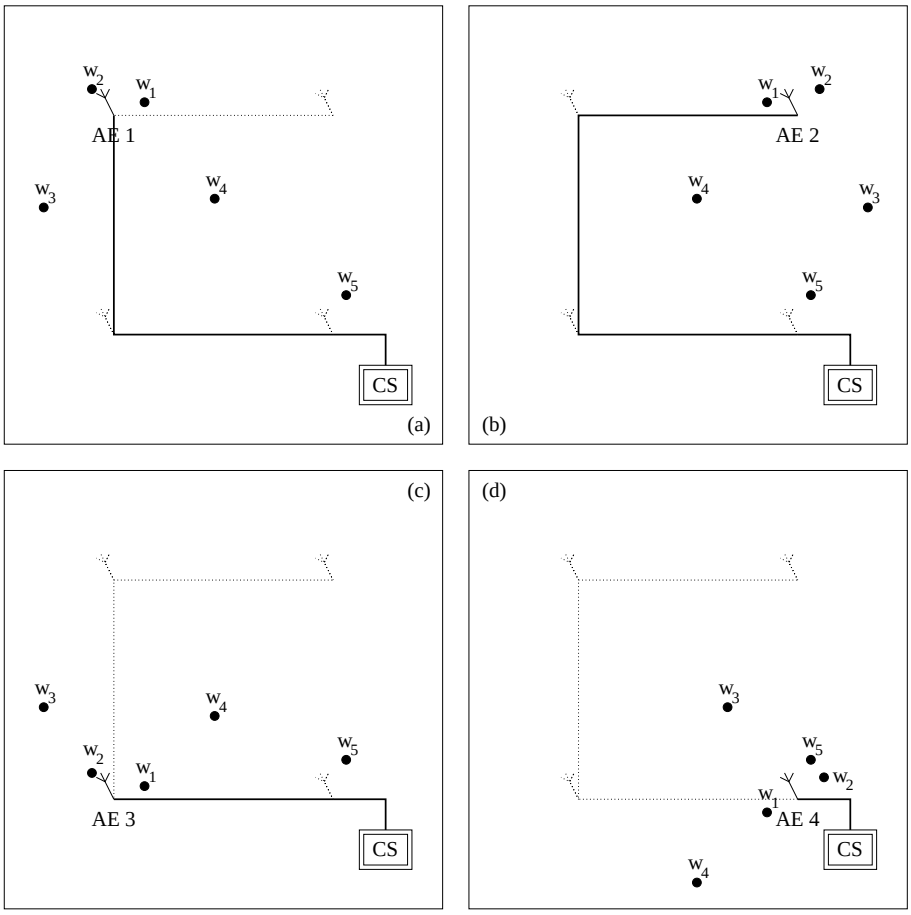


Figure 4.2: Approximate equivalent situation felt at the fingers of the Rake receiver corresponding to 5th user, $w_5$, from each AE in the DA system: (a) 1st finger, (b) 2nd finger, (c) 3rd finger, and (d) 4th finger.

Also, it is worth noting that users $w_4$ and $w_5$ are not close to any AE, therefore, for the noPC case, the SIR values for these two users are expected to be significantly lower than those for the other three users.

Finally, we note the effect of PC: it is observed from Table 4.1 that for this given case, when there is no PC, there is a difference of approximately 22 dB between the highest and lowest SIR values; on the other hand, this difference is less than 1 dB for the case of PBPC. Even more important is the fact that, the lowest SIR value is increased more than 17 dB when PBPC is employed instead of noPC.

### 4.1.3 SDA Systems

Since PBPC works well in DA systems, it would be logical to investigate the performance of this PC scheme in SDA systems.

| $\Gamma_{ij}/N$ (dB) | | | | | | $\Gamma_i/N$ |
|---|---|---|---|---|---|---|
| DA noPC | $w$\AE | AE1 | AE2 | AE3 | AE4 | $\sum$ |
| | $w_1$ | -34.99 | -40.08 | -1.37 | -33.30 | -1.37 |
| | $w_2$ | -2.06 | -37.63 | -37.91 | -43.70 | -2.06 |
| | $w_3$ | -28.73 | -42.23 | -24.80 | -41.53 | -23.21 |
| | $w_4$ | -28.68 | -26.92 | -32.48 | -31.39 | -23.30 |
| | $w_5$ | -40.96 | -32.48 | -37.13 | -6.49 | -6.47 |
| DA PBPC | $w$\AE | AE1 | AE2 | AE3 | AE4 | $\sum$ |
| | $w_1$ | -38.24 | -43.33 | -6.03 | -36.55 | -6.02 |
| | $w_2$ | -6.03 | -40.46 | -40.74 | -46.53 | -6.02 |
| | $w_3$ | -12.26 | -25.98 | -7.94 | -25.29 | -6.47 |
| | $w_4$ | -12.11 | -10.22 | -16.06 | -14.94 | -6.71 |
| | $w_5$ | -40.60 | -32.12 | -36.78 | -6.05 | -6.03 |

Table 4.1: $\Gamma_{ij}/N$ and $\Gamma_i/N$ values, in dB, for DA without power control (noPC) and with power balanced power control (PBPC).

In an SDA system, since a substantial portion of the multiple access interference is rejected, SIR takes the following form:

$$\Gamma_{i,\mathrm{SDA}} = \sum_{j=1}^{L} \Gamma_{ij} = N \sum_{j=1}^{L} \frac{G_{ij}\tilde{P}_i}{\left(\sum_{k=1}^{K} G_{kj}\tilde{P}_k\right) - G_{ij}\tilde{P}_i}. \tag{4.6}$$

When PBPC is employed, it is, in general, not accurate to approximate the denominator of the above expression (inside the summation) by the first term which is in parentheses. Moreover, even if this were possible, it would not yield an SIR expression independent of user index, because the summation $\sum_{i=1}^{K} G_{ij}\tilde{P}_i$ depends on the AE index $j$, and thus, does not yield a constant. Therefore, in an SDA system employing PBPC, SIR for different users may vary significantly.

In order to illustrate this point in a quantitative manner, we continue with the example given in Sec. 4.1.2; this time we consider an SDA system instead of a DA type. The $\Gamma_{ij}/N$ and $\Gamma_i/N$ values for all users, in dB, without power control and with PBPC, are given in Table 4.2. In the preparation of this table, the same assumptions are made as in the preparation of Table 4.1. It is observed from Table 4.2 that for this exemplary case, the lowest SIR value is increased by more than 14 dB, by using PBPC instead of noPC. Moreover, the difference between the highest and lowest SIR values is decreased from almost 36 dB to about 15 dB. Although these are significant improvements, the 15 dB difference in SIR values among various users is still unacceptably high

| $\Gamma_{ij}/N$ (dB) | | | | | | $\Gamma_i/N$ |
|---|---|---|---|---|---|---|
| SDA noPC | $w$\AE | AE1 | AE2 | AE3 | AE4 | $\sum$ |
| | $w_1$ | -30.86 | -14.59 | 20.00 | -25.96 | 20.00 |
| | $w_2$ | 20.94 | -12.03 | -34.20 | -36.37 | 20.94 |
| | $w_3$ | -24.60 | -16.79 | -21.08 | -34.19 | -14.87 |
| | $w_4$ | -24.54 | 3.55 | -28.77 | -24.04 | 3.57 |
| | $w_5$ | -36.83 | -6.21 | -33.42 | 21.47 | 21.48 |
| SDA PBPC | $w$\AE | AE1 | AE2 | AE3 | AE4 | $\sum$ |
| | $w_1$ | -33.21 | -32.87 | 0.88 | -30.23 | 0.89 |
| | $w_2$ | 2.43 | -30.01 | -36.33 | -40.21 | 2.43 |
| | $w_3$ | -6.63 | -15.42 | -2.09 | -18.93 | -0.57 |
| | $w_4$ | -6.45 | 14.25 | -11.46 | -8.14 | 14.32 |
| | $w_5$ | -35.57 | -21.64 | -32.37 | 7.64 | 7.65 |

Table 4.2: $\Gamma_{ij}/N$ and $\Gamma_i/N$ values, in dB, for SDA without power control (noPC) and with power balanced power control (PBPC).

(this difference is less than 1 dB in the DA case with PBPC [see Table 4.1]). It is worth noting that, for a given set of users, it is not that important how large the maximum SIR value is, since the limiting factor is the minimum SIR value. Therefore, it is most desirable to find a PC algorithm that would maximize the minimum SIR value.

After giving the above example for the purpose of developing insight into the PC problem, we provide the CDF's of $\Gamma_{\text{SDA,PBPC}}$'s in Fig. 4.3, for the cases of $L=4, K=5$, and $L=4, K=100$.[3] It is observed from Fig. 4.3 that the disparity among the SIR values is more significant in unloaded (low $K/L$ ratio) systems compared to that in loaded (high $K/L$ ratio) ones. This is the result of the averaging effect in the loaded systems: despite the possible extensive differences (many orders of magnitude) among the entries of the $\mathbf{P}$ matrix, the column sums, $(\sum_{i=1}^{K} G_{ij}\tilde{P}_i)$ tend to be in the same order of magnitude when $K$ is large. Therefore, PBPC performs worse in unloaded systems.

We conclude from the discussions in this section that there is a need to search for a better PC algorithm.

[3]The assumptions made and the simulation parameters used to plot the curves in Fig. 4.6 are discussed in Sec. 4.4.

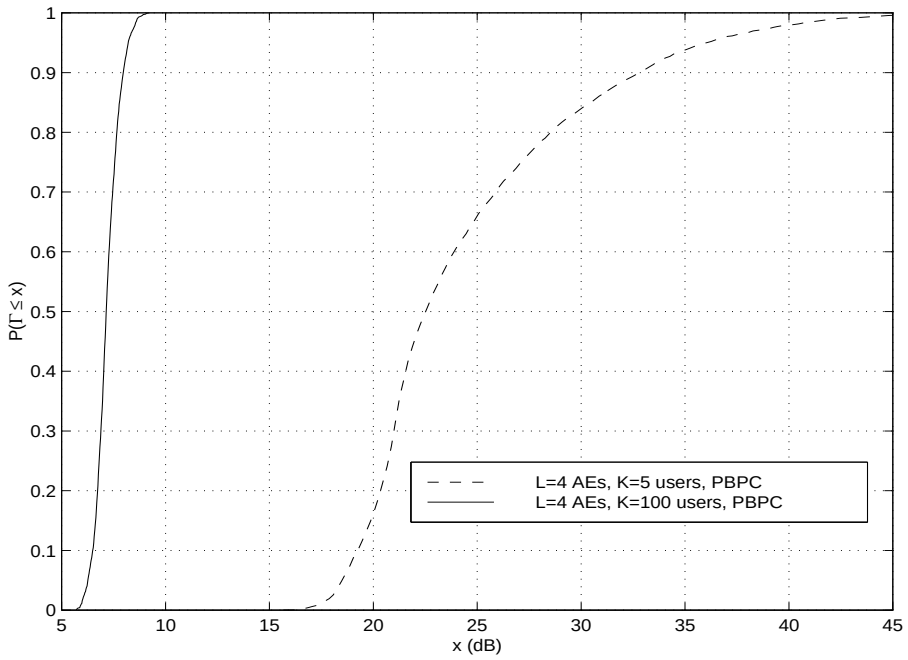


Figure 4.3: CDF of $\Gamma_{\mathrm{SDA,PBPC}}$ for $L=4, K=5$, and $L=4, K=100$.

## 4.2 SIR-Balanced PC in CA Systems

Since the system performance depends on the SIR, not on the received power level, a PC scheme which balances SIR, rather than the received power, would be expected to perform better. Moreover, this is a *fair* PC scheme since it yields the same SIR level for all users. In fact, PC algorithms which *balance* the SIR value have been studied in the literature, for conventional cellular systems with CA's, under the name *SIR-balancing*.

The concept of SIR-balancing was first introduced in [51] in the context of interference management in satellite communications. These results are broadened in [52–54] and applied to non-fading cellular DS-CDMA systems. Subsequently, an optimal global PC algorithm that minimizes outage probability using SIR-balancing with cell removal was demonstrated in [55]; this PC algorithm is applicable mainly for TDMA and FDMA systems. The main drawback of this algorithm is that it requires continuous access to *all* radio paths in the system; therefore, its use in practical cellular systems is very difficult. Nevertheless, the results provide estimates for the optimal performance. An almost-distributed algorithm that converges to the optimal one is discussed in [56]. In that study, each BS (and user) would control its own transmit power based on only limited knowledge about the link gain matrix. It is shown in [57] that maximizing the minimum SIR level, or equivalently minimizing the maximum one, is equivalent to SIR-balancing.

In [51–56], the problem of SIR-balanced PC, which we will refer to as SBPC, is first presented

in matrix notation, then transformed into an eigenvalue problem, and finally, solved analytically using matrix algebra. However, there is a major difference between those cases and the SDA system that we are analyzing: in the SDA system there is diversity reception which complicates the PC problem significantly.

In the conventional cellular systems, in the absence of macro diversity, each user communicates with only one BS. Obviously, this is significantly different than the SDA system where each user communicates with all the AE's. Consequently, modelling of such a conventional cellular system is quite different than that of an SDA type. If we use the same $L$ and $K$ values for both systems, then for the conventional cellular case, there would be $L$ different cells each with one CA, compared to one cell with $L$ AE's in the case of an SDA system. Also, the number of users in each of the conventional cells would be $K/L$, assuming uniform user distribution.

## 4.3 SIR-Balanced Macro PC (SBMPC)

In this section, a PC algorithm that balances SIR in SDA systems is given; we refer to this algorithm as SIR-balanced macro PC (SBMPC).

**SBMPC Algorithm:** find $\{\tilde{P}_i\}_{i=1}^{K}$ subject to

$$\Gamma_{i,\mathrm{SDA,SBMPC}} = N \sum_{j=1}^{L} \frac{G_{ij}\tilde{P}_i}{\left(\sum_{k=1}^{K} G_{kj}\tilde{P}_k\right) - G_{ij}\tilde{P}_i} = \gamma, \ \forall i. \tag{4.7}$$

Because of the outmost summation ($\sum_j$) in Eqn. 4.7, which appears as a result of diversity combining, the set of equations given in Eqn. 4.7 become nonlinear. Therefore, the eigenvalue method described in the previous section does not apply here.

However, we can find the transmit power vector, $\tilde{\mathbf{P}}$, by solving Eqn. 4.7 iteratively. Note that there are $K$ equations, but $K+1$ unknowns, namely, $\gamma$ and $\{\tilde{P}_i\}_{i=1}^{K}$. Therefore, $\tilde{P}_i$'s will be obtained within a multiplicative constant. We fix $\tilde{P}_1$ and find $\{\tilde{P}_i\}_{i=2}^{K}$ as proportional to $\tilde{P}_1$. Therefore, $\tilde{P}_1$ at the $\nu$th step of iterations is $\tilde{P}_1^{(\nu)} = \tilde{P}_1^{(0)}$.

First, we rearrange Eqn. 4.7, and denote the $i$th equation by $\mathcal{E}_i$, as follows:

$$\mathcal{E}_1: \quad \gamma = N \sum_{j=1}^{L} \frac{G_{1j}\tilde{P}_1}{\left(\sum_{k=1}^{K} G_{kj}\tilde{P}_k\right) - G_{1j}\tilde{P}_1}, \tag{4.8}$$

$$\mathcal{E}_i: \quad \tilde{P}_i = \frac{\gamma}{N \sum_{j=1}^{L} \frac{G_{ij}}{\left(\sum_{k=1}^{K} G_{kj}\tilde{P}_k\right) - G_{ij}\tilde{P}_i}}, \quad i = 2, 3, \ldots, K. \tag{4.9}$$

Now, we can state the iterative solution.

**SBMPC Iterative Solution Algorithm I:**[4]

$$\begin{aligned}
\tilde{\mathbf{P}}^{(0)} = \quad & \left\{\tilde{P}_i^{(0)}\right\} = \left\{\left(\sum_{j=1}^{K} G_{ij}\right)^{-1}\right\}, \quad i = 1, 2, \ldots, K, \\
\gamma^{(\nu+1)} = \quad & \mathcal{E}_1\left(\tilde{\mathbf{P}}^{(\nu)}\right), \\
\tilde{P}_1^{(\nu+1)} = \quad & \tilde{P}_1^{(\nu)}, \\
\tilde{P}_i^{(\nu+1)} = \quad & \mathcal{E}_i\left(\gamma^{(\nu+1)}, \tilde{\mathbf{P}}^{(\nu)} - \left\{\tilde{P}_i^{(\nu)}\right\}\right), \quad i = 2, 3, \ldots, K.
\end{aligned}$$

The algorithm starts with an initial vector which is calculated according to PBPC. In the above algorithm, $\mathcal{E}_i(.)$ denotes inserting the variables in the brackets into $\mathcal{E}_i$ given in Eqn.s 4.8 and 4.9.

Obviously, one very important concern is the termination criterion for the iterations. This nontrivial issue is discussed in the next section.

## 4.4 Termination Criterion for Iterations

Simulations are carried out to determine the convergence characteristics of the iterative solution for the SBMPC algorithm introduced in the previous section. The objective is to find a termination criterion that would yield low disparities among the SIR levels of different users for a reasonable number of iterations (NoI's). In the simulations, we make the same assumptions stated in Sec. 3.3.

Let us denote the final step of iterations by $\nu_t$, i.e., NoI = $\nu_t$. The yielding SIR vector, $\mathbf{\Gamma}^{(\nu_t)} = \{\Gamma_i^{(\nu_t)}\}_{i=1}^{K}$, can be calculated by using $\tilde{\mathbf{P}}^{(\nu_t)}$ (which is obtained from Eqn. 4.10) in Eqn. 4.7. The SIR error for a user $i$ after $\nu_t$ steps of iteration, $\Lambda_i^{(\nu_t)}$, is defined as a measure that shows the difference between $\Gamma_i^{(\nu_t)}$ and the optimal value, $\gamma^*$:[5]

$$\Lambda_i^{(\nu_t)} = 10\left|\log\left(\Gamma_i^{(\nu_t)}/\gamma^*\right)\right| \text{ dB}. \tag{4.10}$$

In the simulations, for a certain set of random user locations, first, the $\mathbf{G}$ matrix is formed, and then the balanced SIR value is calculated through the iterative solution of the SBMPC algorithm introduced in the previous section. This process is repeated for different user location sets in order to collect enough data to plot accurate CDF's for NoI's and $\Lambda$.

One straightforward termination criterion would be

$$\text{stop if} \quad 10\left|\log\left(\gamma^{(\nu+1)}/\gamma^{(\nu)}\right)\right| \leq \epsilon \text{ dB}, \tag{4.11}$$

[4]Two other algorithms (II and III) will be discussed in Sec. 4.8.

[5]The optimal values of $\tilde{\mathbf{P}}$ and $\gamma$ are denoted by $\tilde{\mathbf{P}}^*$ and $\gamma^*$, respectively.

where $\epsilon$ is sufficiently close to 0. However, this criterion does not yield satisfactory results, because of the nature of the convergence characteristics of the iterations, which varies according to $L$ and $K$ values, and shows occasional anomalies.

Three types of problems are encountered; we refer to them as type I, type II, and type III

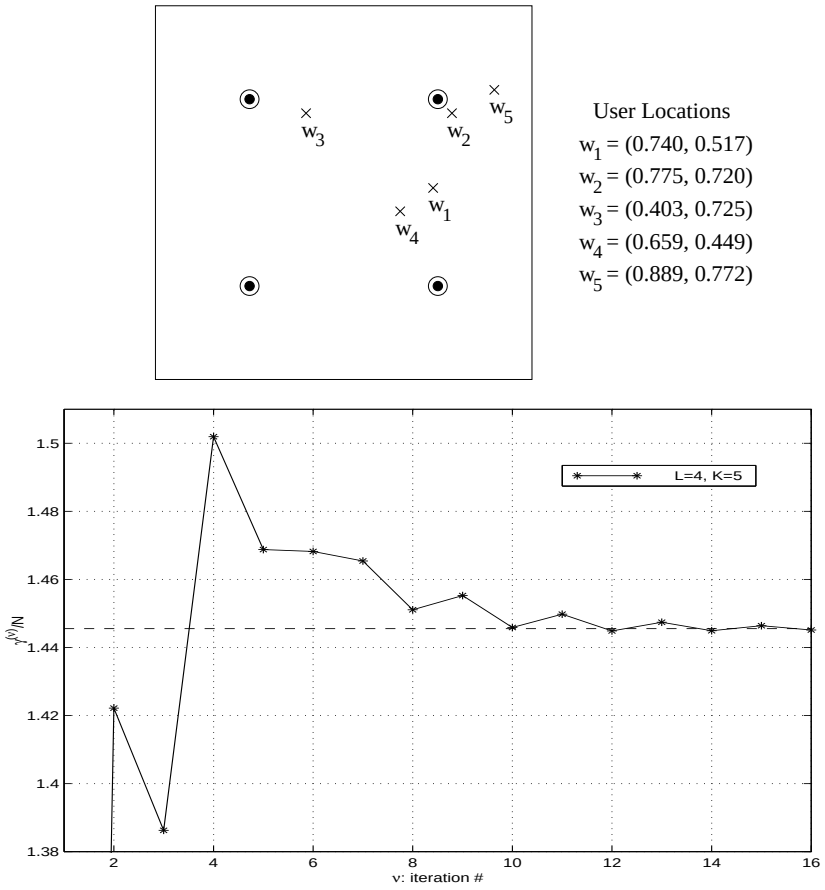


Figure 4.4: A set of user locations that cause a type I problem, for the case of $(L = 4, K = 5)$, and the resulting irregular oscillations in $\gamma/N$ ($\bullet$ and $\times$ denote the AE and user locations, respectively).

problems.

A type I problem occurs when

$$10\left|\log\left(\gamma^{(\nu+1)}/\gamma^{(\nu)}\right)\right| \leq \epsilon \text{ dB}, \quad \ldots, \quad 10\left|\log\left(\gamma^{(\nu+\eta)}/\gamma^{(\nu+\eta-1)}\right)\right| \leq \epsilon \text{ dB},$$
$$\text{but, } 10\left|\log\left(\gamma^{(\nu+\eta+1)}/\gamma^{(\nu+\eta)}\right)\right| > \epsilon \text{ dB}, \tag{4.12}$$

for some integer $\eta \geq 1$. If the termination criterion given in Eqn. 4.11 is used, a type I problem will cause a premature stop, and this will yield high $\Lambda$ values. Such a case is shown in Fig. 4.4[6]

[6] In order to illustrate the relation between the user locations and the corresponding convergence characteristics, fading is not taken into account in the examples shown in Fig.s 4.4–4.6.

where $\epsilon$ is taken to be 0.04 dB.[7] It is observed from this figure that although $10|\log(\gamma^{(6)}/\gamma^{(5)})| \leq \epsilon$

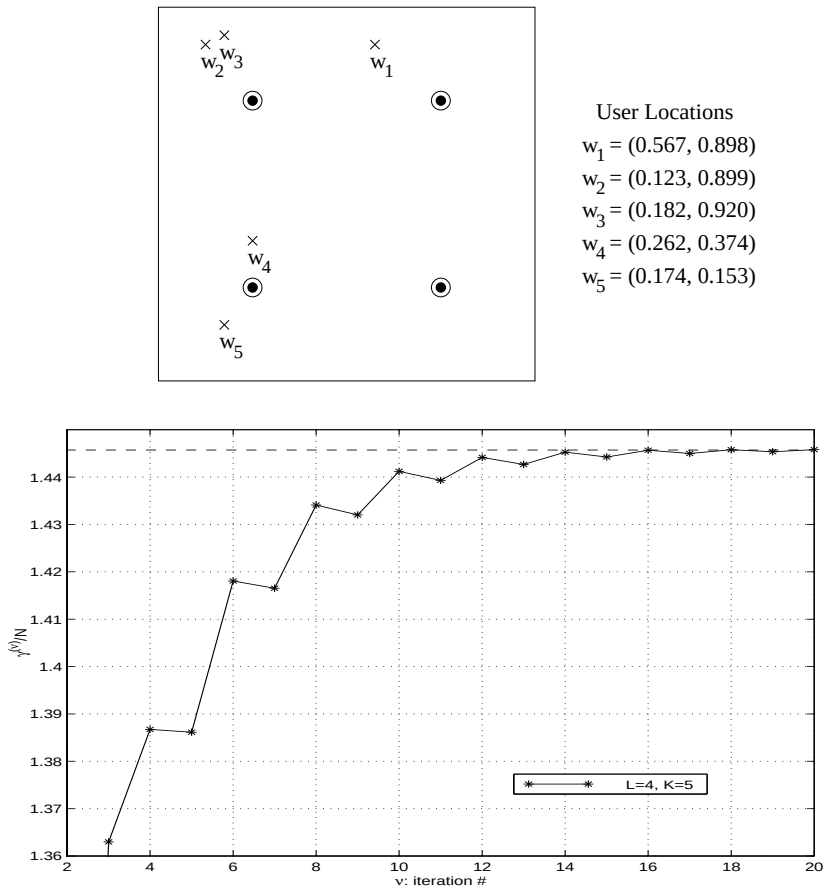


Figure 4.5: Another set of user locations that cause a type I problem, for the case of $(L=4, K=5)$, and the resulting oscillations in $\gamma/N$.

dB and $10|\log(\gamma^{(7)}/\gamma^{(6)})| \leq \epsilon$ dB, $10|\log(\gamma^{(8)}/\gamma^{(7)})| > \epsilon$ dB (which corresponds to $\eta=2$). Type I problems are observed when the users are unevenly located in the cell, as shown in Fig. 4.4. Another example of a type I problem is shown in Fig. 4.5; this case corresponds to $\eta=1$.

A type II problem occurs, on the other hand, when the convergence speed of iterations is very slow. This causes the NoI's to be very high (however, such cases yield small $\Lambda$ values). Type II problems are observed when each user is close to an AE; such a case is shown in Fig. 4.6.

In the simulations, the occasional type I and type II problems are encountered only in the cases that correspond to unloaded systems. In loaded systems, on the other hand, another type of problem, type III, is observed occasionally. For some user positions, $\gamma$ first reaches a maximum and then converges to $\gamma^*$; in such cases, there is the possibility of premature termination (similar to type I problem). Examples of type III problem are shown in Fig.s 4.7 and 4.8.

[7] In Fig.s 4.4–4.8, a linear scale (rather than a dB type) is used.

For an $\epsilon$ arbitrarily close to 0 in Eqn. 4.11, all the anomalies of type I can be handled. But this would yield a very high NoI for all types of problems (and an unnecessarily high accuracy). Therefore, the solution is not making $\epsilon$ close to 0, but rather considering a multi-stage termination criterion.

The flow chart of such a multi-stage termination criterion is shown in Fig. 4.9. We note that the "update $\gamma$" and "update $\tilde{\mathbf{P}}$" lines in the flow chart are performed according to Eqn.s 4.8 and 4.9, respectively. After the final stop, $\mathbf{\Gamma} = \{\Gamma_i\}$ is calculated using Eqn. 4.7.

## 4.5 Observations

Simulations are carried out for a wide range of $L$ and $K$ values ($L=4$ and $K=5$ to 100, and $L=16$ and $K=20$ to 400). In all the cases, the iterations have always converged; that is, $\lim_{\nu\to\infty} \tilde{\mathbf{P}}^{\nu} = \tilde{\mathbf{P}}^{*}$, and $\lim_{\nu\to\infty} \gamma^{\nu} = \gamma^{*}$. The assumptions made in the simulations are the same as those described in Sec. 3.3.

Initial transmit power vectors, $\tilde{\mathbf{P}}^{(0)}$, other than that given in Eqn. 4.10 are also considered, and it is observed that the resulting NoI's are similar (although, $\tilde{\mathbf{P}}^{(0)}$ given in Eqn. 4.10 yields slightly lower NoI's). Therefore, the iterative solution algorithm is very robust with respect to the choice of $\tilde{\mathbf{P}}^{(0)}$; in other words, whatever $\tilde{\mathbf{P}}^{(0)}$ is, the iterative algorithm converges to $\tilde{\mathbf{P}}^{*}$.

CDF's for NoI's and $\Lambda$ are given in Fig.s 4.10-4.11 for $\epsilon = 0.1$ dB, and $m=1, 3$, and 5, where $m$ denotes the number of stages in the multi-stage stop criterion (see Fig. 4.9)[8]. It is observed from these figures that NoI's are lower for the loaded systems [$(L=4, K=100)$, and $(L=16, K=400)$] compared to the unloaded ones [$(L=4, K=5)$, and $(L=16, K=400)$]. This demonstrates efficiency since the required computation at each iteration step for the loaded systems is much more than that for the unloaded ones (due to the size of the link gain matrix $\mathbf{G}$).

We note from Fig. 4.11 that there is significant improvement in the statistics of $\Lambda$, when a 3-stage stop criterion is used instead of a 1-stage type. This is due to the fact that most of the type I problems are eliminated by using a 3-stage stop criterion. On the other hand, NoI's increase for $m=3$ case compared to the $m=1$ case (see Fig. 4.11), as expected, however, the

[8] As it is described in Sec. 4.3, in the iterative solution algorithm, one of the users' transmit power is kept at a constant level throughout the iterations, and powers of the rest of the users are calculated in proportion to the constant one. In our analysis, without loss of generality, user 1's transmit power is kept fixed. As a consequence of this choice, $\mathcal{E}_1(.)$ is used to compute the updated values of $\gamma$ (refer to Eqn. 4.8), which means that the termination of iterations is based on the convergence characteristics of user 1's SIR. At a certain simulation run, user 1 may experience different convergence behavior compared to the other users. Nevertheless, the averaging effect holds, since the simulations are run for very large number of times, and the results shown in Fig.s 4.10-4.11, which are obtained by observing user 1's SIR, adequetly reflect the overall convergence characteristics.

increase is not substantial. Therefore, $m=3$ constitutes a good compromise.

## 4.6 Comparison with Hanly's Work [1] – Part I: Correction to Hanly's Theorem 1

In Ch. 3, we found the range for the balanced-SIR, $\gamma$, for given $K$ and $L$ values (see Eqn.s 3.7 and 3.8). The value of $\gamma$, in this range, depends on the link gain matrix $\mathbf{G}$ (which, in turn, is dependent on the user locations and the fading conditions). In our case, since all the users have the same SIR, we consequently assume that they all have the same quality of service requirement.

Hanly considered a more general case in [1], where the users have different quality of service requirements; in that case, the objective is to achieve a target SIR vector $\mathbf{\Gamma} = \{\Gamma_1, \Gamma_2, \ldots, \Gamma_K\}$, rather than balancing all the users to a common SIR value, $\gamma$. Hanly tries to determine whether there exists a unique $\tilde{\mathbf{P}}^*$ which will yield the target $\mathbf{\Gamma}$, for given $K$ and $L$ values.

**Hanly's Theorem 1** [1]:

a) If $\sum_{i=1}^{K} \Gamma_i \geq NL$, then there is no solution to $\mathbf{\Gamma}$.

b) If $\sum_{i=1}^{K} \Gamma_i < NL$, then there exists a unique solution $\tilde{\mathbf{P}}^*$ to $\mathbf{\Gamma}$.

Based on the above theorem, Hanly states [1]: "We use this power control problem to derive the network capacity region and find that the feasibility of a configuration of users is *independent* of their positions in the network; each user can be assigned a bandwidth that is independent of the user's position in the network. ... An important feature from a network management point of view is that this constraint is *linear*; each user can be assigned a bandwidth. ... The surprising conclusion from Theorem 1 is that ($\mathbf{G}$,$\mathbf{\Gamma}$) is feasible if and only if $\sum_{i=1}^{K} \Gamma_i < NL$, a condition independent of $\mathbf{G}$. This suggests that call admission is very easy in a spread spectrum network with macrodiversity. To see if $K$ users with SIR requirements $(\Gamma_1, \Gamma_2, \ldots, \Gamma_K)$ can be accommodated, we simply add up ... and compare with ... $NL$."

Now, let us compare Hanly's Theorem 1 with our results. Our case corresponds to a special target $\mathbf{\Gamma}$ vector, such that $\Gamma_i = \gamma$, $\forall i$. The results found in Sec. 3.2, in particular, Eqn.s 3.7 and 3.8, indicate that $\Gamma_i \leq \Gamma_{\text{SDA,SBMPC,LL}}$ can always be achievable, and $\Gamma_i > \Gamma_{\text{SDA,SBMPC,UL}}$ cannot be achievable. Moreover, achievability in the region $\Gamma_{\text{SDA,SBMPC,LL}} < \Gamma_i \leq \Gamma_{\text{SDA,SBMPC,UL}}$ depends on the entries of the link gain matrix, that is, on the positions of the users in the network! From Eqn.s 3.7 and 3.8, we calculate that $\sum_{i=1}^{K} \Gamma_{\text{SDA,SBMPC,LL}} = NLK/(K-1)$, and $\sum_{i=1}^{K} \Gamma_{\text{SDA,SBMPC,UL}} = NLK/(K-L)$. In Hanly's Theorem 1, there are two regions with one threshold ($NL$) separating them, but according to our results there should be three regions with two thresholds [$NLK/(K-1)$ and $NLK/(K-L)$].

The discrepancy between Hanly's Theorem 1 and our results is due to an approximation in Hanly's modelling. He includes the user's own signal in the interference; that is, he omits the subtracted term in the denominator of Eqn. 3.5. In that case, Eqn. 3.7 would be $\Gamma_{\text{SDA,SBMPC,LL}} = NL/K$, and Eqn. 3.8 would be $\Gamma_{\text{SDA,SBMPC,UL}} = N/(K/L)$; so, with that approximation, the two thresholds merge to a single one, $NL$, and Hanly's Theorem 1 holds.

Based on the above discussion, we present the corrected version of Hanly's Theorem 1:[9]

**Hanly's Theorem 1 – Revised:**

a) If $\sum_{i=1}^{K} \Gamma_i > NLK/(K-L)$, then there is no solution to $\mathbf{\Gamma}$.

b) If $\sum_{i=1}^{K} \Gamma_i \leq NLK/(K-1)$, then there exists a unique solution $\tilde{\mathbf{P}}^*$ to $\mathbf{\Gamma}$.

c) If $NLK/(K-1) < \sum_{i=1}^{K} \Gamma_i \leq NLK/(K-L)$, then the existence of a unique solution $\tilde{\mathbf{P}}^*$ to $\mathbf{\Gamma}$ depends on the $\mathbf{G}$ matrix.

It is worth noting that $NLK/(K-1) \sim NL$ for $K \gg 1$, $NLK/(K-L) \sim NL$ for $K/L \gg 1$, and $\Gamma_{\text{SDA,SBMPC,LL}}/\Gamma_{\text{SDA,SBMPC,UL}} \sim 1$ (see Eqn. 3.11), once again, for $K/L \gg 1$. Therefore, although Hanly's Theorem 1 is not exact, it is a good approximation of the Revised Theorem given above, especially for loaded systems.

It is interesting to note that the revision of Hanly's Theorem 1 has almost no effect on Hanly's above quoted statements. In order to demonstrate why this is so, let us consider a network with $K-1$ users and assume that a new user (user $K$) is asking permission for admission into the network. If with the prospective user $K$, condition b) in the Revised Theorem is satisfied, then, obviously, user $K$ can be admitted into the network. However, if condition a) is satisfied, then user $K$ should not be admitted. Alternatively, if condition c) were satisfied, then user $K$ should still not be admitted, even with the existence of $\tilde{\mathbf{P}}^*$. The reason is that condition c) depends on $\mathbf{G}$; therefore, even if $\tilde{\mathbf{P}}^*$ exists for this moment, there is no guarantee of its existence in the following moment, due to the mobility of the users and the change in the fading conditions. Thus, the appropriate strategy is to admit the prospective user $K$ only if condition b) is satisfied. This means that the decision to admit is independent of $\mathbf{G}$, as Hanly stated.

We will continue the comparison of this work with that of Hanly's in the next chapter.

## 4.7 Chapter Summary and Remarks

In an SDA system, a power control algorithm that balances the SIR should be considered, since the conventional power-balanced power control algorithm results in considerable disparities among the SIR levels of different users. In this chapter, a nonlinear SIR-balanced PC algorithm, which

[9] We are intending to send a correction/comment note to *IEEE Trans. Commun.* on this theorem.

is referred to as the SIR-balanced macro PC (SBMPC) because of its handling of macro diversity, is developed for CDMA SDA systems.

In SBMPC, the set of equations to be solved are nonlinear (due to diversity) which makes the solutions for SIR-balancing algorithms, given in the literature, inapplicable. Therefore, we propose an iterative solution to the SBMPC algorithm which always converges. Because of the non-smooth convergence characteristics of the iterations, finding a suitable termination criterion for the iterations is a nontrivial problem. We suggest a multi-stage criterion which yields very low disparities among the SIR levels of different users for reasonably low numbers of iterations.

Although the SBMPC algorithm and its iterative solution addressed in this chapter are presented in the context of SDA systems, they may have other important applications. One such application is the power control problem in cellular systems employing macro diversity [1]. Our results are compared with those in [1], and Theorem 1 in that paper is corrected accordingly.

In the iterative solution of the SBMPC algorithm, it is assumed that we have instantaneous access to the entire link gain matrix $\mathbf{G}$. Since all the AE's are connected to a CS, this is not an unrealistic assumption.

## 4.8 Future Research Directions

### 4.8.1 Other SBMPC Iterative Solution Algorithms

An iterative algorithm (Algorithm I) for the solution of SBMPC is given in Sec. 4.3, and its convergence characteristics are analyzed in Sec.s 4.4 and 4.5, through exhaustive simulations. The main conclusion drawn from these simulations is that algorithm I *always* converges, although the speed of convergence may be low for certain user positions (see Fig.s 4.10 and 4.11). In this section, we will discuss two other iterative algorithms for the solution of SBMPC.

**SBMPC Iterative Solution Algorithm II:**

$$
\begin{aligned}
\tilde{\mathbf{P}}^{(0)} = \quad & \left\{\tilde{P}_i^{(0)}\right\} = \left\{\left(\sum_{j=1}^{K} G_{ij}\right)^{-1}\right\}, \quad i = 1, 2, \ldots, K, \\
\gamma^{(\nu+1)} = \quad & \mathcal{E}_1\left(\tilde{\mathbf{P}}^{(\nu)}\right), \\
\tilde{P}_1^{(\nu+1)} = \quad & \tilde{P}_1^{(\nu)}, \\
\tilde{P}_i^{(\nu+1)} = \quad & \mathcal{E}_i\left(\gamma^{(\nu+1)}, \left\{\tilde{P}_1^{(\nu+1)}, \ldots, \tilde{P}_{i-1}^{(\nu+1)}, \tilde{P}_{i+1}^{(\nu)}, \ldots, \tilde{P}_K^{(\nu)}\right\}\right), \quad i = 2, 3, \ldots, K.
\end{aligned}
$$

The difference between Algorithms I and II is as follows: in Algorithm II, within a step of iteration, while updating the transmit power of a user $i$, the already updated transmit power values for

users 1 to $i-1$ are used. In Algorithm I, however, the updated $\tilde{P}_i$'s are not used until the next step of iterations.

**SBMPC Iterative Solution Algorithm III:**

$$
\begin{aligned}
\tilde{\mathbf{P}}^{(0)} &= \left\{\tilde{P}_i^{(0)}\right\} = \left\{\left(\textstyle\sum_{j=1}^{K} G_{ij}\right)^{-1}\right\}, \quad i = 1, 2, \ldots, K, \\
\gamma^{(\nu+1,0)} &= \mathcal{E}_1\left(\tilde{\mathbf{P}}^{(\nu)}\right), \\
\tilde{P}_1^{(\nu+1)} &= \tilde{P}_1^{(\nu)}, \\
\gamma^{(\nu+1,1)} &= \mathcal{E}_1\left(\left\{\tilde{P}_1^{(\nu+1)}, \tilde{P}_2^{(\nu)}, \ldots, \tilde{P}_K^{(\nu)}\right\}\right), \\
\tilde{P}_i^{(\nu+1)} &= \mathcal{E}_i\left(\gamma^{(\nu+1,i-1)}, \left\{\tilde{P}_1^{(\nu+1)}, \ldots, \tilde{P}_{i-1}^{(\nu+1)}, \tilde{P}_{i+1}^{(\nu)}, \ldots, \tilde{P}_K^{(\nu)}\right\}\right), \\
\gamma^{(\nu+1,i)} &= \mathcal{E}_1\left(\left\{\tilde{P}_1^{(\nu+1)}, \ldots, \tilde{P}_i^{(\nu+1)}, \tilde{P}_{i+1}^{(\nu)}, \ldots, \tilde{P}_K^{(\nu)}\right\}\right),
\end{aligned}
\quad \Bigg\} \; i = 2, \ldots, K.
$$

The difference between Algorithms II and III is as follows: in Algorithm III, within each step of iteration, the update of the transmit power of each user is followed by an update of $\gamma$. In other words, within each step of iteration, $\gamma$ is updated $K$ times, unlike Algorithm II (and I) where $\gamma$ is updated only once. Obviously, these extra updates would increase the required computation for Algorithm III, compared to Algorithms I and II.

We made an initial analysis of the convergence speed of Algorithms II and III, and realized that these algorithms have convergence problems; that is, for certain $K$ and $L$ values they do not balance the SIR for certain user locations. To be more precise, the occasional converge problems occurred for $(L = 4, K = 5)$, $(L = 4, K = 10)$, $(L = 16, K = 5)$, and $(L = 16, K = 20)$ cases for Algorithm II, and for the $(L = 4, K = 5)$ case for Algorithm III. Obviously, all of these cases correspond to unloaded systems. The simulations run for some other $K$ and $L$ combinations suggest that there is no convergence problem for loaded cases; however, the results are not conclusive due to the limited number of simulations run.

In this initial analysis, Algorithm II seemed to be somewhat faster than Algorithm I for the cases where Algorithm II did converge, and more interestingly, Algorithm III seemed to be significantly faster than the other two algorithms, whenever it did converge. Once again, exhaustive simulations should be run to verify these initial findings.

If the above findings are true, that is, if Algorithm III always converges for loaded cases with a speed significantly faster than those of the other two algorithms, then, perhaps, a threshold (e.g. $\mu$) in terms of $K/L$ (which would separate the loaded and unloaded cases), can be found.

In [1], Hanly proved the convergence of a somewhat similar PC algorithm (in [1], there is no discussion on the speed of convergence though). Perhaps, a similar proof technique (monotonicity in cooperative systems) can be used to show that Algorithm III always converges for $K/L > \mu$.

If this is possible, then, for given $K$ and $L$ values we can apply the following strategy:

$$\text{use} \begin{cases} \text{Algorithm I}, & \text{if } K/L \leq \mu \\ \text{Algorithm III}, & \text{if } K/L > \mu. \end{cases}$$

Such a strategy would be very useful for the following reason: for the cases where Algorithm III is employed (loaded ones), the computational complexity would be great due to the size of the problem (large $K/L$ ratio); therefore, the high convergence speed of Algorithm III would be a definite asset.

### 4.8.2 More Realistic Initial Conditions

In the convergence speed study we performed, for each simulation, we generate a new $\mathbf{G}$ matrix based on random user locations and log-normal shadow fading conditions. Then, the iterations start from a power-balanced $\tilde{\mathbf{P}}$ vector, and we try to analyze how fast the SIR-balanced condition is achieved. We discussed in Sec. 4.1.3 that the set of transmit powers in power-balancing may, in fact, be significantly different from the corresponding set in SIR-balancing.

In a real system the situation will be somewhat different. Let us consider a system which is SIR-balanced at some point in time, say at $t=t_o$; we denote this system by the pair $(\mathbf{G}_{t_o}, \tilde{\mathbf{P}}^*_{t_o})$. The system may become unbalanced in the next moment, at $t = t_o+\Delta t$, because of two reasons: as a result of the user movements and the change in fading, the entries of the $\mathbf{G}$ matrix may change (but only slightly), and/or a user may enter or leave the system, thus changing the size of the $\mathbf{G}$ matrix.

Probably, such an unbalanced system as $(\mathbf{G}_{t_o+\Delta t}, \tilde{\mathbf{P}}^*_{t_o})$, would be closer to the SIR-balanced case $(\mathbf{G}_{t_o+\Delta t}, \tilde{\mathbf{P}}^*_{t_o+\Delta t})$, than the power-balanced initial condition case that we employ in the simulations. Therefore, the system may become rebalanced faster than our analysis would indicate; in that case, our results would be pessimistic.

On the other hand, we mentioned in Sec. 4.5 that the convergence is *rather* insensitive to the initial choice of the $\tilde{\mathbf{P}}$ vector. Therefore, it is unlikely that our results are *significantly* pessimistic. This issue may be worth investigating more carefully.

Let us present the procedure for an improved simulation. One should start from an SIR-balanced system $(\mathbf{G}_{t_o}, \tilde{\mathbf{P}}^*_{t_o})$, and then, disturb the system a little bit; that is, generate $\mathbf{G}_{t_o+\Delta t}$ from $\mathbf{G}_{t_o}$ (this step requires additional thought on *how* to generate $\mathbf{G}_{t_o+\Delta t}$ from $\mathbf{G}_{t_o}$). Finally, one should use $\tilde{\mathbf{P}}^*_{t_o}$ as the initial condition, and analyze the speed of convergence to $\tilde{\mathbf{P}}^*_{t_o+\Delta t}$.

### 4.8.3 Other Termination Criteria for Iterations

A multi-stage criterion for the termination of iterations is given in Sec. 4.4, and the resulting NoI's and error statistics are studied in Sec. 4.5. Although the multi-stage termination criterion works well, it is not necessarily ideal. By a more careful analysis of the encountered problems and anomalities during the iterations, even better termination criteria may be found.

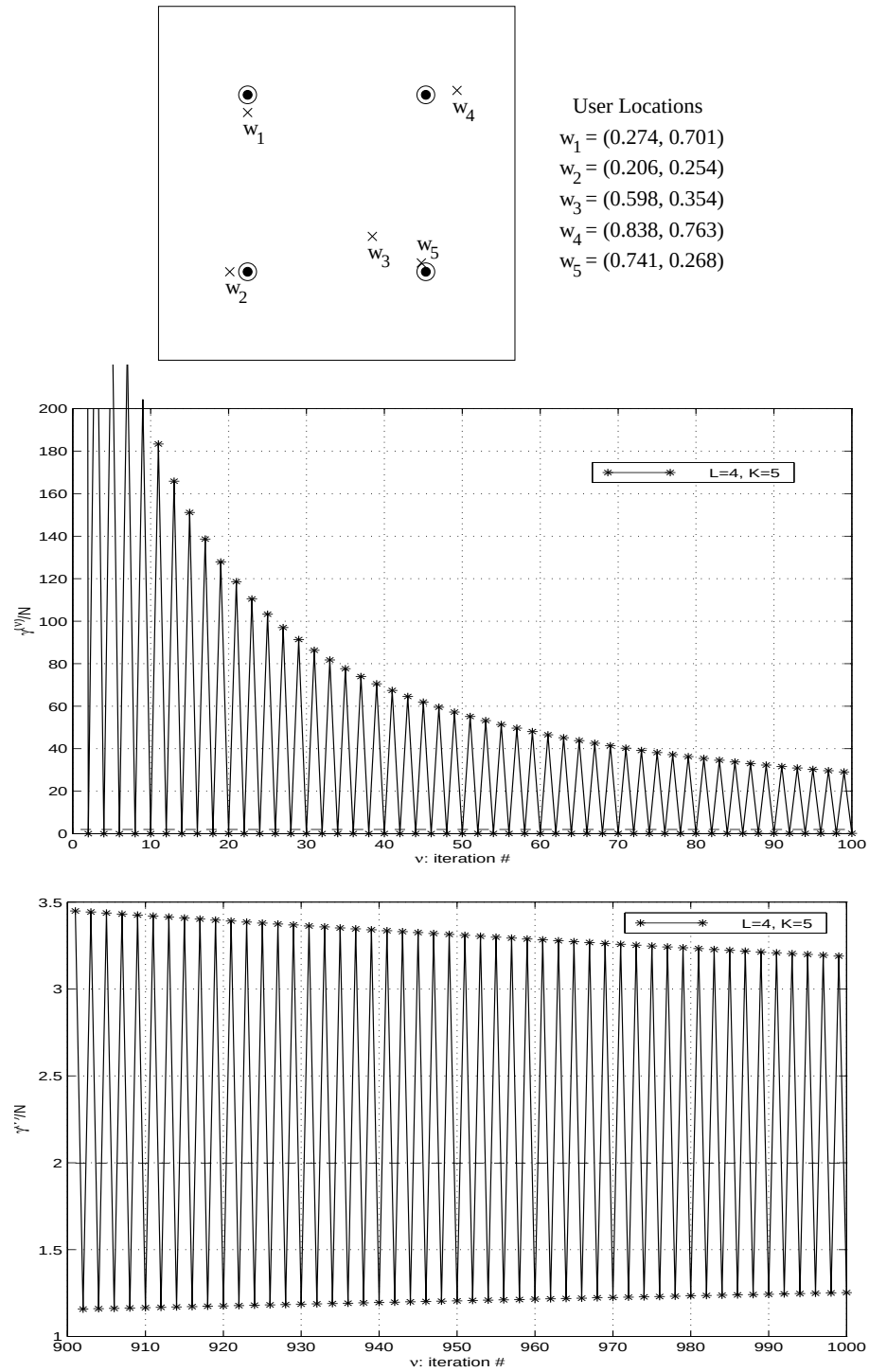


Figure 4.6: A set of user locations that cause a type II problem, for the case of $(L = 4, K = 5)$, and the resulting oscillations in $\gamma/N$.

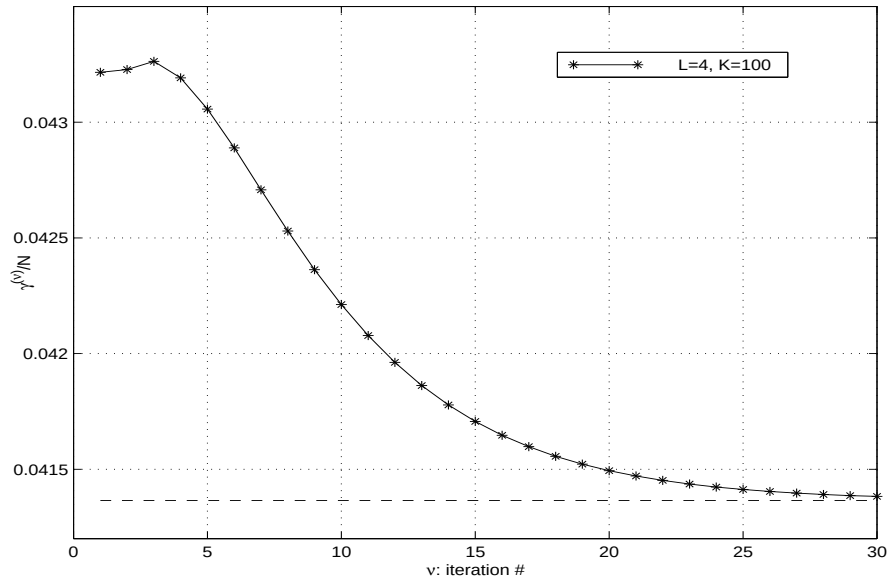


Figure 4.7: A type III problem for the case of $(L=4, K=100)$.

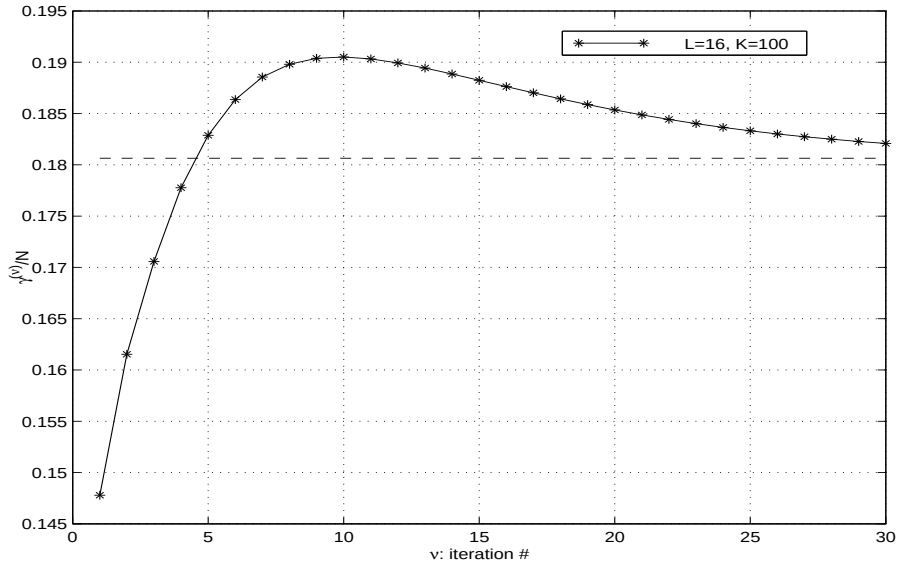


Figure 4.8: A type III problem for the case of $(L=16, K=100)$.

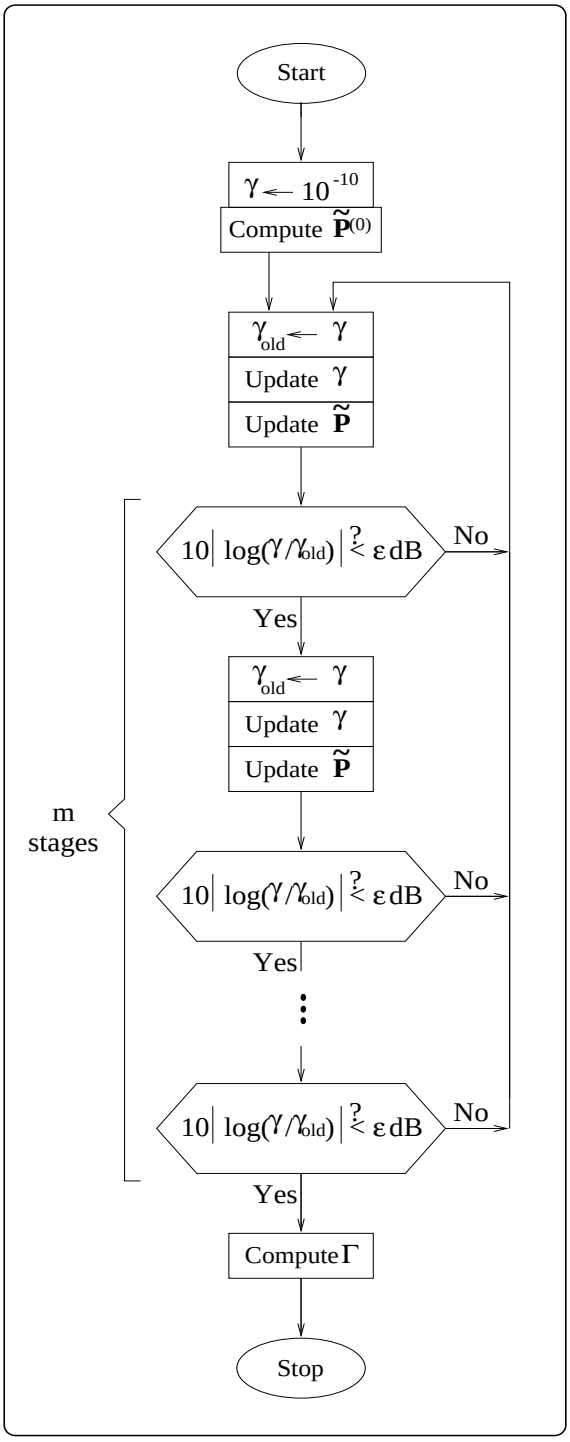


Figure 4.9: The flow chart of the multi-stage termination program.

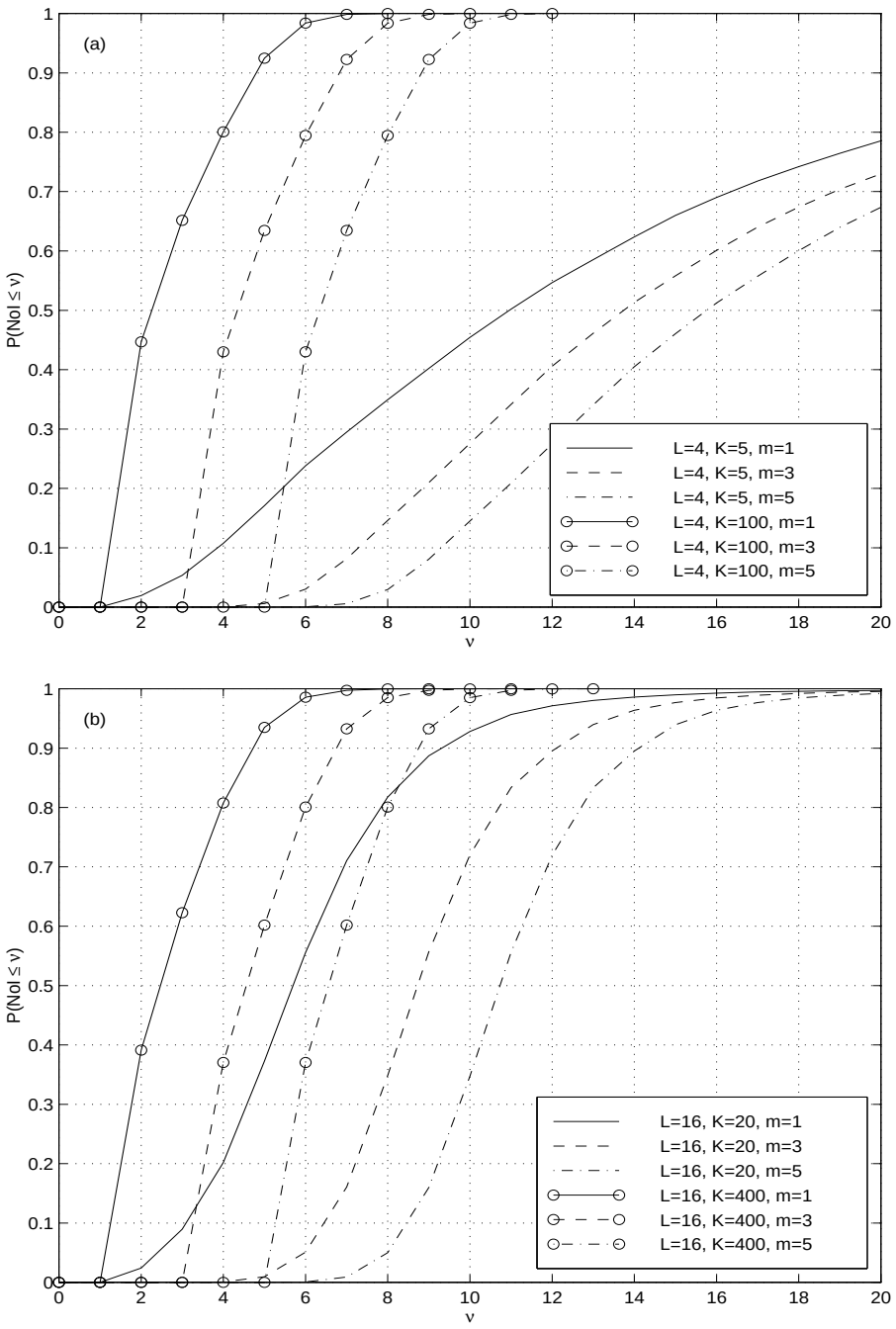


Figure 4.10: CDF of NoI's, for (a) $(L=4, K=5)$, and $(L=4, K=100)$, (b) $(L=16, K=20)$, and $(L=16, K=400)$. In all curves $\epsilon=0.1$ dB.

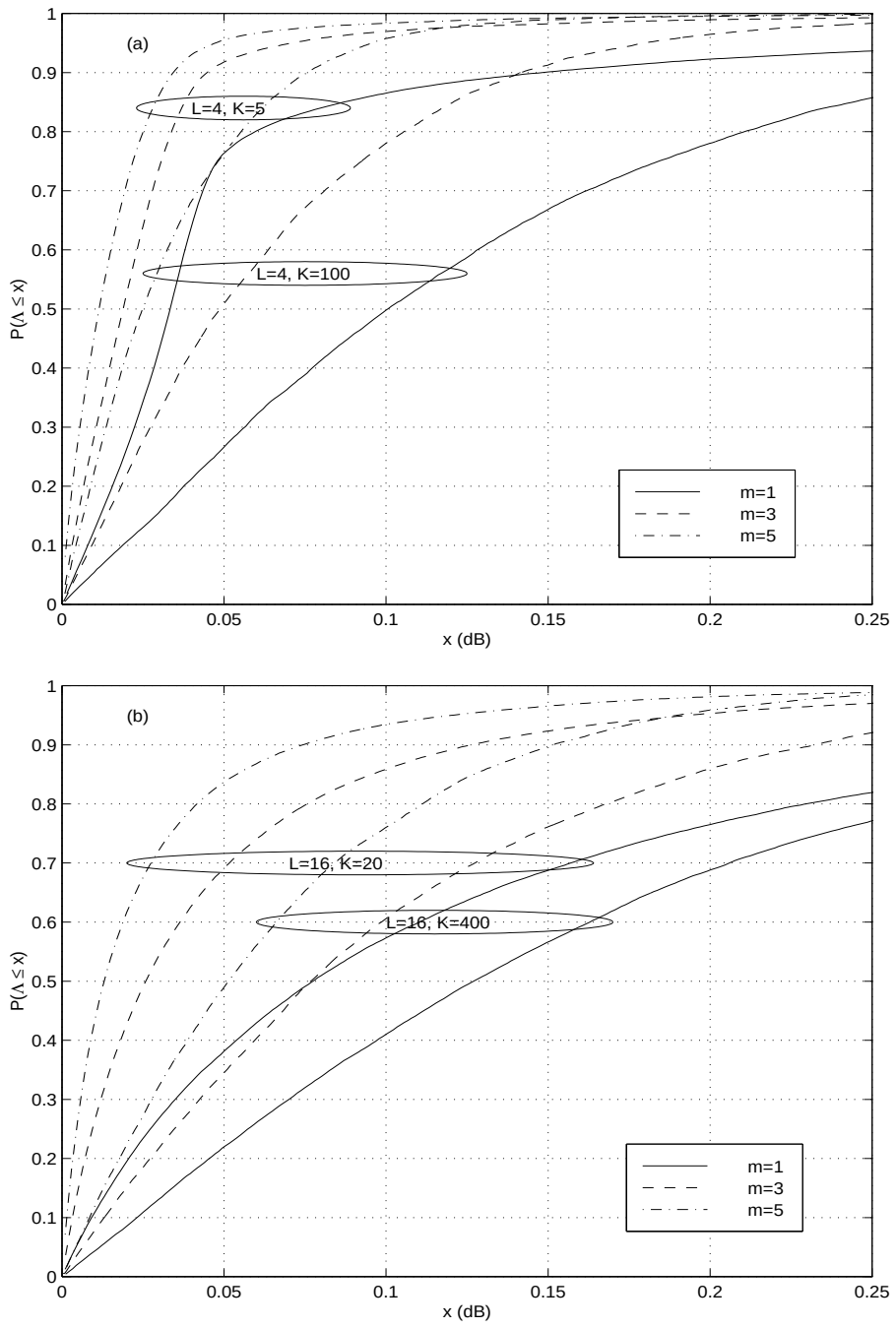


Figure 4.11: CDF of SIR error, $\Lambda$, for (a) $(L=4, K=5)$, $(L=4, K=100)$, (b) $(L=16, K=20)$, and $(L=16, K=400)$. In all curves $\epsilon=0.1$ dB.

# Chapter 5

## Correlated Interference Analysis in SDA Systems

### 5.1 Introduction

It has been demonstrated in Ch.s 3 and 4 that the total interference experienced in the reverse link of an SDA system with $L$ AE's is $L$ times less than that experienced in a conventional single antenna system. This yields an approximately $L$-fold increase in the reverse link SIR (signal-to-interference ratio), which can be transformed into an equivalent increase in the capacity and/or information rate. The reverse link capacity of a network of antennas is also investigated in [1]. Although the approach in that study is different than that used in this thesis, the results are in agreement.

However, one may suspect intuitively that the law of diminishing returns should apply with increasing number of AE's, since, when the number of AE's (and thus the number of users) increases, the AE's (as well as the users) would inevitably become closer to each other. In such a case, we may suspect that the signals received by different AE's may no longer be independent. In this thesis and in [1], the maximal ratio combining (MRC) scheme is used. In order for the MRC scheme to maximize the output SIR, the interference components at the branches of the combiner must be uncorrelated (independent). If this is the case, then the output SIR becomes equal to the algebraic sum of the branch SIR's. If, however, the interference components are correlated, then the output SIR will be less than the sum of the branch SIR's. In fact, in the case of significant correlation between the noise components of different branches, the MRC scheme will cease to be the preferred linear combining technique.

In order to demonstrate this fact, let us consider a hypothetical case, where the signal components at the branches of the combiner are different but the noise components are identical. In such a case, the best linear combining technique would be the selection combining; that is, selecting the branch with the highest SIR. In the limiting case of identical signal and interference components at the branches, there is no gain at all from combining, since amplification does not

increase the SIR. Therefore, in multi-antenna systems, it is critical to investigate the presence of correlated interference in the branches of the combiner. In this chapter, we will present an initial correlated interference analysis that may eventually enable us to determine whether the returns plateau with the increasing number of AE's.

The correlated interference analysis in a multi-antenna system is quite complicated, and thus, this is a rather long chapter. We will start from the simplest non-trivial case and then will analyze the more general cases in sequence. To be more specific, an SDA system with 2 AE's and 2 users will be considered first; then, the obtained results will be generalized for a system with 2 AE's and $K$ users, and finally, the most general case of $L$ AE's and $K$ users will be investigated. The effects of system parameters (such as the processing gain and size of the coverage region) and the user & AE locations on the correlated interference will be demonstrated.

To the best of our knowledge, there exists almost no literature in this topic. Therefore, we believe that our work will lay down a foundational framework that may yield a comprehensive understanding of the relationship between the number of AE's and the yielding system capacity in CDMA multi-antenna systems.

## 5.2 Definitions and Observations

We consider an SDA system with 2 AE's which are denoted as AE $I$ and AE $II$, and 2 users. We assume that user 1 is the user of interest.

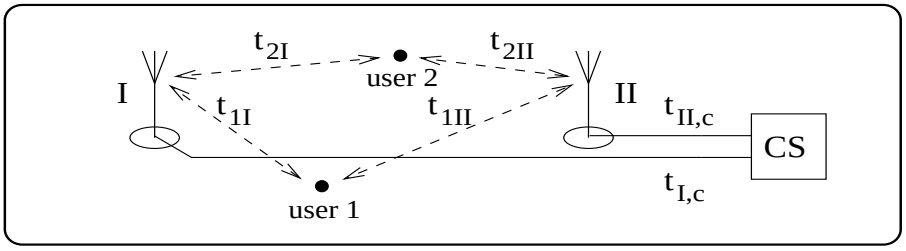


Figure 5.1: Propagation delays in an SDA system with $L = 2$ and $K = 2$.

Fig. 5.1 shows the propagation delays in the system. $t_{1I,t}$ is the total propagation time from user 1 to the CS through AE $I$, and it is equal to

$$t_{1I,t} = t_{1I} + t_{I,c}, \tag{5.1}$$

where $t_{1I}$ is the propagation time in the air from user 1 to AE $I$, and $t_{I,c}$ is that in the cable from AE $I$ to the CS. We note that $t_{I,c}$ does not depend on the location of user 1. Similarly,

$$t_{1II,t} = t_{1II} + t_{II,c}, \tag{5.2}$$

where $t_{1II,t}$ is the total propagation time from user 1 to the CS through AE $II$, $t_{1II}$ is that in the air from user 1 to AE $II$, and $t_{II,c}$ is that in the cable from AE $II$ to the CS. Propagation times regarding user 2 are defined in a similar way, and are obvious from Fig. 5.1.

The modulation process for the two users and the demodulation process for user 1 at the CS are illustrated in Fig. 5.2. Also, the spreading code and the related assumptions are depicted

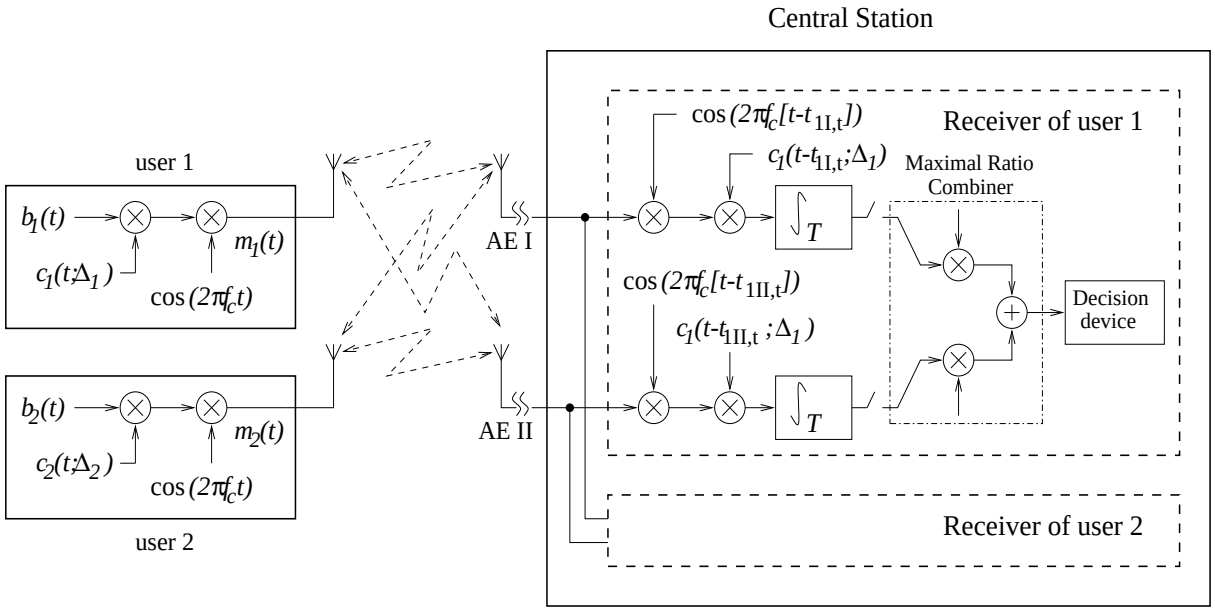


Figure 5.2: The modulation and demodulation processes in the reverse link of an SDA system with $L=2$ and $K=2$.

in Fig. 5.3. At user 1's receiver, the despreading at the $I$st branch is performed by multiplying

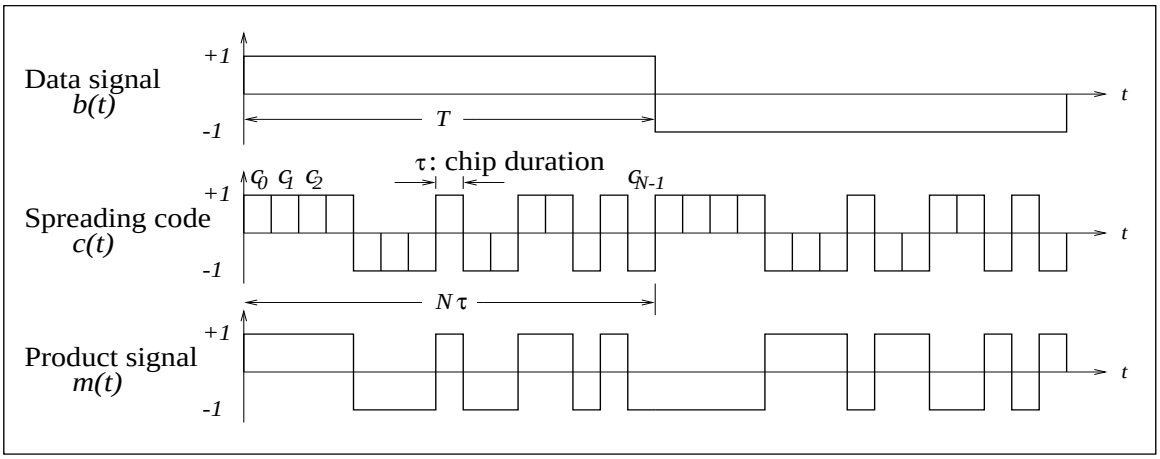


Figure 5.3: The data signal, $b(t)$, the spreading code, $c(t)$, and the product signal, $m(t) = b(t)c(t)$.

the received signal by $c_1(t - t_{1I,t}; \Delta_1)$, where $c_1(t)$ is the spreading code for user 1 and $\Delta_1$ is the

corresponding (normalized) code phase. $\Delta_1$ is represented in terms of $\tau$; in other words,

$$c_1(t - t_{1I,t}; \Delta_1) = c_1(t - t_{1I,t} - \Delta_1 \tau). \tag{5.3}$$

The situation at the *II*nd branch of user 1's receiver is similar; obviously, in this case the despreading is performed by $c_1(t - t_{1II,t}; \Delta_1)$.

Let $\zeta_{1I}$ and $\zeta_{1II}$ be the interference (noise) components (after demodulation) at the branches of the maximal ratio combiner of user 1, corresponding to AE's *I* and *II*, respectively. $\zeta_{1I}$ and $\zeta_{1II}$ are composed of two components as follows

$$\zeta_{1I} = \psi_{1I}\, n_{1I}, \tag{5.4}$$

$$\zeta_{1II} = \psi_{1II}\, n_{1II}, \tag{5.5}$$

where $\psi_{1I}$ and $\psi_{1II}$ are the deterministic components at the *I*st and *II*nd branches, respectively, and

$$n_{1I} = \langle c_1(t - t_{1I,t}; \Delta_1) c_2(t - t_{2I,t}; \Delta_2) \rangle\,, \tag{5.6}$$

$$n_{1II} = \langle c_1(t - t_{1II,t}; \Delta_1) c_2(t - t_{2II,t}; \Delta_2) \rangle\,, \tag{5.7}$$

are the random components, again at the *I*st and *II*nd branches, respectively. In Eqn.s 5.6 and 5.7, $\langle . \rangle$ denotes the inner product, i.e.,

$$\langle c_1(t) c_2(t) \rangle = \int_T c_1(t) c_2(t) dt, \tag{5.8}$$

where $T$ is the bit duration (refer to Fig. 5.3).

We are interested in evaluating the correlation coefficient of the random variables $\zeta_{1I}$ and $\zeta_{1II}$, $\rho_{12,I\text{–}II}$, which is defined as

$$\rho_{12,I\text{–}II} = \frac{\mathbf{E}(\zeta_{1I}\,\zeta_{1II}) - \mathbf{E}(\zeta_{1I})\mathbf{E}(\zeta_{1II})}{\sqrt{\mathbf{E}(\zeta_{1I}^2) - \mathbf{E}^2(\zeta_{1I})}\,\sqrt{\mathbf{E}(\zeta_{1II}^2) - \mathbf{E}^2(\zeta_{1II})}}. \tag{5.9}$$

One can easily show that Eqn. 5.9 reduces to

$$\rho_{12,I\text{–}II} = \frac{\mathbf{E}(n_{1I}\, n_{1II}) - \mathbf{E}(n_{1I})\mathbf{E}(n_{1II})}{\sqrt{\mathbf{E}(n_{1I}^2) - \mathbf{E}^2(n_{1I})}\,\sqrt{\mathbf{E}(n_{1II}^2) - \mathbf{E}^2(n_{1II})}}. \tag{5.10}$$

We conclude from Eqn.s 5.9 and 5.10 that the deterministic components $\psi_{1I}$ and $\psi_{1II}$ do not have any effect on the correlation coefficient. Therefore, in the rest of this chapter we will focus on $n_{1I}$ and $n_{1II}$.

We also define (normalized) differential code phase, $\Delta_{12}$, as the difference between the spreading code phases of users 1 and 2; i.e.,

$$\Delta_{12} = \Delta_1 - \Delta_2. \tag{5.11}$$

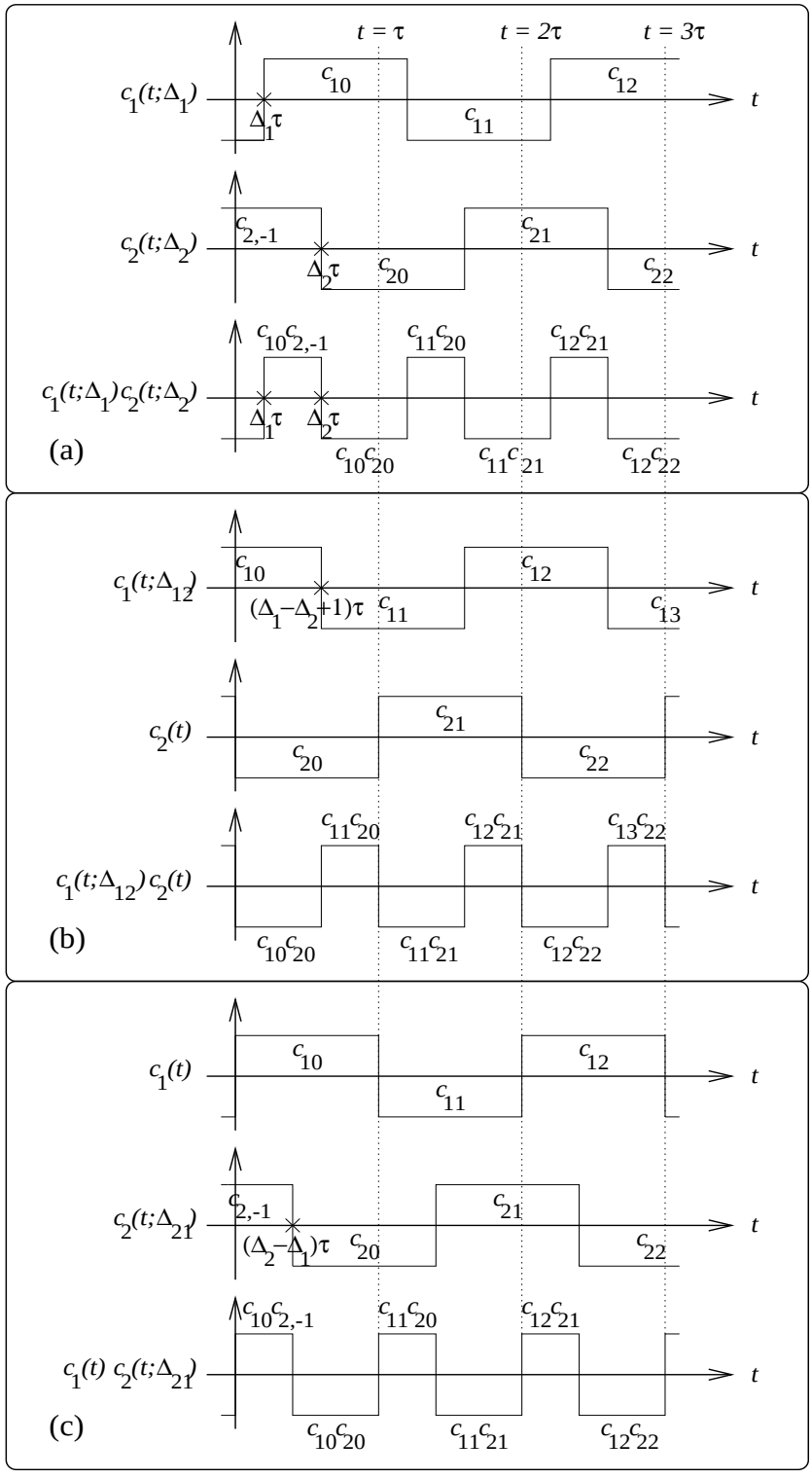


Figure 5.4: Demonstration of Eqn. 5.13: although (a) $c_1(t;\Delta_1)\ c_2(t;\Delta_2)$, (b) $c_1(t;\Delta_{12})\ c_2(t)$, and (c) $c_1(t)\ c_2(t;\Delta_{21})$, are all different time functions, $\langle c_1(t;\Delta_1)\ c_2(t;\Delta_2)\rangle = \langle c_1(t;\Delta_{12})\ c_2(t)\rangle = \langle c_1(t)\ c_2(t;\Delta_{21})\rangle$.

Without loss of generality, $\Delta_{12}$ is modeled as a uniform random variable in the interval $[0, 1)$.

Before we proceed, we will present some observations that will be used later in this chapter. We start by noting that although $c_1(t)c_2(t) \neq c_1(t-t_0)c_2(t-t_0)$, where $t_0$ denotes some delay, the following equation holds:

$$\langle c_1(t)c_2(t)\rangle = \langle c_1(t-t_0)c_2(t-t_0)\rangle. \tag{5.12}$$

From Eqn.s 5.3 and 5.12, we make the second observation:

$$\langle c_1(t;\Delta_1)c_2(t;\Delta_2)\rangle = \langle c_1(t;\Delta_{12})c_2(t)\rangle = \langle c_1(t)c_2(t;\Delta_{21})\rangle, \tag{5.13}$$

where $\Delta_{12}$ and $\Delta_{21}$ are defined according to Eqn. 5.11. The result of Eqn. 5.13 is depicted in Fig. 5.4. Also from Eqn. 5.12, the third observation follows right away:

$$\langle c_1(t-t_1)c_2(t-t_2)\rangle = \langle c_1(t-[t_1-t_2])c_2(t)\rangle = \langle c_1(t)c_2(t-[t_2-t_1])\rangle, \tag{5.14}$$

where $t_1$ and $t_2$ denote some delays. Finally, from Eqn.s 5.13 and 5.14, the most general case can be obtained as

$$\langle c_1(t-t_1;\Delta_1)c_2(t-t_2;\Delta_2)\rangle = \langle c_1(t-[t_1-t_2];\Delta_{12})c_2(t)\rangle = \langle c_1(t)c_2(t-[t_2-t_1];\Delta_{21})\rangle. \tag{5.15}$$

However, it is important to note that for some delays $t_{11}$ and $t_{12}$, with $t_{11} \neq t_{12}$,

$$\langle c_1(t-t_{11})c_2(t)\rangle\langle c_1(t-t_{12})c_2(t)\rangle \neq \langle c_1(t-[t_{11}-t_{12}])c_2(t)\rangle\langle c_1(t)c_2(t)\rangle; \tag{5.16}$$

but rather, the left hand side depends on the actual values of $t_{11}$ and $t_{12}$. It will become apparent in Section 5.3 that this result will complicate our analysis.

## 5.3 Correlation Coefficient Analysis for Synchronous Users

In this section and the next one, the correlation coefficient corresponding to the noise components at the *I*st and *II*nd branches of the maximal ratio combiner of user 1, $\rho_{12,I\text{–}II}$, will be determined. As a starting point, we make the assumption that users are synchronized, in other words, $\Delta_1 = \Delta_2$, that is, $\Delta_{12} = 0$. The general case, where $\Delta_{12}$ is a uniform random variable in the region $[0, 1)$, will be considered in Section 5.4.

We will start by demonstrating the dependence of $\rho_{12,I\text{–}II}$ on the propagation delays incurred in the system.

### 5.3.1 Dependence of Correlation Coefficient on Propagation Delays

Eqn. 5.15 can be used to simplify $n_{1I}$ and $n_{1II}$, defined by Eqn.s 5.6 and 5.7, as

$$n_{1I} = \langle c_1(t-t_{1I,t};\Delta_1)c_2(t-t_{2I,t};\Delta_1)\rangle = \langle c_1(t-t_{12I})c_2(t)\rangle, \tag{5.17}$$

$$n_{1II} = \langle c_1(t - t_{1II,t}; \Delta_1) c_2(t - t_{2II,t}; \Delta_1) \rangle = \langle c_1(t - t_{12II}) c_2(t) \rangle, \tag{5.18}$$

where,

$$t_{12I} \;=\; t_{1I,t} - t_{2I,t} \;=\; (t_{1I} + t_{I,c}) - (t_{2I} + t_{I,c}) \;=\; t_{1I} - t_{2I}, \tag{5.19}$$

$$t_{12II} \;=\; t_{1II,t} - t_{2II,t} \;=\; (t_{1II} + t_{II,c}) - (t_{2II} + t_{II,c}) \;=\; t_{1II} - t_{2II}. \tag{5.20}$$

In the simplification of $t_{12I}$ and $t_{12II}$, Eqn.s 5.1 and 5.2 are used. It is observed from Eqn.s 5.19 and 5.20 that $t_{12I}$ and $t_{12II}$ depend only on the propagation delays in the air.

Without loss of generality we will first assume that $0 \leq t_{12I} \leq \tau$; we will consider the most general case later in this section.

Now, $n_{1I}$ can be computed as (refer to Fig. 5.4)

$$n_{1I} = \sum_{k=0}^{N-1} \left[ (\tau - t_{12I}) c_{1,k}\, c_{2,k} + t_{12I}\, c_{1,k}\, c_{2,k+1} \right]. \tag{5.21}$$

We assume that $\{c_{ik}\}$ are independent identically distributed equi-probable Bernoulli random variables with values equal to $\pm 1$. With this assumption, it is easy to show that

$$\mathbf{E}(n_{1I}) = 0. \tag{5.22}$$

The variance of $n_{1I}$ can be computed from Eqn. 5.21, by realizing that $c_{ik}^2 = 1$, as

$$\mathbf{E}(n_{1I}^2) = N \left( (\tau - t_{12I})^2 + t_{12I}^2 \right). \tag{5.23}$$

It is observed from Eqn. 5.21 that in order for $n_{1I}$ and $n_{1II}$ to be correlated, $n_{1II}$ should have components in the form of $c_{1k}\, c_{2k}$ and/or $c_{1k}\, c_{2,k+1}$. It is not difficult to show that for $t_{12II} < -\tau$ or $t_{12II} > 2\tau$, $n_{1II}$ does not have such components. We will investigate the remaining range for $t_{12II}$ in three intervals, namely, $-\tau \leq t_{12II} \leq 0$, $0 \leq t_{12II} \leq \tau$, and $\tau \leq t_{12II} \leq 2\tau$.

If $-\tau \leq t_{12II} \leq 0$, then $n_{1II}$ can be shown to be equal to

$$n_{1II} = \sum_{k=0}^{N-1} \left[ -t_{12II}\, c_{1,k}\, c_{2,k-1} + (t_{12II} + \tau) c_{1,k}\, c_{2,k} \right] \tag{5.24}$$

The mean and variance of $n_{1II}$ are found as

$$\mathbf{E}(n_{1II}) = 0, \tag{5.25}$$

$$\mathbf{E}(n_{1II}^2) = N \left( (t_{12II} + \tau)^2 + t_{12II}^2 \right). \tag{5.26}$$

Now, using Eqn.s 5.21 and 5.24, the correlation, $\mathbf{E}(n_{1I}\, n_{1II})$, can be computed as

$$\mathbf{E}(n_{1I}\, n_{1II}) = N(\tau - t_{12I})(t_{12II} + \tau). \tag{5.27}$$

Substituting Eqn.s 5.23, 5.26, and 5.27, in Eqn. 5.10, $\rho_{12,I-II}$ can be obtained as

$$\rho_{12,I-II} = \frac{(\tau - t_{12I})(t_{12II} + \tau)}{\sqrt{(\tau - t_{12I})^2 + t_{12I}^2}\sqrt{t_{12II}^2 + (t_{12II} + \tau)^2}}. \tag{5.28}$$

The calculations are similar for the other intervals. If $0 \leq t_{12II} \leq \tau$, then $n_{1II}$ is found as

$$n_{1II} = \sum_{k=0}^{N-1} \left[(\tau - t_{12II})c_{1,k}\, c_{2,k} + t_{12II}\, c_{1,k}\, c_{2,k+1}\right]. \tag{5.29}$$

From above, the mean and variance are obtained as

$$\mathbf{E}(n_{1II}) = 0, \tag{5.30}$$

$$\mathbf{E}(n_{1II}^2) = N\left(t_{12II}^2 + (\tau - t_{12II})^2\right) \tag{5.31}$$

From Eqn.s 5.21 and 5.29, the correlation is calculated as

$$\mathbf{E}(n_{1I} n_{1II}) = N\left[(\tau - t_{12I})(\tau - t_{12II}) + t_{12I}\, t_{12II}\right], \tag{5.32}$$

and from Eqn.s 5.23, 5.31, and 5.32, the correlation coefficient is found as

$$\rho_{12,I-II} = \frac{(\tau - t_{12I})(\tau - t_{12II}) + t_{12I}\, t_{12II}}{\sqrt{(\tau - t_{12I})^2 + t_{12I}^2}\sqrt{t_{12II}^2 + (\tau - t_{12II})^2}}. \tag{5.33}$$

Finally, for $\tau \leq t_{12II} \leq 2\tau$, $n_{1II}$ is found as

$$n_{1II} = \sum_{k=0}^{N-1} \left[(2\tau - t_{12II})c_{1,k}\, c_{2,k+1} + (t_{12II} - \tau)\, c_{1,k}\, c_{2,k+2}\right], \tag{5.34}$$

with

$$\mathbf{E}(n_{1II}) = 0, \tag{5.35}$$

$$\mathbf{E}(n_{1II}^2) = N\left((2\tau - t_{12II})^2 + (t_{12II} - \tau)^2\right). \tag{5.36}$$

The correlation is calculated from Eqn.s 5.21 and 5.34 as

$$\mathbf{E}(n_{1I}\, n_{1II}) = N t_{12I}(2\tau - t_{12II}), \tag{5.37}$$

and $\rho_{12,I-II}$ is computed using Eqn.s 5.23, 5.36, and 5.37 as

$$\rho_{12,I-II} = \frac{t_{12I}(2\tau - t_{12II})}{\sqrt{(\tau - t_{12I})^2 + t_{12I}^2}\sqrt{(\tau - t_{12II})^2 + (t_{12II} - \tau)^2}}. \tag{5.38}$$

From Eqn.s 5.28, 5.33, and 5.38, $\rho_{12,I-II}$ is plotted for various values of $t_{12I}$, in the range of $[0, \tau]$, in Fig. 5.5. As it is already discussed, if $0 < t_{12I} < \tau$ then the range of $t_{12II}$ for nonzero $\rho_{12,I-II}$ is $(-\tau, 2\tau)$. Also, the 3-dimensional plot of $\rho_{12,I-II}$ in the analyzed intervals of $0 \leq t_{12I} \leq \tau$, and $-\tau \leq t_{12II} \leq 2\tau$ is shown in Fig. 5.6. We note that in Fig. 5.6, the intersection

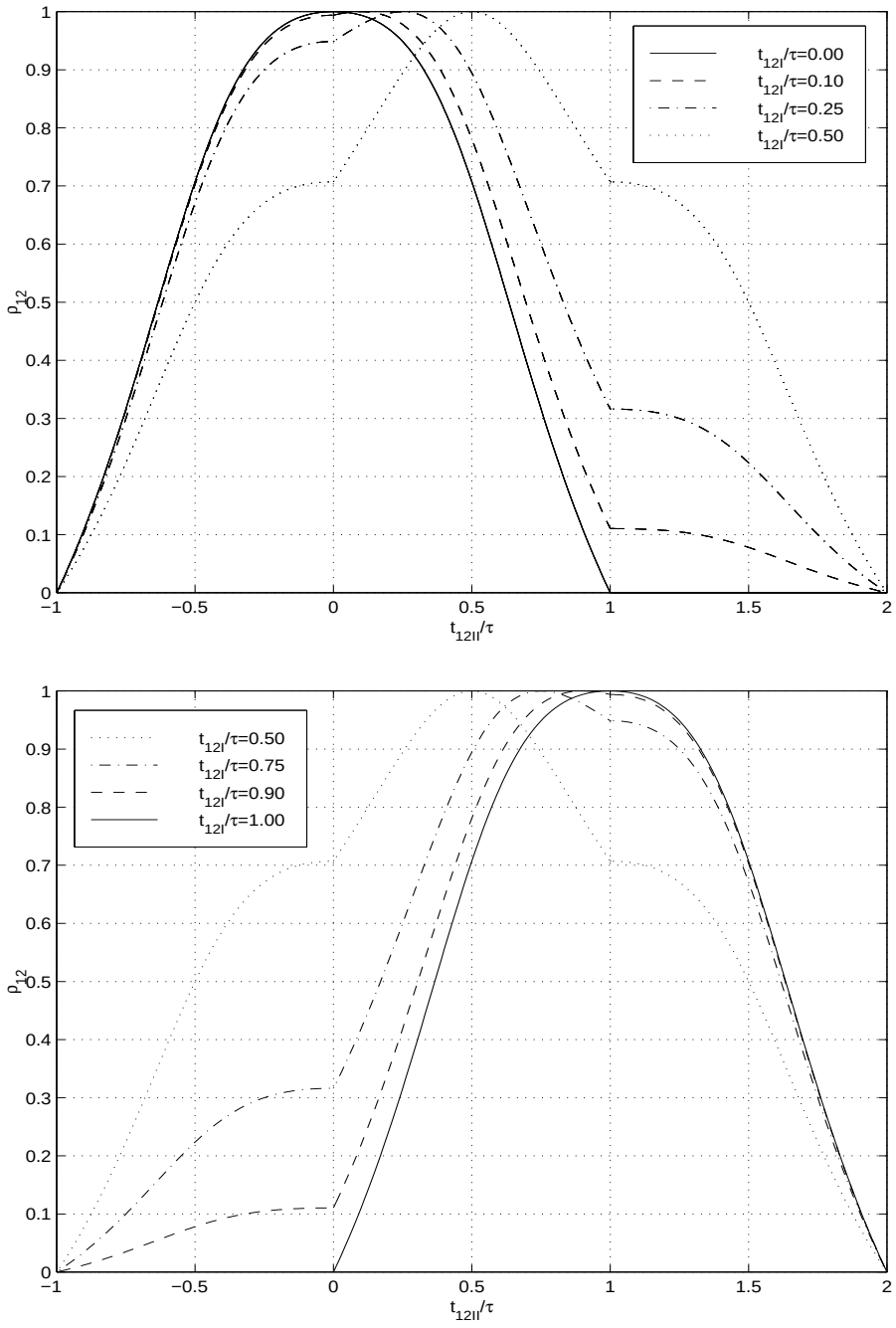


Figure 5.5: Correlation coefficient as a function of $t_{12II}$, for $t_{12I}/\tau = 0.00$, 0.10, 0.25, 0.50, 0.75, 0.90, and 1.00, for synchronous users ($\Delta_{12}=0$).

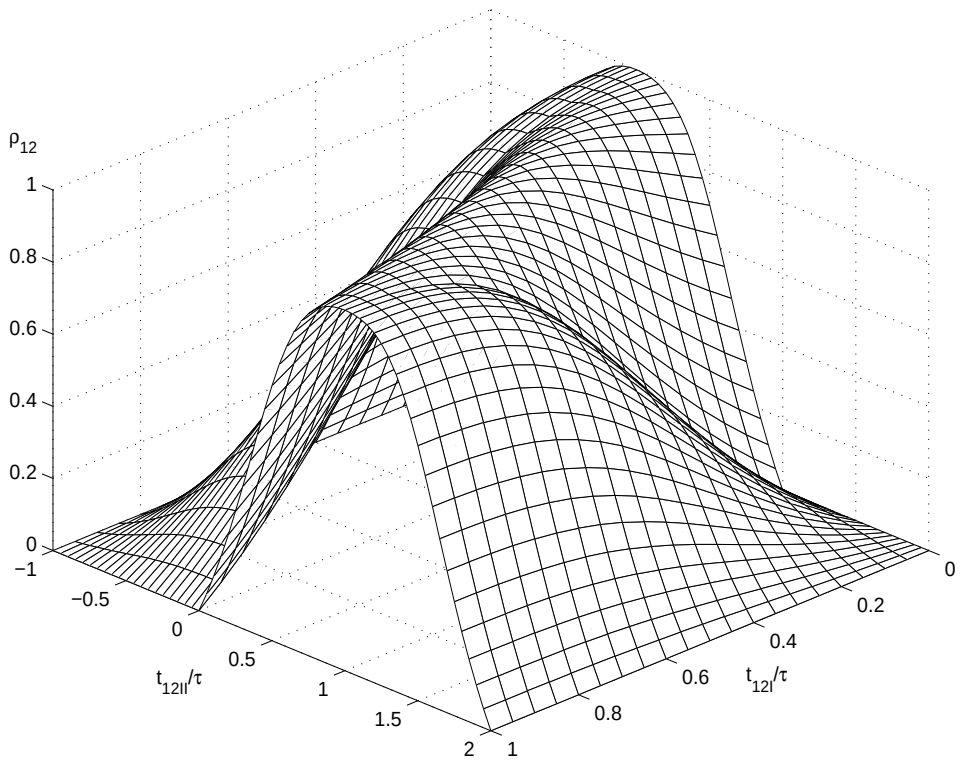


Figure 5.6: Correlation coefficient as a function of $t_{12I}$ and $t_{12II}$, for $0 \leq t_{12I} \leq \tau$ and $-\tau \leq t_{12II} \leq 2\tau$, for synchronous users ($\Delta_{12}=0$).

of the vertical $\rho_{12,I\text{–}II}$–$t_{12II}$ plane with the 3-dimensional plot at certain values of $t_{12I}$ yield the curves shown in Fig. 5.5.

The results obtained so far for the case of $0 \leq t_{12I} \leq \tau$, can be generalized for $t_{12I}$ values in any interval. Without giving the details, we will state $\rho_{12,I\text{–}II}$ for the general case of $n\tau \leq t_{12I} \leq$

$(n+1)\tau$, where $n$ is an integer:

$$\rho_{12,I-II} = \begin{cases} \dfrac{[(n+1)\tau - t_{12I}][t_{12II} - (n-1)\tau]}{\sqrt{[(n+1)\tau - t_{12I}]^2 + (t_{12I} - n\tau)^2}\sqrt{(n\tau - t_{12II})^2 + [t_{12II} - (n-1)\tau]^2}}, \\ \qquad\qquad \text{if } (n-1)\tau \le t_{12II} \le n\tau; \\ \dfrac{[(n+1)\tau - t_{12I}][(n+1)\tau - t_{12II}] \; + \; (t_{12I} - n\tau)(t_{12II} - n\tau)}{\sqrt{[(n+1)\tau - t_{12I}]^2 + (t_{12I} - n\tau)^2}\sqrt{[(n+1)\tau - t_{12II}]^2 + (t_{12II} - n\tau)^2}}, \\ \qquad\qquad \text{if } n\tau \le t_{12II} \le (n+1)\tau; \\ \dfrac{(t_{12I} - n\tau)[(n+2)\tau - t_{12II}]}{\sqrt{[(n+1)\tau - t_{12I}]^2 + (t_{12I} - n\tau)^2}\sqrt{[(n+2)\tau - t_{12II}]^2 + [t_{12II} - (n+1)\tau]^2}}, \\ \qquad\qquad \text{if } (n+1)\tau \le t_{12II} \le (n+2)\tau. \end{cases} \tag{5.39}$$

Then, $\rho_{12,I-II}$ given by Eqn.s 5.28, 5.33, and 5.38 corresponds to the $n=0$ case. In Fig. 5.7, the

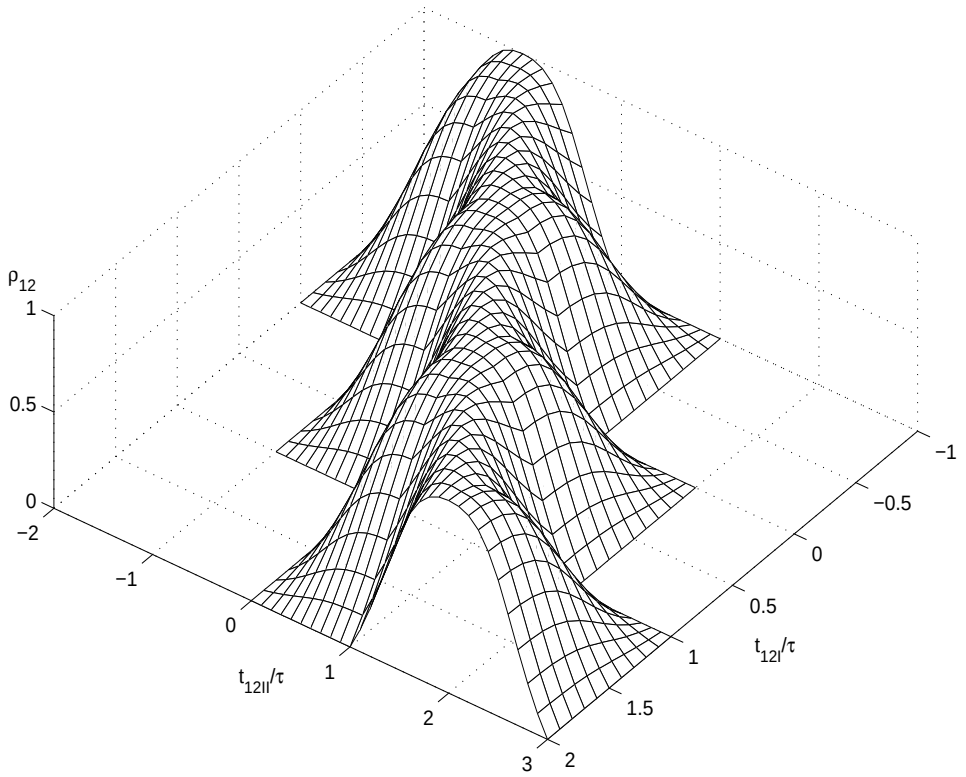


Figure 5.7: Correlation coefficient as a function of $t_{12I}$ and $t_{12II}$, for synchronous users ($\Delta_{12} = 0$).

general expression for $\rho_{12,I-II}$ given in Eqn. 5.39 is plotted with respect to $t_{12I}$ and $t_{12II}$.

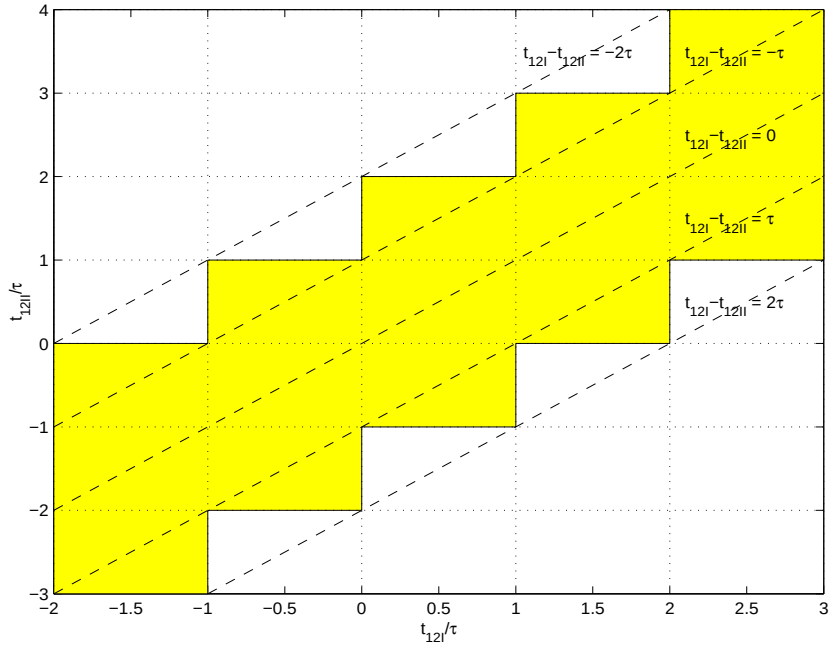


Figure 5.8: Non-zero $\rho_{12,I-II}$ region in terms of $t_{12I}$ and $t_{12II}$, for synchronous users ($\Delta_{12}=0$).

It is observed from Eqn. 5.39 and Fig. 5.7 that

$$\begin{aligned} t_{12I} = n\tau \longrightarrow & \begin{cases} \rho_{12,I-II} = 0, & \text{for } t_{12II} \le (n-1)\tau \text{ and } t_{12II} \ge (n+1)\tau \\ 0 < \rho_{12,I-II} \le 1, & \text{for } (n-1)\tau < t_{12II} < (n+1)\tau, \end{cases} \\ n\tau < t_{12I} < (n+1)\tau \longrightarrow & \begin{cases} \rho_{12,I-II} = 0, & \text{for } t_{12II} \le (n-1)\tau \text{ and } t_{12II} \ge (n+2)\tau \\ 0 < \rho_{12,I-II} \le 1, & \text{for } (n-1)\tau < t_{12II} < (n+2)\tau, \end{cases} \end{aligned} \tag{5.40}$$

where $n$ is an integer. The regions of $t_{12I}$ and $t_{12II}$ for which $\rho_{12,I-II}$ is nonzero is shown in Fig. 5.8 by the shaded area. Fig. 5.8 can be thought of as looking at Fig. 5.7 from above (the z-axis).

So far, the dependence of $\rho_{12,I-II}$ on $t_{12I}$ and $t_{12II}$ is investigated. Since the propagation time depends on the distance, there is an equivalent dependence of $\rho_{12,I-II}$ on the location of users and AE's.

### 5.3.2 Dependence of Correlation Coefficient on User and AE Locations

In this section, the dependence of $\rho_{12,I-II}$ on the user and AE locations will be investigated. The goal is to find the region for user 2 which will result in a non-zero $\rho_{12,I-II}$, for a given set of AE and user 1 locations. The time domain requirements for this region is already known from Eqn. 5.40. Therefore, the task is to find the equivalent of Eqn. 5.40 in terms of distance.

As it is well known, the propagation time, $t$, depends on the distance, $d$, as

$$t = \frac{d}{c}, \tag{5.41}$$

where $c$ is the speed of light which will be taken as $3 \times 10^8$ m/sec. Therefore, from Eqn.s 5.19, 5.20, and 5.41, $t_{12I}$ and $t_{12II}$ can be stated in terms of distances as

$$t_{12I} = \frac{d_{1I} - d_{2I}}{c}, \tag{5.42}$$

$$t_{12II} = \frac{d_{1II} - d_{2II}}{c}, \tag{5.43}$$

where $d_{ij}$ is the distance between user $i$ and AE $j$, $i \in \{1, 2\}$, $j \in \{I, II\}$.

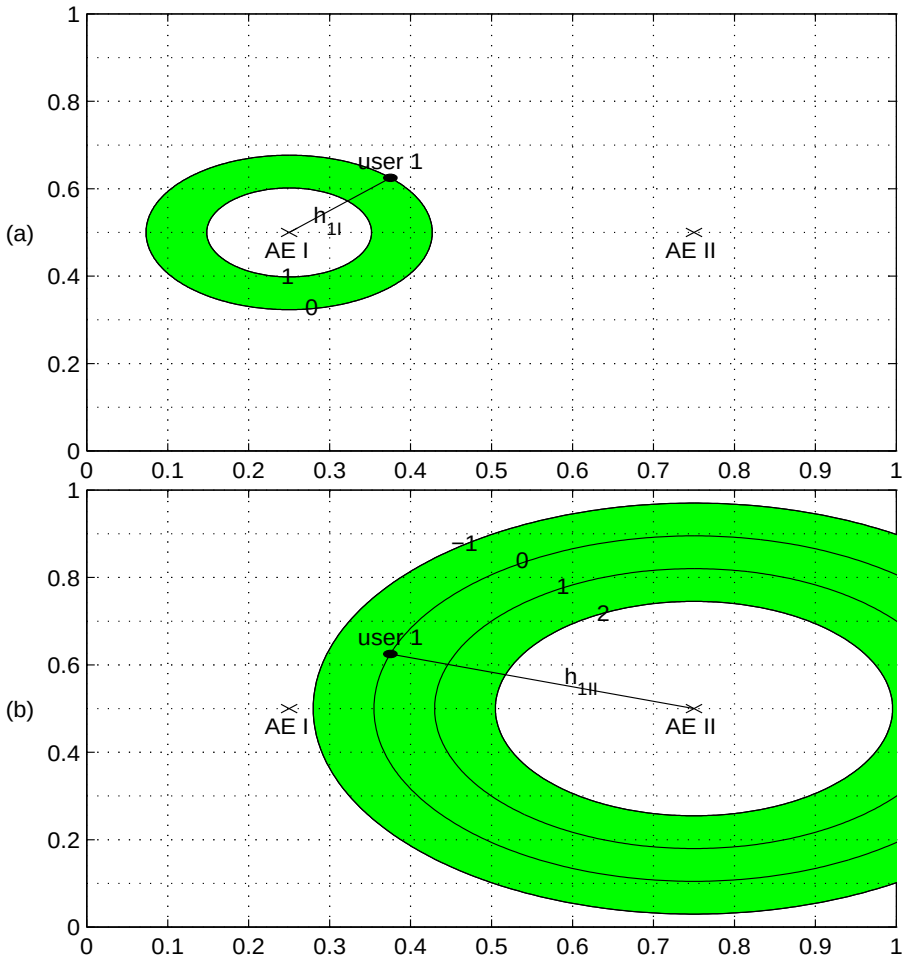


Figure 5.9: For synchronous users ($\Delta_{12}=0$), the shaded areas show the following regions: (a) $0 < t_{12I} < \tau \equiv 0 < (h_{1I} - h_{2I}) < 0.075$, (b) $-\tau \leq t_{12II} \leq 2\tau \equiv -0.075 < (h_{1II} - h_{2II}) < 0.15$. In both figures $s=400$ and $R_c=10$ Mcps.

We will work on a unit square region with side 1 m. Distances in this unit region will be denoted by $h$. In other words, $h$ is the normalized distance which is related to the actual

distance, $d$, as

$$d = h\, s, \tag{5.44}$$

where $s$ is the scaling factor. For instance, if $s=500$, this means that the service region has the shape of a square with side length 500 meters. Also, we define the chip rate, $R_c$, as

$$R_c = \frac{1}{\tau}. \tag{5.45}$$

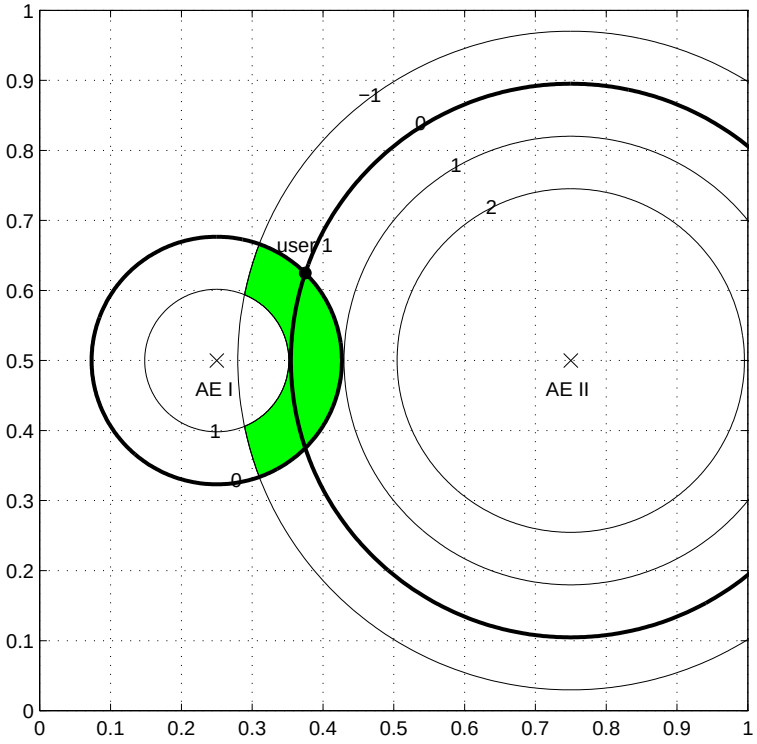


Figure 5.10: For synchronous users ($\Delta_{12}=0$), the shaded area shows the following region: $0 < (h_{1I} - h_{2I}) < 0.075$ and $-0.075 < (h_{1II} - h_{2II}) < 0.15$ ($s$=400 and $R_c$=10 Mcps).

We will first find the region corresponding to $n\tau < t_{12I} < (n+1)\tau$. This region is a function of the locations of users 1 and 2, and AE $I$ (but, not AE $II$). Then, we will find the region corresponding to $(n-1)\tau < t_{12II} < (n+2)\tau$, which is a function of the locations of users 1 and 2, and AE $II$ (but, not AE $I$).

We start by analyzing the $n=0$ case. Using Eqn.s 5.42, 5.43 and 5.44, we can write

$$0 \;<\; t_{12I} = t_{1I} - t_{2I} \;<\; \tau \;\;\longrightarrow\;\; 0 \;<\; (h_{1I} - h_{2I}) \;<\; \frac{c\tau}{s}, \tag{5.46}$$

$$-\tau \;<\; t_{12II} = t_{1II} - t_{2II} \;<\; 2\tau \;\;\longrightarrow\;\; -\frac{c\tau}{s} \;<\; (h_{1II} - h_{2II}) \;<\; 2\frac{c\tau}{s}. \tag{5.47}$$

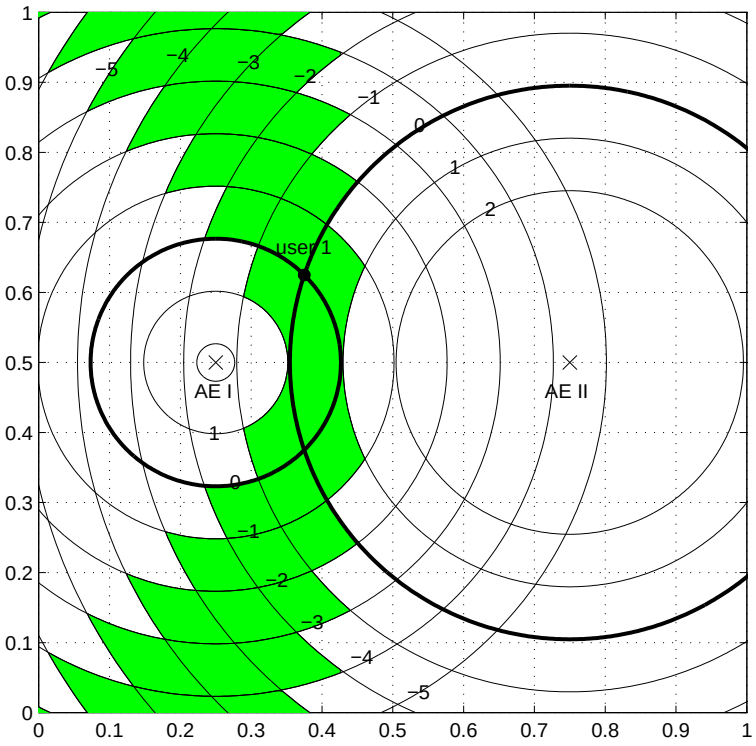


Figure 5.11: The *caution zone* for user 1 ($s = 400$ and $R_c = 10$ Mcps), for synchronous users ($\Delta_{12}=0$).

It is observed from Eqn. 5.40 that the intersection of these two regions yields the non-zero $\rho_{12,I\text{–}II}$ region for user 2 for $n = 0$. In a similar way, the corresponding regions for other $n$ values can also be found. We call the union of all such regions the *caution zone* for user 1; because, the interference resulting from a user in this zone, at the $I$st branch of user 1's combiner at the CS, will be correlated with the corresponding interference at the $II$nd branch.

As an example, we consider a system with $s = 400$ and $R_c = 10$ Mcps (Mega chips/sec). Then, $c\tau/s = 0.075$. We assume that AE's $I$, $II$, and user 1 are placed at the coordinates (.25,.5), (.75,.5), and (.375,.625), respectively, on the unit service region. The region for which $0 < (h_{1I}-h_{2I}) < 0.075$ is shown in Fig. 5.9(a) by the shaded area. In Fig. 5.9(a), the numbers "0" and "1" on the circles indicate that for any user 2 location on those circles, $(t_{1I}-t_{2I})/\tau=0$, and 1, respectively. In the same way, the region $-0.075 < (h_{1II}-h_{2II}) < 0.15$ is shown in Fig. 5.9(b) by the shaded area. Similar to Fig. 5.9(a), the numbers "-1" through "2" on the circles in Fig. 5.9(b) indicate that for any user 2 location on those circles, $(t_{1II}-t_{2II})/\tau=-1$, through 2, respectively.

The intersection of the regions shown in Fig.s 5.9(a) and (b) is depicted in Fig. 5.10. Similarly, using Eqn.s 5.40, 5.42, 5.43 and 5.44, the corresponding regions for other $n$ values can also be

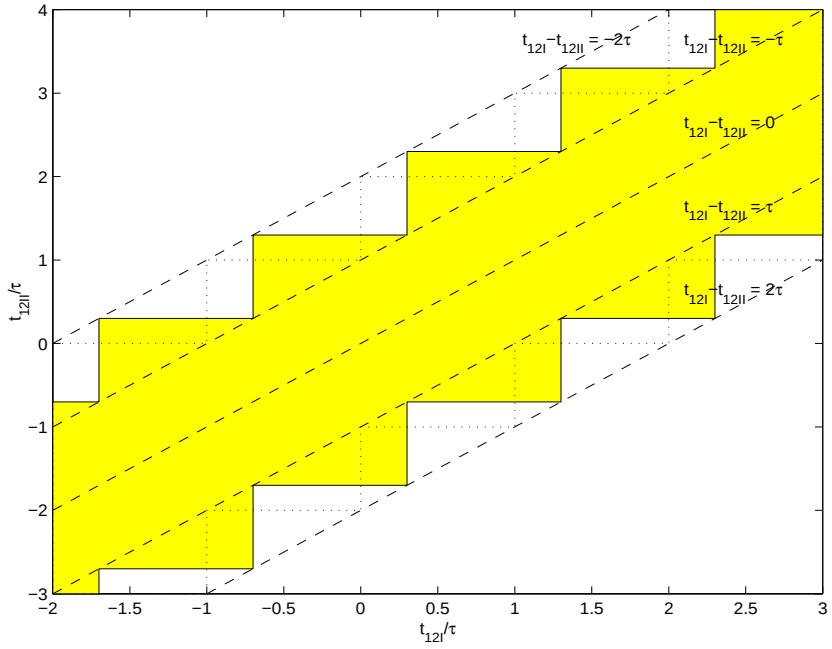


Figure 5.12: Non-zero $\rho_{12,I-II}$ region in terms of $t_{12I}$ and $t_{12II}$, for asynchronous users ($\Delta_{12} = 0.7$).

found. We realize that for $n \geq 1$, the conditions given in Eqn.s 5.46 and 5.47 do not yield an overlapping region. In Fig. 5.11 the *caution zone* for user 1 is shown, which is the union of the regions corresponding to $n = -6, -5, \cdots, 0$.

We note that the analysis presented so far is for the case where the users are synchronized. Next, we will investigate the general case where users 1 and 2 are asynchronous.

## 5.4 Correlation Coefficient Analysis for Asynchronous Users

In this section, we turn our attention to the effect of the chip phase in the correlation analysis. Based on Eqn.s 5.6, 5.7, 5.13, 5.19, and 5.20, $n_{1I}$ and $n_{1II}$ can be written as

$$n_{1I} = \langle c_1(t - t_{12I}; \Delta_{12}) c_2(t) \rangle, \tag{5.48}$$

$$n_{1II} = \langle c_1(t - t_{12II}; \Delta_{12}) c_2(t) \rangle. \tag{5.49}$$

Using Eqn. 5.3, the above $n_{1I}$ and $n_{1II}$ expressions take the following form:

$$n_{1I} = \langle c_1(t - t_{12I} - \Delta_{12}\tau) c_2(t) \rangle, \tag{5.50}$$

$$n_{1II} = \langle c_1(t - t_{12II} - \Delta_{12}\tau) c_2(t) \rangle. \tag{5.51}$$

Defining $t'_{12I}$ and $t'_{12II}$ as

$$t'_{12I} = t_{12I} + \Delta_{12}\tau, \tag{5.52}$$

$$t'_{12II} = t_{12II} + \Delta_{12}\tau, \tag{5.53}$$

Eqn.s 5.50 and 5.51 can be rewritten as

$$n_{1I} = \langle c_1(t - t'_{12I})c_2(t)\rangle, \tag{5.54}$$

$$n_{1II} = \langle c_1(t - t'_{12II})c_2(t)\rangle. \tag{5.55}$$

Comparing Eqn.s 5.54 and 5.55 with those for the synchronous users, namely, Eqn.s 5.17 and 5.18, we notice that both sets of equations are in the same form with the only difference that $t_{12I}$ and $t_{12II}$ in Eqn.s 5.17 and 5.18 are replaced with $t'_{12I}$ and $t'_{12II}$, respectively, in Eqn.s 5.54 and 5.55. Therefore, we conclude that the $\rho_{12,I\text{–}II}$ expressions found in the previous section (such as Eqn. 5.39) as well as the curves plotted in Fig.s 5.5 and 5.7 are still valid provided that $t_{12I}$ and $t_{12II}$ are substituted by $t'_{12I}$ and $t'_{12II}$, respectively.

Based on Eqn.s 5.52, 5.53, and the above observation, Eqn. 5.40 can be modified as

$$\begin{aligned}
&t_{12I} = (n - \Delta_{12})\tau \;\longrightarrow \\
&\qquad \begin{cases} \rho_{12,I\text{–}II} = 0, & \text{for } t_{12II} \le [(n-1) - \Delta_{12}]\tau \text{ and } t_{12II} \ge [(n+1) - \Delta_{12}]\tau \\ 0 < \rho_{12,I\text{–}II} \le 1, & \text{for } [(n-1) - \Delta_{12}]\tau < t_{12II} < [(n+1) - \Delta_{12}]\tau, \end{cases} \\
&(n - \Delta_{12})\tau < t_{12I} < [(n+1) - \Delta_{12}]\tau \;\longrightarrow \\
&\qquad \begin{cases} \rho_{12,I\text{–}II} = 0, & \text{for } t_{12II} \le [(n-1) - \Delta_{12})]\tau \text{ and } t_{12II} \ge [(n+2) - \Delta_{12}]\tau \\ 0 < \rho_{12,I\text{–}II} \le 1, & \text{for } [(n-1) - \Delta_{12}]\tau < t_{12II} < [(n+2) - \Delta_{12}]\tau. \end{cases}
\end{aligned} \tag{5.56}$$

In fact, Eqn. 5.40 can be obtained from Eqn. 5.56 for the special case of $\Delta_{12}=0$.

Similar to Fig. 5.8 which is drawn based on Eqn. 5.40, the region for non-zero $\rho_{12,I\text{–}II}$ is shown in Fig. 5.12 which is drawn based on Eqn. 5.56. In Fig. 5.12, $\Delta_{12}$ is taken to be 0.7. Also in this figure, the dotted lines show the boundary of the non-zero $\rho_{12,I\text{–}II}$ region for the synchronous case (refer to Fig. 5.8) for comparison.

Following the same steps presented in Section 5.3.2, the time domain expressions, given in Eqn. 5.56 and shown in Fig. 5.12 for the non-zero $\rho_{12,I\text{–}II}$ region, can be converted into the expressions in terms of distances on the unit service region. For this conversion, Eqn.s 5.42, 5.43, 5.44, 5.52, and 5.53 should be used in Eqn. 5.56. Since the procedure is very similar to the one presented in Section 5.3.2, we will skip the analytical intermediate expressions and will show only the resulting *caution zone* for user 1.

We continue with the example introduced in Section 5.3.2 (a system with $s = 400$ and $R_c = 10$ Mcps). In Fig. 5.13, the *caution zone* for user 1 is shown for the case of $\Delta_{12} = 0.5$. The shaded

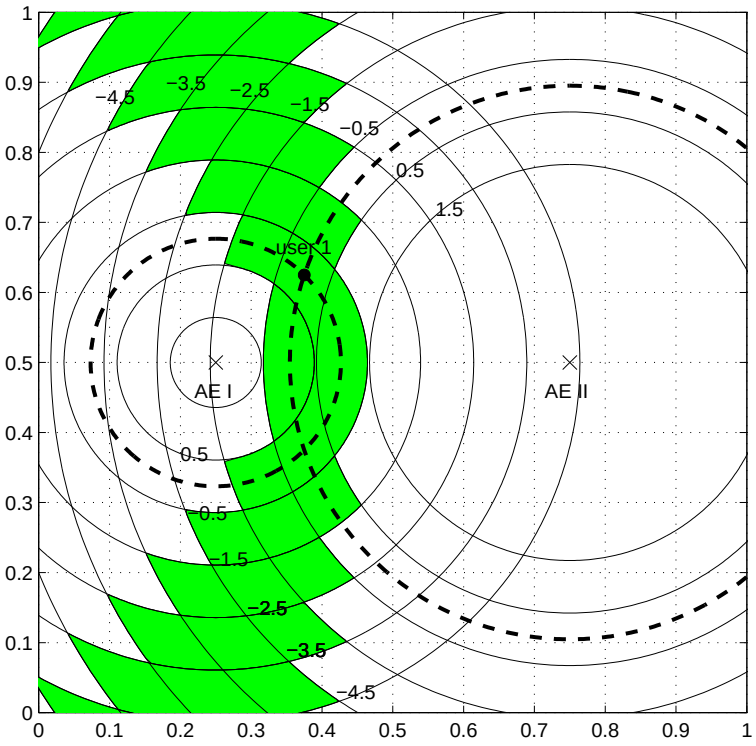


Figure 5.13: The *caution zone* for user 1 ($s = 400$ and $R_c = 10$ Mcps), for asynchronous users ($\Delta_{12} = 0.5$).

regions in Fig. 5.13 correspond to $n = 1, 2, \cdots, 7$. Similar to Fig. 5.11, the numbers "-4.5" through "0.5" on the circles in Fig. 5.13, which have centers at AE $I$, indicate that for any user 2 location on those circles, $(t_{1I} - t_{2I})/\tau = -4.5$, through 0.5, respectively. In the same way, the numbers "-4.5" through "1.5", on the circles which have centers at AE $II$, indicate that for any user 2 location on those circles, $(t_{1II} - t_{2II})/\tau = -4.5$, through 1.5, respectively.

Finally, caution zones for other $\Delta_{12}$ values in the range $[0, 1)$ can also be drawn following the same procedure described in this section.

## 5.5 Approximation of the Caution Zones

We start by defining the differential delay, $\Delta t_{12,I-II}$, from $t'_{12I}$ and $t'_{12II}$ (refer to Eqn.s 5.19, 5.20, 5.52, and 5.53) as

$$\Delta t_{12,I-II} = t'_{12I} - t'_{12II} = (t_{12I} + \Delta_{12}) - (t_{12II} + \Delta_{12}) = t_{12I} - t_{12II} = (t_{1I} - t_{2I}) - (t_{1II} - t_{2II}), \quad (5.57)$$

which can be rewritten as

$$\Delta t_{12,I-II} = (t_{1I} - t_{1II}) - (t_{2I} - t_{2II}). \quad (5.58)$$

We note from Eqn.s 5.57 and 5.58 that $\Delta t_{12,I-II}$ is independent of the differential code phase, $\Delta_{12}$, that is, $\Delta t_{12,I-II}$ is the same for both synchronous and asynchronous users. In Fig.s 5.8 and 5.12, the parallel dashed lines correspond to $\Delta t_{12,I-II} = -2\tau, -\tau, 0, \tau$, and $2\tau$.

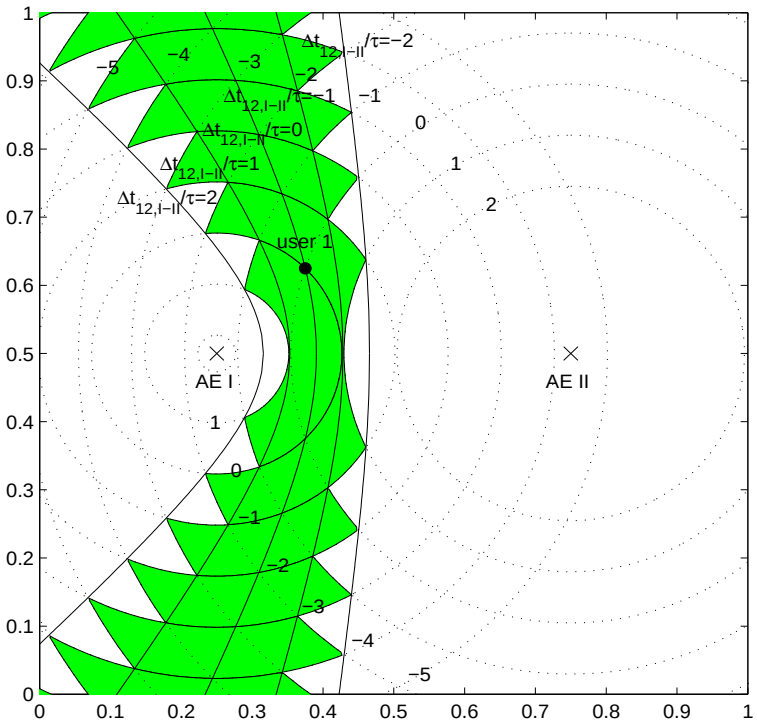


Figure 5.14: The $\Delta t_{12,I-II}/\tau = -2, -1, 0, 1$, and 2 lines along with the caution zone for user 1, for the case of synchronous users ($\Delta_{12}=0$), with $s=400$ and $R_c=10$ Mcps.

We notice from Eqn.s 5.39, 5.40, and 5.56 that $\rho_{12,I-II}$ depends on the actual values of $t_{12I}$ and $t_{12II}$, rather than their difference, $\Delta t_{12,I-II}$. In fact, it is observed from Fig. 5.7 that $\rho_{12,I-II}$ exhibits periodicity with respect to $\Delta t_{12,I-II}$ when $-2\tau < \Delta t_{12,I-II} < 2\tau$. The correlation analysis would have been much simpler if $\rho_{12,I-II}$ were constant (rather than being periodic) with respect to $\Delta t_{12,I-II}$. In that case, a (2-dimensional) plot of $\rho_{12,I-II}$, as a function of $\Delta t_{12,I-II}$ would have been sufficient.

Let us investigate the dependence of $\rho_{12,I-II}$ on $\Delta t_{12,I-II}$ more closely. It is clear from Fig.s 5.5-5.7 that $t_{12I} = t_{12II}$ corresponds to the worst case and $|t_{12I} - t_{12II}| > 2\tau$ guarantees the uncorrelatedness. In other words, (using Eqn. 5.57) it can be stated that

$$\frac{|\Delta t_{12,I-II}|}{\tau} = 0 \quad \longrightarrow \quad \rho_{12,I-II} = 1, \tag{5.59}$$

$$\frac{|\Delta t_{12,I-II}|}{\tau} \geq 2 \quad \longrightarrow \quad \rho_{12,I-II} = 0. \tag{5.60}$$

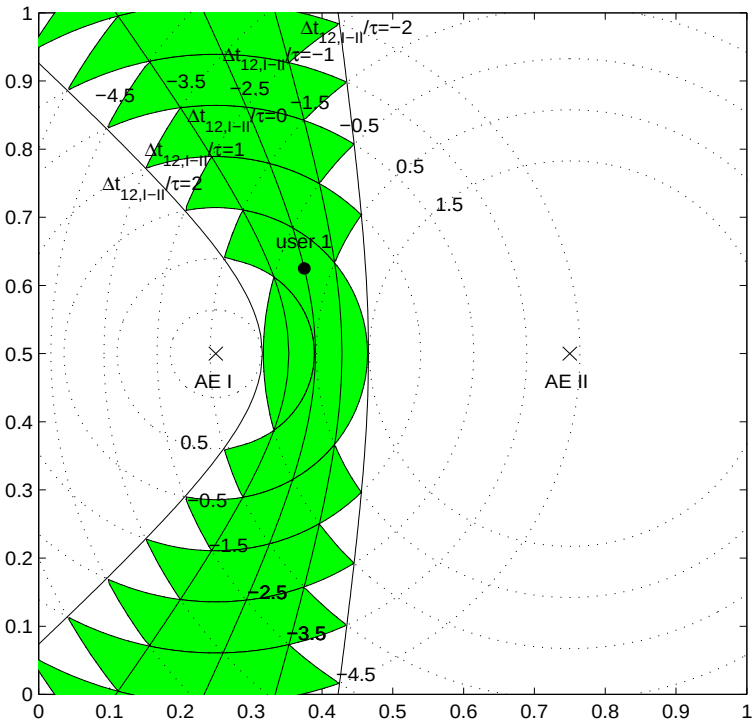


Figure 5.15: The $\Delta t_{12,I\text{–}II}/\tau = -2, -1, 0, 1$, and 2 lines along with the caution zone for user 1, for the case of asynchronous users ($\Delta_{12} = 0.5$), with $s = 400$ and $R_c = 10$ Mcps.

One other important observation from Fig. 5.5 is that

$$1 \leq \frac{|\Delta t_{12,I\text{–}II}|}{\tau} < 2 \quad \longrightarrow \quad 0 \leq \rho_{12,I\text{–}II} \leq 0.5. \tag{5.61}$$

Obviously, it is desirable to have $\rho_{12,I\text{–}II} = 0$. However, it is important to note that even in the case of a $\rho_{12,I\text{–}II}$ very close to unity, such as $\rho_{12,I\text{–}II} = 0.99$, analytically there would still be some gain from diversity combining, although this gain would be minuscule. Even in the limiting case of $\rho_{12,I\text{–}II} = 1$, although there would be no gain from diversity combining, there would be no harm either. In a practical system, however, there are other factors to be taken into consideration besides SIR. If $\rho_{12,I\text{–}II}$ is close to unity, the insignificant returns in SIR would not justify the increased processing, complexity, and thus, cost.

It would be efficient if a threshold value for $\rho_{12,I\text{–}II}$ is determined, say $\rho_o$, such that it can be argued that if $0 \leq \rho_{12,I\text{–}II} \leq \rho_o$, then there would be benefit from diversity, however, if $\rho_o < \rho_{12,I\text{–}II} \leq 1$, then practically there would not be much gain from diversity. We note that in order for the output SIR in a MRC scheme to be the sum of the branch SIR's, $\rho_{12,I\text{–}II}$ should be equal to 0. Therefore, for $\rho_{12,I\text{–}II} = \rho_o$, as described above, the output SIR will be less than the sum of the branch SIR's.

We choose a conservative value for $\rho_o$:

$$\rho_o = 0.5. \tag{5.62}$$

Based to Eqn.s 5.59 and 5.61, setting $\rho_o$ to 0.5 is equivalent to the following inequality:

$$\frac{|\Delta t_{12,I-II}|}{\tau} > 1. \tag{5.63}$$

It is obvious from the discussion so far that $|\Delta t_{12,I-II}|/\tau$ is a critical quantity in the correlation analysis.

Fig.s 5.14 and 5.15 show the $\Delta t_{12,I-II}/\tau = -2, -1, 0, 1$, and 2 lines along with the caution zone for $\Delta_{12} = 0$, and 0.5, respectively, for the example case ($s = 400, R_c = 10$ Mcps). Fig.s 5.14 and 5.15 are in conformity with Eqn. 5.60, in other words, $\rho_{12,I-II} = 0$ for $\Delta t_{12,I-II}/\tau > 2$. Also from Fig.s 5.14 and 5.15, Eqn. 5.58 is confirmed, that is, $\Delta t_{12,I-II}/\tau$ does not depend on $\Delta_{12}$.

The implications of Eqn.s 5.62 and 5.63 is that the caution zones (the shaded areas) in Fig.s 5.14 and 5.15 can be approximated by the area between the $\Delta t_{12,I-II}/\tau = -1$ and 1 lines. We know from Eqn. 5.61 that $\rho_{12,I-II}$ is less than 0.5 in the shaded regions outside the approximated caution zones, therefore, the performance degradation introduced by such an approximation is expected to be insignificant.

## 5.6 The Hyperbolic Grid

In this section, a systematic way of finding the approximate caution zones on the unit service region will be presented. We assume that AE locations are fixed and given.

For a given user 1 location, we calculate $h_{1I} - h_{1II}$ (refer to Eqn. 5.44), and denote this difference by $\vartheta_1$. From analytic geometry, it is known that "a hyperbola is the set of all points in a plane the difference of whose distances from two fixed points is a constant" [58, pp. 595]. Then, for the given user 1 location, a hyperbola can be drawn for representing all the points which satisfy

$$h_{1I} - h_{1II} = \vartheta_1. \tag{5.64}$$

We note that for a given AE *I* and *II* locations, there is only a unique hyperbola through the user 1 location.

For an arbitrary user 2 location, we similarly calculate $h_{2I} - h_{2II}$, and denoted it by $\vartheta_2$. A corresponding hyperbola can also be drawn for representing all the points which satisfy

$$h_{2I} - h_{2II} = \vartheta_2. \tag{5.65}$$

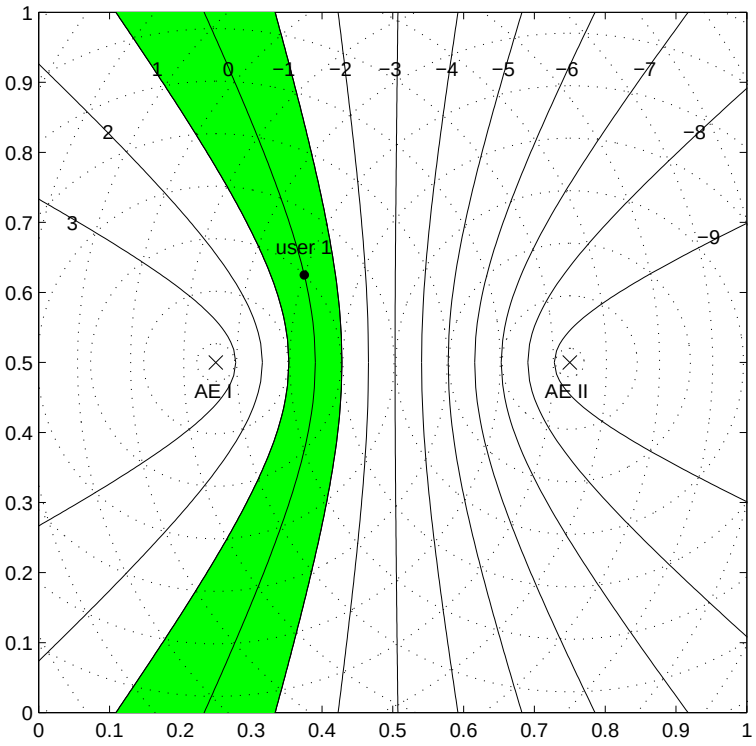


Figure 5.16: The hyperbolic grid and approximate caution zone, for $s = 400$, $R_c = 10$ Mcps, and user 1 location (.375,.625).

The importance of the expression $\Delta t_{12,I-II}/\tau$ has been discussed in Section 5.5; now, we will express this expression in terms of $\vartheta_1$ and $\vartheta_2$. From Eqn.s 5.42, 5.44, 5.45, and 5.58, $\Delta t_{12,I-II}/\tau$ can be written as

$$\frac{\Delta t_{12,I-II}}{\tau} = \frac{sR_c}{c}\left[(h_{1I} - h_{1II}) - (h_{2I} - h_{2II})\right]. \tag{5.66}$$

From Eqn.s 5.64 and 5.65, Eqn. 5.66 takes the form

$$\frac{\Delta t_{12,I-II}}{\tau} = \frac{sR_c}{c}(\vartheta_1 - \vartheta_2). \tag{5.67}$$

We emphasize that user 1 location is given and our goal is to find the approximate caution zone for user 1; in other words, $\vartheta_1$ is known but $\vartheta_2$ is to be found. For a given user 1 location, we first compute $\vartheta_1$ from Eqn. 5.64. Next, in order to find the boundaries of the approximate caution zone, we solve the equation (refer to Eqn. 5.63)

$$\frac{sR_c}{c}(\vartheta_1 - \vartheta_2) = \pm 1 \tag{5.68}$$

for $\vartheta_2$, and denote the two solutions as $\vartheta_{21}$ and $\vartheta_{22}$. Then, using Eqn. 5.65, we draw the hyperbolas corresponding to $\vartheta_{21}$ and $\vartheta_{22}$. The approximate caution zone is the area between these two hyperbolas.

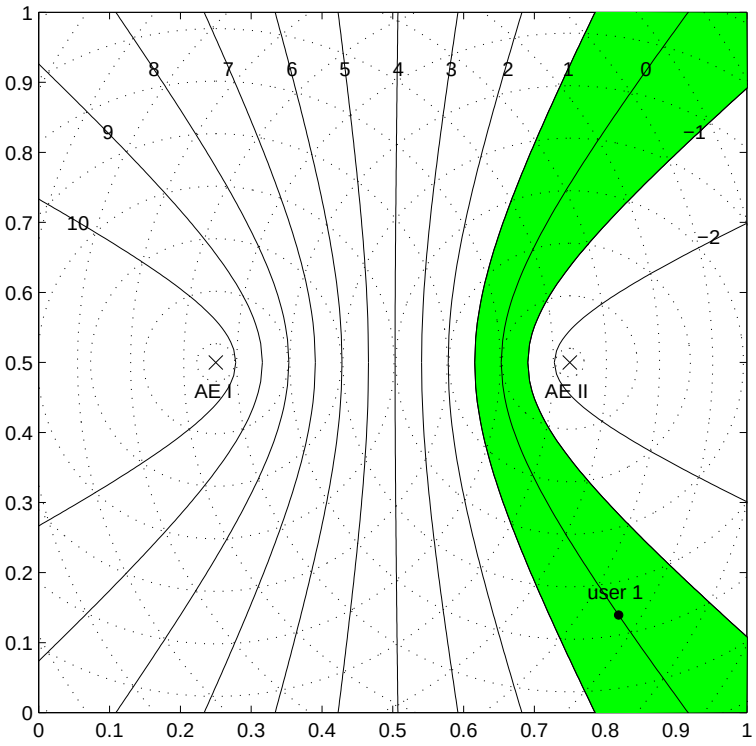


Figure 5.17: The hyperbolic grid and approximate caution zone, for $s=400$, $R_c=10$ Mcps, and user 1 location (.819,.139).

For the exemplary system given in Section 5.3.2, these two hyperbolas and the approximate caution zone for user 1 are shown in Fig. 5.16. In this figure, all the hyperbolas for which $(\vartheta_1-\vartheta_2)sR_c/c$ is an integer are also shown; we call this set of hyperbolas *the hyperbolic grid*. On each hyperbola in the hyperbolic grid, the corresponding $(\vartheta_1-\vartheta_2)sR_c/c$ value is written; it is observed from Eqn. 5.67 that these integers are indeed $\Delta t_{12,I\text{–}II}/\tau$ values. We note that the "origin" of the hyperbolic grid is the hyperbola on which user 1 is located.

It is worth emphasizing that in Fig. 5.16, if user 1 were not at the given location but were at some other location on the same hyperbola which satisfies $h_{1I}-h_{1II}=\vartheta_1$ (that is, the hyperbola indicated by "0" in Fig. 5.16), the locations of the other hyperbolas and the approximate caution zone would still be the same. Similarly, as far as the correlation analysis is concerned, as long as user 2 is on a particular hyperbola, it does not matter where it is on that hyperbola.

Similar to Fig. 5.16, the hyperbolic grid and approximate caution zone for user 1 are shown in Fig. 5.17, this time for some other user 1 location: (.819,.139). In Fig. 5.17, the same $s$ and $R_c$ values introduced in the example given in Section 5.3.2 are used ($s=400$, $R_c=10$ Mcps).

## 5.7 The Effects of System Parameters on the Caution Zone

### 5.7.1 The $sR_c$ Product

As it has already been stated $|\Delta t_{12,I-II}|/\tau$ is a critical quantity in the correlation analysis (refer to Eqn. 5.63). It is observed from Eqn. 5.66 that $|\Delta t_{12,I-II}|/\tau$ depends on a few parameters. In

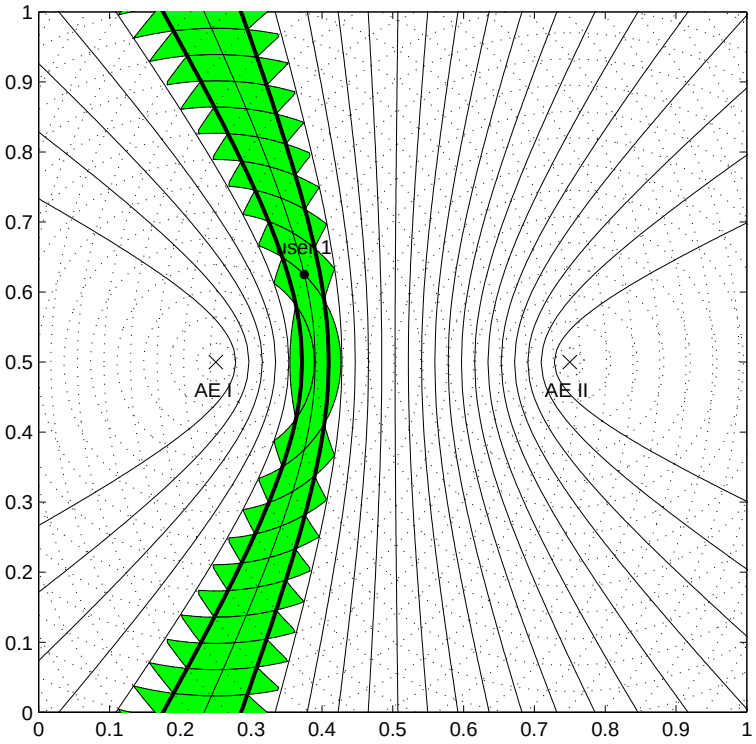


Figure 5.18: The hyperbolic grid, actual and approximate caution zones, for $s = 800$, $R_c = 10$ Mcps, and user 1 location (.375,.625).

the right hand side of Eqn. 5.66, $c$ is a constant, and $h_{ij}$, $i \in \{1, 2\}$, $j \in \{I, II\}$, depends on the user and AE locations. Therefore, the product $sR_c$ is the most important system parameter. It is also noticed that for a certain value of the product $sR_c$, the actual values of $s$ and $R_c$ do not matter. Hence, as long as the correlation analysis is concerned, a system with $s=400$ and $R_c=10$ Mcps is equivalent to the one with $s=1000$ and $R_c=4$ Mcps.

Let us investigate the effect of $sR_c$ more closely. For a large $sR_c$ value, the hyperbolic grid will be denser; in other words, the hyperbolas, for which $(\vartheta_1 - \vartheta_2)sR_c/c$ is an integer, will be closer to each other. Since the approximate caution zone is the area between the hyperbolas -1 and 1, this area will be smaller. Therefore, it is desirable to have a large $sR_c$ value. In Fig. 5.18, the hyperbolic grid, the actual and approximate (thick lines) caution zones for user 1 are shown for the case of $sR_c = 8 \times 10^9$, with user 1 location (.375,.625). This may, for instance, correspond

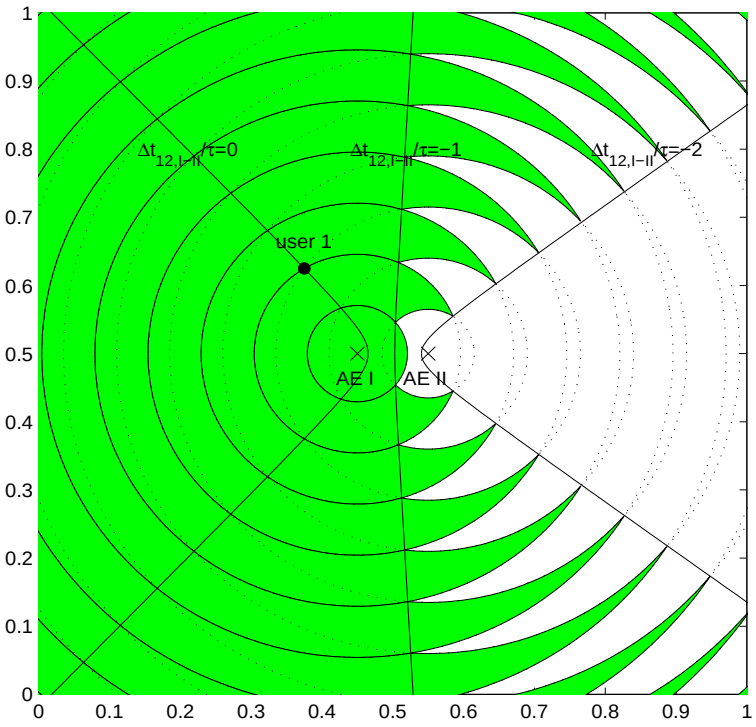


Figure 5.19: The hyperbolic grid and approximate caution zone, for $s = 400$, $R_c = 10$ Mcps, user 1 location (.375,.625), and AE *I* & *II* locations (.45,.5) and (.55,.5), respectively.

to a system with $s = 800$ and $R_c = 10$ Mcps. We note that in the example given in Sec. 5.3.2, $sR_c = 4 \times 10^9$ (see Fig. 5.16).

### 5.7.2 AE Locations

The density and orientation of the hyperbolic grid also depend on the AE locations in the service area. For a given $sR_c$ value, the density of the hyperbolic grid will increase with the increasing distance between the AE's. Therefore, to minimize the caution zone (and thus, the correlation effect), AE's must be placed as far apart as possible — an intuitively satisfying result.

We will demonstrate this result by two examples. Fig. 5.19 shows the hyperbolic grid and the actual caution zone for a system where the two AE's are in very close proximity. In this case, the approximate caution zone covers almost half of the service area! Fig. 5.20, on the other hand, shows the hyperbolic grid and the approximate caution zone for a system where the two AE's are far apart. As expected, the corresponding approximate caution zone is much smaller. Note that for both of the systems illustrated in Fig.s 5.19 and 5.20, $sR_c$ value ($s = 400$ and $R_c = 10$ Mcps) and the user 1 location (.375,.625) are the same.

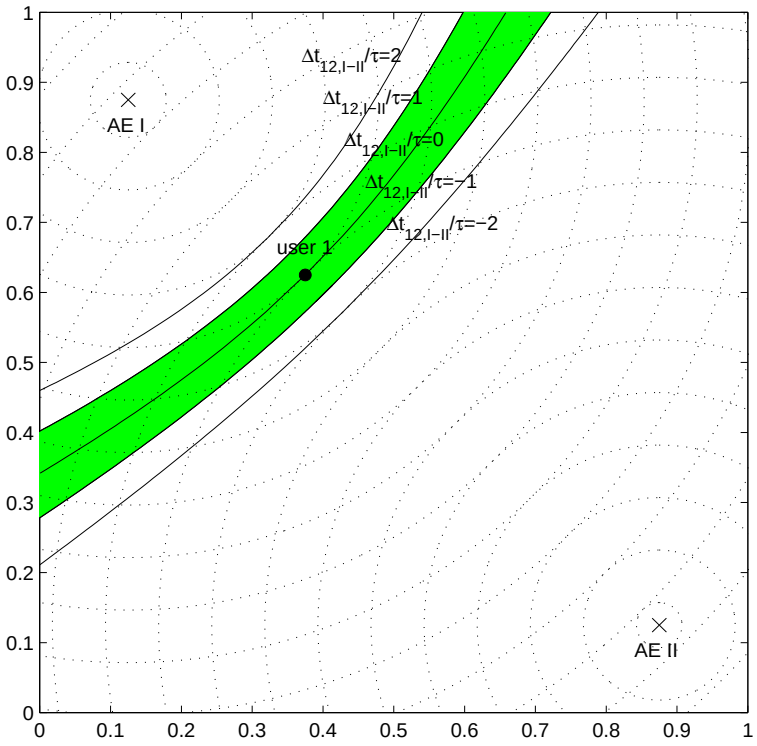


Figure 5.20: The approximate caution zone, for $s = 400$, $R_c = 10$ Mcps, user 1 location (.375,.625), and AE *I* & *II* locations (.125,.875) and (.875,.125), respectively.

In the rest of this thesis, the term *caution zone* will be used to indicate the approximate caution zone (that is, the area between the hyperbolas $\Delta t_{12,I-II}/\tau = -1$ and 1), unless otherwise stated.

## 5.8 Correlation Analysis for $L=2$ with Many Users

The analysis we performed so far corresponds to the special case of $L=2$ AE's with $K=2$ users. In this section, we will extend our analysis to the more general case of $L=2$ with many users.

In a system with $K$ users, for each user $i$, we determine whether the remaining $K-1$ users are in the caution zone for user $i$. By this way, we construct a $K \times K$ correlation matrix, $\mathbf{U} = \{u_{ij}\}$ such that

$$u_{ij} = \begin{cases} 0, & \text{if user } j \text{ is not in the caution zone for user } i, \\ 1, & \text{if user } j \text{ is in the caution zone for user } i. \end{cases} \tag{5.69}$$

We note that $u_{ii} = 0$, $i = 1, 2, \ldots, K$, since a user does not create interference to itself. Also, it can be shown that if user $j$ is in the caution zone for user $i$, then user $i$ must be in the caution zone for user $j$. It can further be shown that if user $j$ is in the caution zone for user $i$, and user $k$

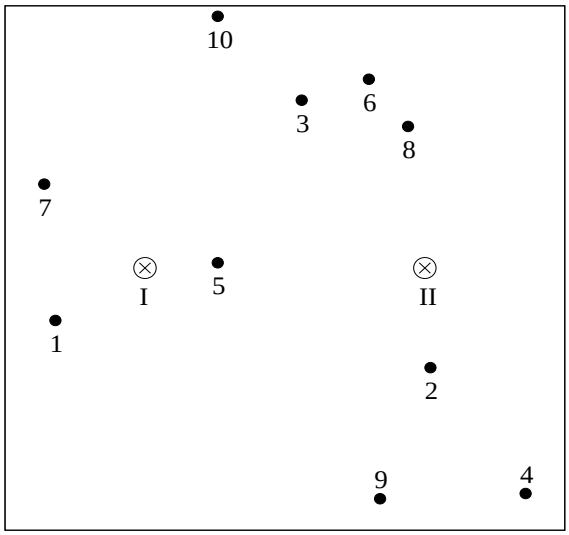


**U:** Correlation Matrix

| | 1 | 2 | 3 | 4 | 5 | 6 | 7 | 8 | 9 | 10 |
|---|---|---|---|---|---|---|---|---|---|---|
| 1 | 0 | 0 | 0 | 0 | 0 | 0 | 1 | 0 | 0 | 0 |
| 2 | 0 | 0 | 0 | 1 | 0 | 0 | 0 | 1 | 0 | 0 |
| 3 | 0 | 0 | 0 | 0 | 0 | 0 | 0 | 0 | 0 | 0 |
| 4 | 0 | 1 | 0 | 0 | 0 | 0 | 0 | 1 | 0 | 0 |
| 5 | 0 | 0 | 0 | 0 | 0 | 0 | 0 | 0 | 0 | 0 |
| 6 | 0 | 0 | 0 | 0 | 0 | 0 | 0 | 0 | 1 | 0 |
| 7 | 1 | 0 | 0 | 0 | 0 | 0 | 0 | 0 | 0 | 0 |
| 8 | 0 | 1 | 0 | 1 | 0 | 0 | 0 | 0 | 0 | 0 |
| 9 | 0 | 0 | 0 | 0 | 0 | 1 | 0 | 0 | 0 | 0 |
| 10 | 0 | 0 | 0 | 0 | 0 | 0 | 0 | 0 | 0 | 0 |

Figure 5.21: A system with $L=2$ and $K=10$, and the corresponding correlation matrix, $\mathbf{U}$, for $s=400$ and $R_c=10$ Mcps.

is in the caution zone for user $j$, then this does not necessarily mean that user $k$ will be in the caution zone for user $i$. The conclusion from the above two sentences, in mathematical terms, is that $\mathbf{U}$ is a symmetric non-transitive matrix.

In Fig. 5.21, a system with $L=2$ and $K=10$ is illustrated and the corresponding $\mathbf{U}$ matrix is given ($s=400$ and $R_c=10$ Mcps). In Fig. 5.21, the caution zones are not drawn. But, if we were to draw the caution zone for user 8, for instance, then users 2 and 4 would be in that caution zone. Consequently, $u_{82}=1$, $u_{84}=1$, and all the other entries in the 8th row of the $\mathbf{U}$ matrix are 0's.

In the worst case, all of the $K-1$ entries in a row of $\mathbf{U}$ will be 1's, and in the best case, all of those entries will be 0's. Based on this observation, we define a quantity which we call percent correlation, $\phi$, as follows

$$\phi_i = \frac{\#\text{ of 1's in the } i\text{th row of the } \mathbf{U} \text{ matrix}}{K-1} \times 100, \quad i = 1, 2, \ldots, K. \tag{5.70}$$

It is worth noting that $\phi$ is not equal to the correlation coefficient.

Based on the discussion in Sec. 5.7, the percent correlation for a user will depend on that particular user's location in the system, as well as the AE locations, and $s$ and $R_c$ values. Simulations have been run to obtain the $\phi$ values for various combinations of these system parameters. For each such combination, 100 systems (each with $L=2$ and $K=100$) are randomly (uniform user distribution) generated; consequently, a total of 10,000 $\phi$ values are collected. The arithmetic means of these values, $\overline{\phi}$, for various combinations of the system parameters, are given in Fig. 5.22.

K = 100 users

$R_c$ = 10 Mcps

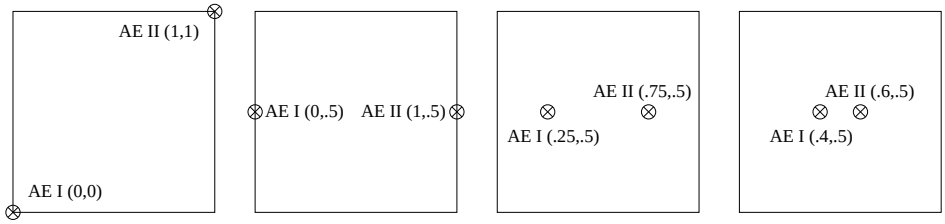


| | | | | |
|---|---|---|---|---|
| s = 1000 | 3.70 | 3.46 | 5.95 | 15.06 |
| s = 400 | 9.23 | 8.67 | 14.26 | 32.58 |
| s = 200 | 18.37 | 17.07 | 27.09 | 52.41 |
| s = 40 | 75.33 | 69.02 | 90.11 | 100.00 |

Figure 5.22: The average percent correlation, $\overline{\phi}$, values for various combinations of AE locations, and $s$ and $R_c$ values, in systems with $L=2$ and $K=100$.

## 5.9 Correlation Analysis for Many AE's with Many Users

In this section, we extend our analysis to the most general case of $L$ AE's with $K$ users.

In this case, for each user, a total of $L(L-1)/2$ caution zones exist, each of which corresponds to a particular AE pair. Therefore, the **U** matrix is composed of $L(L-1)/2$ submatrices (one for each antenna pair), with sizes $K \times K$. Consequently, the correlation matrix, **U**, is 3-dimensional with size $[L(L-1)/2] \times K \times K$. Such a system, for the case of $L=4$ and $K=10$, is illustrated in Fig. 5.23.

For a user $i$, the most disadvantageous situation will occur if all of the remaining $K-1$ users are in all of the $L(L-1)/2$ caution zones for user $i$. Obviously, this is an event with a very low likelihood! Such a situation will yield $(K-1)[L(L-1)/2]$ 1's in the 2-dimensional $i$th row of the **U** matrix. Based on this observation, we define the percent correlation, $\phi$, as

$$\phi_i = \frac{\#\text{ of 1's in the 2-dimensional } i\text{th row of the } \mathbf{U} \text{ matrix}}{(K-1)\dfrac{L(L-1)}{2}} \times 100, \quad i = 1, 2, \ldots, K. \qquad (5.71)$$

The size of the simulations grows rapidly due to the $L(L–1)/2$ factor. Therefore, we considered only $L=4$ and $K=100$ case with $s=400$ and $R_c=10$ Mcps. Similar to the simulations in the previous section, 100 systems are randomly (uniform user distribution) generated, and thus, a total of 10,000 $\phi$ values are collected. The average percent correlation, $\overline{\phi}$, is found to be 12.75, as shown in Fig 5.24.

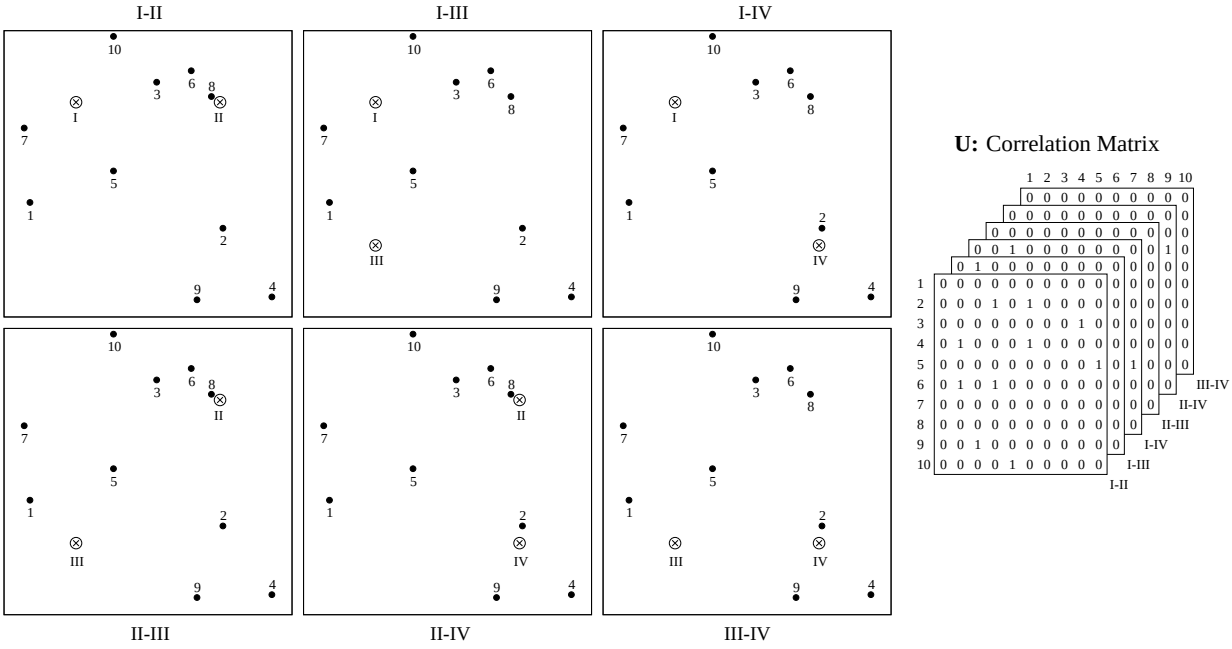


Figure 5.23: A system with $L=4$ and $K=10$, and the corresponding correlation matrix, $\mathbf{U}$, for $s=400$ and $R_c=10$ Mcps.

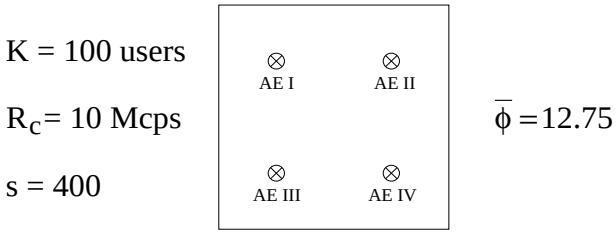


Figure 5.24: The average percent correlation, $\overline{\phi}$, in systems with $L=4$ and $K=100$.

## 5.10 Comparison with Hanly's Work [1] – Part II

In Sec. 4.6, we made some comparisons between our results and those given in a somewhat similar study [1]. In this section, we continue with the comparison. To the best of our knowledge, the only work in the literature on space-related correlation analysis in CDMA macrodiversity systems is Section 7 of [1]. Although the approach of that section to the problem is correct, the discussion is rather brief and qualitative. Based on the rigorous analysis we presented in this chapter, we will comment on some of the statements in [1].

Hanly states in [1]: "... More precisely, for user $u$, let $t_u(j,k)$ be the difference in propagation delays between the user and the receivers $j$ and $k$, respectively. If two users $u$ and $v$ are so close that $|t_u(j,k) - t_v(j,k)|$ is less than a chip time, then the interference at $j$ and $k$, for the decoder of user $u$ (or $v$) will be correlated. ... For example, if $W=20$ MHz, then the chip time

is $5 \times 10^{-8}$ seconds, during which time light travels 15 m. It is clear that the proportion of users in a network that have path differences within 15 m will be very small." In this quotation, $W$ denotes the spread spectrum bandwidth.

The expression $t_u(j,k) - t_v(j,k)$ given in [1] is the equivalent of the differential delay $\Delta_{12,I\text{–}II}$ that we defined in Eqn. 5.57. We have shown throughout this chapter that $|\Delta_{12,I\text{–}II}|/\tau < 1$ corresponds only to an approximation of the areas where the correlated interference exists. The actual such areas (caution zones) depend on the values of $t_u(j,k)$ and $t_v(j,k)$ (refer to, for example, Fig.s 5.7 and 5.8). Therefore, the first part of the above quoted statement is imprecise.

In the second part of the quotation, Hanly considers only a small area around a user as the caution zone. However, we have demonstrated analytically and shown in numerous figures that the caution zones are, in fact, much broader due to the geometry of the problem. Two users that are at different sides of the service region may cause significant correlated interference to one another.

## 5.11 Chapter Summary and Remarks

If the interference (noise) components at the branches of a combiner are uncorrelated, then MRC yields an output SIR that is the algebraic sum of the branch SIR's. If, however, the interference components start becoming correlated, the returns from combining will decrease accordingly. In the limiting case of identical signal and interference components at the branches, there is no gain at all from combining. Therefore, in a CDMA multi-antenna system, the existence of many AE's, and thus, a combiner with many branches, does not automatically guarantee a better performance; we must ensure that the corresponding interference components are uncorrelated (or slightly correlated so that its effect is insignificant). To this end, the objective of this chapter was to evaluate the conditions under which the correlated interference occurs.

We started this chapter by analyzing the simplest non-trivial case of $L = 2$ with $K = 2$, in order to develop some insight into the problem of correlated interference. For this special case, we were able to obtain the correlation coefficient as a function of the distances involved in the service region. Hence, for a given user location, we were able to determine the portions of the service region in which other user(s) would cause correlated interference to the given user; we called this region the caution zone for the given user. We then found an approximate expression (and an approximate caution zone) in simpler terms.

Subsequently, we extended our analysis to the more general case of $L = 2$ with many users. In this case, since obtaining the correlation coefficient would be very tedious, we worked with a simpler quantity which we called the percent correlation. Finally, we considered the most general

case of many AE's with many users.

We observed that the caution zone, for a given user, depends on the location of that particular user, as well as the AE locations, service region size, and the chip rate. Increasing the chip rate, and placing the AE's as far as possible from each other,[1] results in a reduction in the correlation between the interference components at the combiner branches. This implies that for reasonably high chip rates (wideband-CDMA) and for service regions that are not very small, the level of correlation is low if the number of AE's is not very high.

Further investigation is required to make conclusions for the cases with high numbers of AE's.

## 5.12 Future Research Directions

As stated earlier, almost no literature exists on the space-related correlated interference analysis in CDMA multi-antenna systems. Therefore, we believe that our work lays down a foundational framework in this area. Although the simulations that we performed may not be comprehensive, and thus, conclusive for certain cases (such as the ones with high $L$ values), they are still very important, since this initial analysis may eventually enable us to develop a comprehensive understanding of the benefits of the CDMA multi-antenna systems.

Some of the possible research directions are given below:

• We stated that the locations of AE's are very important as far as the correlation effect is considered. For an irregular service region, obtaining the optimal AE locations requires some further investigation. It is interesting to note from Fig. 5.22 that, the system with AE locations (0,.5) and (1,.5) yields a better result than that with AE locations (0,0) and (1,1), although the inter-AE distance is larger in the latter system.

• We defined the percent correlation, $\phi$, in Sec. 5.8. This quantity is very useful in comparing two systems with different parameters; obviously, the one with a lower $\phi$ is preferable. However, what is a reasonable value for $\phi$? In other words, up to what value of $\phi$ can we neglect the effect of correlated interference? These questions should be investigated by analytic methods.

• The simulations should be extended to cover larger $L$ values with different $K/L$ ratios. We obtained $\overline{\phi} = 12.75$ for $L = 4$ and $K = 100$ case, and this is better than 14.26, which is the corresponding value for the $L = 2$ and $K = 100$ case; however, it is unfair to compare these two figures, since $K/L$ ratios in the two systems are different (25 and 50, respectively).

• There still remains a fundamental question: in a given service area that is to be covered by an SDA system, can we put as many AE's as we wish without an upper limit? In an SDA system, putting more AE's would always yield better performance (this is analogous to a dish

[1] For large $L$ values, this is equivalent to distributing the AE's uniformly throughout the service region.

antenna: the greater the diameter, the better the performance). However, the returns in SIR may diminish gradually as $L$ increases, since signals received by different AE's would start being correlated. Taking the increasing complexity and processing in the system into account, adding more AE's would not be worthwhile after a point, which puts an upper limit on the number of AE's. Finding this upper limit may yield an interesting **spatial sampling theorem**.

# Chapter 6

## Antenna Interconnection Strategies

In order to provide high capacity, ubiquitous coverage, and to be able to support compact and lightweight wireless terminals, a very large number of antennas should be deployed in urban areas; according to one estimate, more than 5000 cells would be required in the Tokyo metropolitan area [59]. Therefore, building an affordable infrastructure for the WAN is a major challenge.

In a WAN, there are two main cost factors: the cost of the BS's, and that of the interconnecting infrastructure that links these BS's, which is proportional to the length of the wired-network. In this chapter, antenna interconnection strategies for WAN's are studied in order to determine cost-efficient as well as robust and flexible interconnection architectures. To this end, some results from the theory of minimal networks are used, in particular, those dealing with the well-known problem of Steiner trees.

In Sec. 6.1, the relation between the antenna interconnection architecture and the logical network topology is presented. In Sec. 6.2, the Steiner minimal tree (SMT) architecture is described, and SMT construction in hexagonal and square layouts is discussed. The conduit length comparisons between the star and SMT architectures are presented in Sec. 6.3. In Sec. 6.4, interconnection strategies for linking various central stations are examined. The realization of logical network topologies within the optimal SMT conduit infrastructure is addressed in Sec. 6.5; and finally, concluding remarks are made in Sec. 6.6.

## 6.1 Antenna Interconnection Architectures and Resulting Logical Network Topologies

In the current cellular mobile communication systems (such as AMPS or GSM), T1 lines or microwave radio links are most commonly used for connecting the BS's to the MTSO [60]. In the case of the T1 cables, generally, the star architecture is employed, mainly due to its topological simplicity. In a star architecture, if a new BS is to be added to the network, a cable is laid down

between the new BS and MTSO. Hence, there is no need for coordination with the other BS's. Also, a fault in any BS, or in the cable, would only affect that particular BS, and moreover, the distance between any BS and the MTSO is minimal, which may eliminate the need for amplifiers in the feeder. However, the required cabling for the star architecture is excessive.

### 6.1.1 Complexity/Intelligence Distribution and the Logical Network Topology

Different ways of distributing the complexity/intelligence in the system yield a variety of logical network topologies in which the above mentioned two cost factors (BS and interconnecting infrastructure costs) conflict.

The length and logical topology of a network are closely related. However, simply changing the logical topology of a network, in order to decrease its length, is not necessarily a solution, since doing so may increase the cost of the base stations.

### 6.1.2 Microcellular Systems

Since the radius of a microcell is in the order of a few hundred meters or less, a very large number of microcells will be required to cover metropolitan areas. If a conventional BS is needed for each microcell, then the deployment cost would become extremely high. Furthermore, it is very difficult to find convenient locations for the bulky BS equipment every few hundred meters in urban areas. Therefore, it would be very desirable if the microcell BS (Micro-BS) could contain a minimal amount of hardware, and if most of the processing could be performed at a CS located at a convenient economical site, serving many of these microcells.

Different possible methods of distributing the processing among a Micro-BS and the CS yield a variety of systems. The microcellular systems which have low levels of complexity at the Micro-BS's have naturally logical star topologies, resulting in greater network lengths. On the other hand, the systems with logical bus topologies, have shorter lengths; however, they suffer from a higher level of complexity at the Micro-BS's, since the signals from different Micro-BS's should be distinguishable at the CS.

Ultimately, all the signal specific processing can be moved to the CS, from which the radio signals are delivered to Micro-BS's via fiber optic, coaxial or microwave links [15, 61].

In a metropolitan area where the Micro-BS's are many kilometers away from the CS, it is almost impossible to have line-of-sight links between the utility-post-mounted Micro-BS antennas and the CS. This would yield severe multipath and shadowing phenomena in addition to the path loss. Therefore, despite their easy installation, microwave links are not suitable in many environments (although the networking of CS's may be realized via microwave links as we will address in Section 6.4). The main problems associated with coaxial links are the significant losses

in the cable and the poor frequency response [61]. Even if high-gain RF amplifiers are inserted in the feeder, the resulting SNR is not sufficient, unless the distances between the CS and Micro-BS's are short enough to utilize repeaterless coaxial cables [62].

On the other hand, advances in lightwave technologies, along with the availability of wide-bandwidth, very low-loss (around to 0.2 dB/km) fiber optic cables, enable the tranmission of radio signals between the CS and Micro-BS's without amplification for more than 20 km, using sub-carrier multiplexing (SCM) [59,63]. In this case, the Micro-BS would contain only an optoelectric (O/E) converter and power amplifier (PA) in the forward link, and a low noise amplifier (LNA) and an electrooptic (E/O) converter in the reverse link as shown in Fig. 6.1(a).[1] The fiber optic antenna remoting offers other advantages along with simple and economical Micro-BS's, for instance, centralized control (which is suitable for macro diversity and dynamic channel allocation), and transparency to the modulation scheme (FDMA, TDMA or CDMA) employed [60].

The above described system has a logical star topology because of the point-to-point nature of SCM fiber optic links [Fig. 6.1(a)] [61, 64–66]. The star architecture provides high reliability and easy maintenance due to its topology; however, it requires an enormous investment for the wired network infrastucture. In order to decrease the infrastucture cost, an alternative architecture, the passive double star (PDS), has been proposed which employes optical passive splitters, as illustrated in Fig. 6.1(b) [66]. Although the PDS architecture yields great savings in wired network infrastucture, the simplicity of Micro-BS, which was originally one of the major motivations for using fiber optic links, is lost. This is due to the fact that, since the PDS architecture has a logical bus topology, the CS cannot distinguish between the signals coming from different Micro-BS's unless Micro-BS's are equipped with transmitter/receivers (TX/RX) modems.

One other possibility is to implement a bus architecture, in which case many Micro-BS's are coupled to a fiber optic bus via passive optical couplers as shown in Fig. 6.1(c), and time-division multiplexing (TDM) is employed to distinguish the signals of different Micro-BS's [67]. In this scheme, however, to compensate for the coupling losses, optical amplifiers should be inserted in the cable, and furthermore, hardware should be included at Micro-BS's for TDM. An amplifier chain in the feeder is not desirable since, in such a case, the Micro-BS's that are further away from the CS have much poorer reliability compared to those which are closer.

Hybrid coaxial/SCM-fiber links can also be utilized for the PCS access network [62]. In this system, the Micro-BS's which belong to the same cluster of microcells can be connected to a signal combiner via coaxial cables (as long as the coaxial cable length is less than a few hundred

[1] This concept has been addressed in the literature under different names, such as "antenna remoting" [60], "extension", or "separation" [61], and the Micro-BS has been referred to as the "remote cell site" [60], "microcell base unit" [14], "antenna remote unit" (ARU) [63], and "radio base station" (RBS) [64].

metres so that there is no need for amplification in the feeder), and the combiner is connected to the CS via a fiber optic link. Since the signals from all the microcells in a cluster are summed at the combiner, this architecture, which is suitable for FDMA and TDMA schemes, cannot be used with the CDMA scheme. We note that the hybrid coaxial/fiber network is also a double-star architecture (with a small splitting ratio), and therefore it has a logical bus topology.

### 6.1.3 Distributed Antenna and Sectorized Distributed Antenna Systems

Both DA and SDA systems have logical bus topologies. In the case of a DA scheme, a coaxial bus link can be used to connect the AE's and the CS, as long as the cell is not very large; obviously, a fiber optic bus employing SCM is another possibility. In either case, amplifiers may need to be inserted in the feeder to compensate for the coupling losses. It is worth noting that, unlike the microcellular bus link discussed in the previous section, the DA bus link does not require the use of TDM or frequency conversions at the antenna elements since, in a DA cell, the same signal is fed to all of the AE's.

In the case of an SDA, a separate bus link runs in each sector, which may be either a coaxial or a fiber optic cable, although the fiber may be more approporiate for the farther sectors. A hybrid coaxial/fiber bus link may be another possibility; the radio signal may be delivered to a distant sector via a fiber cable, and in the sector, a coaxial bus may be used. For the limiting case of one AE per sector in an SDA, the architecture is the star type, and transmission without repeaters is possible since there are no coupling losses.

### 6.1.4 Logical Topology versus Conduit Structure

A cable can be installed only on those links of a wired network where a conduit has been placed. Since the conduit placement is far more expensive than the material cost of the cable, the cost-saving cable deployment strategy is to let a conduit path be shared by many different cable routes wherever possible [68]. For instance, in a microcellular network which has logical star topology, there is only one cable route between the CS and a Micro-BS; however, the connections are not necessarily restricted to the "point-to-point" type. In other words, the logical topology and the actual conduit layout do not need to have the same architecture. In the following few sections, the focus will be on constructing efficient conduit architectures, and in Sec. 6.5, a discussion will be presented on how to map a logical cable topology into the optimal conduit infrastructure.

## 6.2 The Steiner Minimal Tree Architecture

Let us consider a typical access network where many AE's (or Micro-BS's) are to be connected to a CS. The straightforward and conventional interconnection structure is the star architecture as shown in Fig. 6.2(a) for the hexagonal layout. However, as mentioned earlier, the main problem in implementing this architecture is the enormous financial investment required for the construction of the conduit infrastructure.

The architectures illustrated in Fig. 6.2 may correspond to DA (or SDA) systems with AE's and CS's, or to microcellular systems with Micro-BS's and CS's. Without loss of generality, however, we will assume that the architectures studied in this paper correspond to DA systems. Thus, a hexagonal region shown by dotted lines in Fig. 6.2 (and also in other figures) does not denote an individual cell; rather, it is the area wherein a wireless user is most likely to receive the strongest signal from the corresponding AE in the center of the region. A cell, then, refers to the area bordered by thick lines in the figures that encloses many AE's and a CS. On the other hand, for the case of a microcellular system, this bordered area would correspond to a service area covered by many Micro-BS's connected to a CS.

### 6.2.1 Shortest Interconnection Network Problem

A network architecture which consists of AE's and transmission links can be represented by a connected graph where the AE's are shown by vertices (points) and the links by edges. Let $\mathbf{\Psi} = \{\Psi_1, \Psi_2, ..., \Psi_L\}$ be a set of $L$ points in the plane, denoting $L$ AE's to be interconnected. Since the objective is to minimize the total conduit length, the corresponding graph that interconnects these $L$ points should not contain any cycles because removing an edge from the cycle will readily reduce the total length (or weight), but this will not disconnect the graph. Therefore, a tree structure that spans all of the vertices and also yields the minimum total length is required.

If no new points are allowed to be added to the original set $\mathbf{\Psi}$ (i.e, if the vertices of the required tree are exactly the points in $\mathbf{\Psi}$), then the shortest network connecting these points is called a minimal spanning tree (MST). Two classical algorithms for finding such a tree are Prim's algorithm (1957), which adds edges which extend the existing tree and do not create cycles, and Kruskal's algorithm (1956), which adds edges which connect components [69, pp. 593–598]. In Fig. 6.2(b) and (c), two different MST's in a hexagonal layout are illustrated. We note that since the lengths (weights) of the edges in the hexagonal layout are not all different, the MST is not unique.

However, it is possible to construct still shorter trees connecting $\Psi_1, ..., \Psi_L$ by adding extra vertices beside the $\Psi_i$. The shortest possible tree constructed in this way is called the Steiner

minimal tree (SMT) and the additional vertices are called Steiner points [70, 71].

A tree interconnecting a set of $L$ points in the plane, by adding extra vertices (Steiner points) if necessary, is called a Steiner tree (ST) if it satisfies the following conditions [72]:

1) No two edges meet at less than 120°.

2) There are at most $L-2$ Steiner points.

3) Each Steiner point has exactly three incident edges.

Conditions 1) and 3) together imply that every Steiner point has exactly three edges meeting at 120°. An SMT is simply the shortest ST; thus, it should be emphasized that not every ST is an SMT. Finally, an ST is called full (FST) if it has exactly $L-2$ Steiner points.

### 6.2.2 SMT Construction Principles

The SMT constructions for $L=3$ and $L=4$ are well known. A summary is presented below for these cases along with the general case of $L$ points.

$\underline{L=3:}$ If $\triangle\Psi_1\Psi_2\Psi_3$ has an angle $\geq 120°$, then adding Steiner points does not help in reducing the total length of the network [Fig. 6.3(a)]. Otherwise, three equilateral triangles are drawn on the sides of $\triangle\Psi_1\Psi_2\Psi_3$. If the far vertex of each equilateral triangle is joined to the opposite $\Psi_i$, then these lines meet at a single Steiner point[2][Fig. 6.3(b)]. The length of the SMT constructed in this way, $\Omega_{\rm SMT} = \Psi_1 S + \Psi_2 S + \Psi_3 S$, satisfies [73, p. 140]:

$$\Omega_{\rm SMT} = \Psi_1 A = \Psi_2 B = \Psi_3 C. \tag{6.1}$$

For the special case of the hexagonal layout, with hexagon radius $a$, it is obvious from Fig. 6.3(c) that

$$\Omega_{\rm SMT} = 3a. \tag{6.2}$$

$\underline{L=4:}$ Similar to the case for $L=3$, equilateral triangles are drawn on the sides $\Psi_1\Psi_3$ and $\Psi_2\Psi_4$ [Fig. 6.3(d)], and then their far vertices ($A$ and $B$, respectively) are joined. The intersection of this line and the circles shown locates Steiner points $S_1$ and $S_2$. It can be shown [74] that in Fig. 6.3(d)

$$\Psi_1 S_1 + \Psi_3 S_1 = A S_1 \quad \text{and} \quad \Psi_2 S_2 + \Psi_4 S_2 = B S_2. \tag{6.3}$$

Therefore, the length of the SMT with vertices $\Psi_1, \Psi_2, \Psi_3, \Psi_4, S_1$ and $S_2$, is equal to $AB$. We note that another ST can be formed [Fig. 6.3(e)] in general; however, the ST with the longer central edge is the SMT. For the special case of hexagonal layout [Fig. 6.3(f) and (g)], $\Omega_{\rm SMT}(= AB)$ is

[2] In Fig.s 6.3 and 6.4, the Steiner points are shown by white dots.

the hypotenuse of a right triangle whose other two sides have lengths $4.5a$ and $\sqrt{3}a/2$; so using the Pythagorean theorem, $L_{SMT}$ can be shown as

$$\Omega_{\rm SMT} = \sqrt{(4.5a)^2 + (\sqrt{3}a/2)^2} = \sqrt{21}a. \tag{6.4}$$

It is worth noting that for the hexagonal layout, both of the possible ST's [Fig.s 6.3(f) and (g)] are SMT's.

<u>$L$-Point Case:</u> If $L \geq 5$, then SMT construction becomes very difficult. The existence of a finite algorithm for SMT construction was proven by Melzak in 1961 [75]; but this problem in the general case is extremely complicated. Melzak's algorithm makes use of the following observation: if the SMT does not have as many as $L-2$ Steiner points, then the SMT will decompose into a number of smaller FST's which meet each other at some subset of the given vertices [74]. Melzak's algorithm makes use of the following facts [76]: SMT($\mathbf{\Psi}$) (which denotes the SMT corresponding to set $\mathbf{\Psi}$) may always be decomposed into sets SMT($\Psi_{L_1}$), SMT($\Psi_{L_2}$), ..., SMT($\Psi_{L_l}$), where $\Psi_{L_1}$, $\Psi_{L_2}$, ..., $\Psi_{L_l}$ are subsets of $\mathbf{\Psi}$ with $\mid \Psi_{L_i} \cap \Psi_{L_j} \mid \leq 1, \quad \forall\ L_i \neq L_j$, where SMT($\Psi_{L_k}$) is an FST for $\Psi_{L_k}$, and the edges of the SMT($\Psi_{L_k}$) form a partition of the edges of SMT($\mathbf{\Psi}$). Fig. 6.4(a) and (b)[3] shows such a decomposition and the yielding SMT, respectively, for a case of $L = 10$. Although we do not know *a priori* how to decompose the given $L$ points into subsets, the total number of possible decompositions is finite [73]. However, if we try all possibilities, their number will grow exponentially. The exponentiality is more of a problem inherent to the SMT rather than just with Melzak's algorithm [71]; indeed, it is shown in [77] that the SMT construction for a general set $\mathbf{\Psi}$ is NP-complete.

### 6.2.3 SMT Construction for Hexagonal Layout

An important consideration for NP-complete problems is the study of special cases. To this end, in this section, we discuss the SMT construction for hexagonal layout. We note the practical importance of this layout since the hexagon is the most commonly used geometrical shape in modeling the service area of an AE in wireless communications.

Let us first introduce the concept of the Steiner ratio. For a given arbitrary set of points $\mathbf{\Psi}$, if $\Omega_{\rm MST}$ and $\Omega_{\rm SMT}$ denote the lengths of the MST and SMT, respectively, then, the following theorem holds (for the proof, see [70, pp. 166–177]):

> **Theorem 1:** $\chi$ *(Steiner ratio)* $= \inf_{\mathbf{\Psi}}(\Omega_{\rm SMT}(\Psi)/\Omega_{\rm MST}(\Psi)) = \sqrt{3}/2 = 0.8660\ldots$,
> *where* "inf" *is taken over all possible sets of* $\mathbf{\Psi}$.

We note that it is quite important to know to what extent a heuristic (like MST) approximates the optimum structure (SMT) since the problem of SMT construction is NP-complete. Since, for

[3] Fig. 6.4(b) is taken from [73, p. 142].

any layout,

$$\chi = \frac{\sqrt{3}}{2} = 0.8660 \leq \frac{\Omega_{\rm SMT}}{\Omega_{\rm MST}} \leq 1, \tag{6.5}$$

the maximum increase in conduit length for constructing an MST instead of the SMT can be calculated as

$$\frac{1-\sqrt{3}/2}{\sqrt{3}/2} \times 100\% \simeq 15\%. \tag{6.6}$$

**Hexagonal Cells**

We start by examining the special case of a hexagonal cell in the hexagonal layout.

> **Theorem 2:** *For a hexagonal cell in the hexagonal layout, the SMT construction is achieved by decomposing the vertices into subsets of 3 points which form equilateral triangles.*

Since the vertices in the hexagonal layout are located at the intersection points of the triangular grid, this decomposing strategy is intuitively satisfying. There are many possible ways of forming these three-point subsets; one of them, along with the corresponding SMT, is illustrated in Fig. 6.5. This theorem is proven in [78] by induction. Here, we will give an alternate proof based on the concept of the Steiner ratio.

> **Proof:** It can be shown that in a hexagonal cell constructed in the hexagonal layout, for a given $n$ (which is the number of AE's at one side of the hexagonal cell), there are
>
> $$L = 3n(n-1)+1 \tag{6.7}$$
>
> AE's (points), for instance, in Fig. 6.5, $n=4$ and $L=37$.
>
> Let $\Omega_0$ be the length of the tree structure illustrated in Fig. 6.5. It is not difficult to show that there are a total of $(L-1)/2$ three-point subsets in such a tree with $L$ points. Since the three-point FST's formed for each subset have lengths of $3a$,
>
> $$\Omega_0 = \frac{L-1}{2}3a. \tag{6.8}$$
>
> It is well known that if a graph is a tree with $L$ vertices, then it has precisely $L-1$ edges. In the hexagonal layout with hexagon radius $a$, the distance between any two neighboring vertices, which is the length of an edge of the MST, is found to be $\sqrt{3}a$. Therefore, $\Omega_{\rm MST}$ for an $L$-point hexagonal cell [see Fig. 6.2(b) and (c)] is
>
> $$\Omega_{\rm MST} = (L-1)\sqrt{3}a. \tag{6.9}$$

If the ratio of the above two equations is taken, we obtain

$$\Omega_0/\Omega_{\rm MST} = \frac{\sqrt{3}}{2}. \tag{6.10}$$

But this is equal to $\chi$, the Steiner Ratio; therefore, $\Omega_{\rm MST} = \Omega_0$. This result shows that the decomposition strategy in the form of three-point subsets depicted in Fig. 6.5 yields SMT's. □

**General Cell Shape**

Based on the proof given in the previous section, many other interconnecting structures for arbitrary cell shapes can also be shown to be SMT's as long as $L$ is an odd number and the exact decomposition of set $\mathbf{\Psi}$ into three-point subsets is possible, as shown in Fig. 6.6(a) and (b). If $L$ is an even number, however, this exact decomposition into subsets of three-points cannot be realized. Even for an odd $L$, there may be cell shapes for which subsets with number of points other than three may needed to be formed; an example is shown in Fig. 6.6(c) where two-point subsets along with a three-point one are formed to construct the SMT. For such cases, where the exact decomposition into subsets of three-points is not possible, however, we can not use the Steiner ratio theorem to prove that these interconnecting structures are indeed SMT's.

Because of the fact stated in Eqn. 6.5, we can be certain that whatever the cell shape is,

$$\chi\,\Omega_{\rm MST} = \frac{3}{2}(N-1)a \le \Omega_{\rm SMT} \le \Omega_{\rm MST} = (L-1)\sqrt{3}a. \tag{6.11}$$

### 6.2.4 SMT Construction for Square Layout

To construct SMT's in a layout other than the hexagonal one is quite challenging. In this section we discuss a square layout with square service regions of $L = n^2$ AE's, with inter-AE distance $a$. For the special case of $n = 2^k$ (or $L = 2^{2k}$), $k = 1, 2, \ldots$, the SMT is constructed by decomposing the set $\mathbf{\Psi}$ into 4-point subsets which form squares [76]. The case for $n = 8$ is shown in Fig. 6.7(a) and the resulting tree structure is illustrated in Fig. 6.7(b). There are a total of $(L-1)/3$ such subsets, with each FST for each subset having a length $(\sqrt{3}+1)a$. Therefore,

$$\Omega_{\rm SMT} = \frac{L-1}{3}(\sqrt{3}+1)a. \tag{6.12}$$

Since, $\Omega_{\rm MST} = (L-1)a$,

$$\frac{\Omega_{\rm SMT}}{\Omega_{\rm MST}} = \frac{\sqrt{3}+1}{3} = 0.9107 > \chi = \frac{\sqrt{3}}{2} = 0.8660. \tag{6.13}$$

Hence, the Steiner ratio theorem cannot be used to prove that this structure is an SMT.

Fig. 6.8 shows the appropriate decompositions that yield the minimum[4] lengths for square service regions.[5] The shortest ST's currently known, for an extended set of points in a square layout, can be found in [79].

## 6.3 Conduit Length Comparisons between Star and SMT Architectures

The ratio of the required conduit lengths for star and SMT architectures, $\Omega_{\mathrm{STAR}}/\Omega_{\mathrm{SMT}}$, is shown in Fig. 6.9(a) for the case of hexagonal cells in a hexagonal layout with the CS in the center of the cell. The remarkable gain in using SMT architecture instead of the star architecture is obvious. Moreover, the proportional cost for using the star architecture increases even more as the network grows; for instance, we observe from Fig. 6.9(a) that for $L=37$, $\Omega_{\mathrm{STAR}}/\Omega_{\mathrm{SMT}}$ is 2.51, but for $L=271$, it is 6.69.

In addition, the conduit length in a star architecture depends on the location of the CS in the cell; $\Omega_{\mathrm{STAR}}$ yields a minimum value if the CS is in the center of the cell, but it may increase considerably if the CS is located in some other part of the cell. However, this is not the case for SMT and also for MST architectures, where the CS can easily be placed in any convenient location without any increase in the conduit length. Therefore, $\Omega_{\mathrm{STAR}}/\Omega_{\mathrm{SMT}}$ further increases if the CS is not in the center of the cell. Let us consider, for instance, the extreme situation where the CS is in the corner. Fig. 6.10(a) and (b) shows the star and SMT architectures, respectively, for such a case; the corresponding MST architecture is also illustrated in Fig. 6.10(c). It is observed from Fig. 6.9(b) that for $L=91$, $\Omega_{\mathrm{STAR}}/\Omega_{\mathrm{SMT}}$ reaches a value of 6.60 if the CS is in the corner; this value is considerably higher than 3.89, which is the value for the case where the CS is in the center.

Furthermore, the conduit length in a star architecture also depends on the shape of the cell; for a fixed cell area, if the cell has the shape of a hexagon (which approximates a circle), then the required conduit length is less than that of almost any other cell shape. For SMT architecture, however, the effect of cell shape on the conduit length is marginal, as described in Section 6.2.3. In Fig. 6.11, rectangular cells in the hexagonal layout with $L=37$ are illustrated. If the CS is in the center of the cell, then $\Omega_{\mathrm{STAR}}/\Omega_{\mathrm{SMT}}$ [see Fig. 6.11(a) and (b)] would be 3.80 [Fig. 6.9(c)]; this is considerably higher than the 2.51 obtained from Fig. 6.9(a), which is the corresponding ratio for a hexagonal cell, again with $L=37$. In Fig. 6.11(c), an MST architecture, for which the

[4] Among all the constructions in Fig. 6.8, only the pattern for the case $n=3$ has been proven to be a SMT [76]; therefore, the expression $\Omega_{\mathrm{MIN}}$ is used to denote the lengths rather than $\Omega_{\mathrm{SMT}}$.

[5] In Fig. 6.8, there is a 3- and a 10-point subset, for the cases $n=6$ and $n=10$, respectively. The construction

conduit length is totally independent of the cell shape, is also shown.

Obviously, for star architecture, the combined effect of the cell shape and the CS location is even more severe on the conduit length. For instance, for the case illustrated in Fig. 6.11(d), where the CS is located in the corner of a rectangular cell with $L=37$, $\Omega_{\mathrm{STAR}}/\Omega_{\mathrm{SMT}}$ increases to 7.21 [Fig. 6.9(d)]; this value is significantly higher than 2.51, which is the corresponding ratio for the case where the CS is in the center of a hexagonal cell.

If a cell grows too large, it may become beneficial or necessary to split it into two (or more) cells. In a star architecture, since all the existing conduits meet in a central location, splitting a cell requires a major reconfiguration; therefore, it is not practical, as shown in Fig. 6.12(a) [80]. An SMT (also MST) architecture, however, can easily be split without any major reconfiguration [Fig. 6.12(b)].

## 6.4 Interconnection of Central Stations

In general, an access network infrastructure consists of AE's, CS's, main switches, and transmission links interconnecting them. In such a network, AE's are connected to the corresponding CS, and various CS's are connected to a main switch, which links the entire network to a fixed network such as the PSTN.

One way to establish this interconnection is to link a CS and the corresponding AE's in the form of an SMT, and then connect the CS's and the main switch, again in an SMT form, as shown in Fig. 6.13(a). We call this structure an *double-SMT* architecture. Such a structure can be thought of as a tree with two stages, as illustrated in Fig. 6.13(b). It is worth noting that, although both levels of this interconnecting tree are constructed as SMT's, the overall tree is not an SMT, nor even an ST. Therefore, the length of a *double-SMT* architecture is (slightly) more than that of a single-SMT type. It is reported in literature, however, that the double-star architecture is significantly shorter than the single-star type [66,80]. Consequently, it is not a good strategy to construct a *double-SMT* architecture instead of a single-SMT type, unlike the case for the star architecture. Nevertheless, a *double-SMT* architecture is still shorter than a double-star type, simply because the SMT in each level of the tree is shorter than the corresponding star type. Fig. 6.14 shows the conduit length comparisons, in terms of hexagon radius $a$, for the one- and two-level architectures, for the cases of 7 cells with 7 AE's, 7 cells with 19 AE's, and 19 cells with 19 AE's. For all of these cases, both the cells and the structures formed by the combination of cells are in hexagonal shapes.

As far as the conduit length is concerned, an improved method of realizing the interconnection

of FST's for these particular subsets are not demonstrated here.

is shown in Fig. 6.15(a). In this case, the overall structure is a single SMT, which we call an *extended SMT* architecture; hence, it yields the minimum total conduit length.

One other possibility is that the interconnection between the CS's and the main switch may be established via radio [Fig. 6.15(b)]. In such a case, the structure can be thought of as a collection of unconnected SMT's; therefore, the conduit length need only be considered for the connections in the first level of the tree shown in Fig. 6.13(a). Although this architecture, which we call a *single-layer SMT*, requires less conduit than the *extended-SMT* type, there is the additional cost of the radio equipment to implement the second level of the tree illustrated in Fig. 6.13(a).

As an example, let us consider the case where a fixed area is served by $M$ cells, each having $N$ AE's. Using Eqn. 6.8, the required conduit lengths for the three architectures described above can be found, in terms of hexagon radius $a$, as

$$\Omega_{\text{extended SMT}} = \frac{3}{2}(ML-1)a, \tag{6.14}$$

$$\Omega_{\text{single-layer SMT}} = \frac{3}{2}M(L-1)a, \tag{6.15}$$

$$\Omega_{\text{double SMT}} = \frac{3}{2}M(L-1)a + \frac{3}{2}(M-1)\sqrt{L}a. \tag{6.16}$$

The required conduit lengths are plotted in Fig. 6.16 for the case of $ML = 3367$. It is observed from Fig. 6.16 that if an *double-SMT* architecture has to be implemented, the best strategy would be to maximize the number of AE's in each cell (or, equivalently, to minimize the number of cells in the fixed service area); this would give a large $L$ and small $M$. However, if the CS's could be connected to the main switch via radio links (*single-layer SMT*), then it would be most efficient to minimize the number of AE's in each cell (or, equivalently, to maximize the number of cells), hence yielding a small $L$ and large $M$.

## 6.5 Cable Configurations in the SMT Conduit Architecture

All the logical topologies described in Section 6.1 can be realized within the optimal SMT conduit infrastructure. Fig. 6.17(a) shows the mapping of a wired network which has logical star topology into an SMT conduit architecture. This network may correspond to a fiber optic microcellular system utilizing SCM, or to an SDA system with one AE per sector. Physical implementation of a wired network with logical bus topology is illustrated in Fig. 6.17(b), which may represent a microcellular system with multilevel star links realized by using 1:2 passive splitters (located at the Steiner points) or a DA system. It is worth noting that both the conduit and cable lengths for the network shown in Fig. 6.17(b) are minimal since, in this case, the actual cable architecture

is in SMT form as well. If we do not take the cost of the splitters (and possible amplifiers in the feeder)[6] into account, this architecture results in the minimal wired network infrastructure cost.

One other way of realizing the Steiner points is to use multifiber optical links. It is a common practice of manufacturers to package a large number of optical fibers within one cable because the manufacturing and installation costs for multifiber and single-fiber cables are not significantly different [81]. In such a case, there is no need for couplers and splitters, and consequently, no loss is induced at the Steiner points. The conduit architectures presented in this chapter are not limited to fiber links; either fiber optic or coaxial cables may be utilized in the conduit.

It is observed from Fig 6.17(a) that mapping a network with logical star topology into the SMT conduit structure results in some increase in the actual cable length. The total cable length for a network with logical star topology mapped into the SMT conduit structure can be calculated as

$$\Omega = 2n(n-1)(2n-1) = \frac{2}{3}(L-1)\sqrt{1+\frac{4}{3}(L-1)}, \tag{6.17}$$

for a hexagonal service area in the hexagonal layout, with the CS in the center of the region. If the ratio of Eqn. 6.17 to Eqn. 6.22, or to Eqn. 6.24, is taken, the increase in the cable length, for using SMT conduit architecture, instead of the star type, can be obtained to be less than 27%, $\forall n$. Taking the results shown in Fig. 6.9 into account, we conclude that the savings from the more expensive conduit layout justify this increase in the cable length.

Finally, we note that both the conduit and cable lengths for the network shown in Fig. 6.17(b) are minimal, since in this case the actual cable architecture is realized in SMT form as well. This structure may correspond to a distributed antenna (DA) system, which may be a promising alternative to a microcellular system in certain environments [37]. In a DA system, since the same signal is transmitted from and received by all the antenna elements, the system has a logical bus topology with a very low level of complexity at the antenna elements. Therefore, SMT architecture for DA systems yield savings in both cable and conduit lengths.

## 6.6 Chapter Summary and Remarks

In this chapter, some concepts from minimal networks theory are utilized in order to determine cost-efficient, as well as robust and flexible antenna interconnection architectures for WAN's.

The optimum SMT and the suboptimum MST architectures both result in a tremendous reduction in conduit length compared to the conventional star type, especially in large networks. The conduit length in a star architecture depends on both the service area shape and CS location

[6] A complete cost analysis should also take into consideration the costs of the other network elements, such as the AE's, couplers, splitters and amplifiers.

in the service area. The conduit length for the SMT architecture, however, is independent of the CS location, and the effect of the service area shape on the conduit structure is marginal. For the MST architecture, these two factors do not have any effect at all on the conduit length. As a result, if the CS is not in the center of the service area and/or if the shape of the service area is not close to a circle, then the relative difference in conduit length between star and SMT (and also MST) architectures becomes even more significant. Furthermore, splitting a service area can be achieved with minimum network reconfiguration for the SMT and MST architectures, unlike the star type which requires major reconfiguration. Therefore, the SMT and MST architectures not only result in significantly less conduit, but they are also much more robust and flexible compared to the star type. Finally, the SMT (or MST) architecture can also be used for interconnecting various CS's in a network.

In this chapter, it is also demonstrated that WAN's having star or bus logical topologies can be realized within the proposed optimal SMT conduit structure. For the systems which have logical bus topologies with centralized complexity, such as the DA systems, the SMT architecture is optimal in both cable and conduit lengths.

The SMT's that are considered in this study are formed for hexagonal and square layouts. In practice, though, the layout almost never has a regular shape. However, even if this were the case, to install the conduit according to an SMT structure may not be practical. Nevertheless, it is quite important to have a general understanding of the interconnection architectures. For an arbitrary layout, the most reasonable strategy may be to use an MST structure; because, as mentioned earlier, there are straightforward algorithms for constructing an MST, however, it may not be possible to construct the SMT as it is an NP-complete problem. Although there is an increase in the conduit length of the MST architecture over that of the SMT type of at most 15%, both architectures still offer substantial savings in conduit length, along with flexibility and robustness, compared to the star architecture.

## 6.7 Appendix

In a hexagonal service region with parameter $n$, there are a total of $n-1$ concentric rings of Micro-BS's around the CS. Let $\Omega_q$ denote the total length of the links between the Micro-BS and the CS for the $q$-th ring; such a case with $n=8$ and $q=7$ is illustrated in Figure 6.18. Therefore,

$$\Omega_{\mathrm{STAR}} = \sum_{q=2}^{n} \Omega_q. \tag{6.18}$$

For the sake of simplicity, let $a = 1$. Then, making use of the symmetry of the layout, $\Omega_q$ can be calculated for the odd- and even-numbered layers as

$$\begin{aligned}\Omega_q &= 12\sum_{i=1}^{\frac{q-3}{2}}\sqrt{\left[\frac{3}{2}(q-1)\right]^2+\left[(2i)\frac{\sqrt{3}}{2}\right]^2} \\ &\quad + 6\left[2(q-1)\frac{\sqrt{3}}{2}+\frac{3}{2}(q-1)\right],\ q:\text{odd};\end{aligned} \tag{6.19}$$

$$\begin{aligned}\Omega_q &= 12\sum_{i=1}^{\frac{q-2}{2}}\sqrt{\left[\frac{3}{2}(q-1)\right]^2+\left[(2i-1)\frac{\sqrt{3}}{2}\right]^2} \\ &\quad + 6\left[2(q-1)\frac{\sqrt{3}}{2}\right],\ q:\text{even}.\end{aligned} \tag{6.20}$$

We first consider the case where $n$ is an odd number. Now, $\Omega_{\text{STAR}}$ can be calculated by making the following substitution

$$m = \left\{\begin{array}{ll} 2j+1, & q\text{: odd} \\ 2j, & q\text{: even}\end{array}\right\},\ j = 1,\ldots,\frac{n-1}{2} \tag{6.21}$$

in Eqn.s 6.19 and 6.20, and then by using Eqn.s 6.19 and 6.20 in Eqn 6.18:

$$\begin{aligned}\Omega_{\text{STAR}} &= 3\sqrt{3}n(n-1)+\frac{9}{4}(n^2-1) \\ &\quad + 12\sum_{j=2}^{\frac{n-1}{2}}\sum_{i=1}^{j-1}\left[\sqrt{9j^2+3i^2}+\sqrt{9(j-\frac{1}{2})^2+3(i-\frac{1}{2})^2}\right], \\ &\quad n\text{: odd}.\end{aligned} \tag{6.22}$$

For the case where $n$ is an even number, instead of Eqn. 6.21, the following substitution should be made in Eqn.s 6.19 and 6.20:

$$q = \left\{\begin{array}{lll} 2j+1, & j = 1,\ldots,(n-1)/2, & q\text{: odd} \\ 2j, & j = 1,\ldots,n/2, & q\text{: even}.\end{array}\right. \tag{6.23}$$

Following the same procedure described for the $n$: odd case, $\Omega_{\text{STAR}}$ can be calculated as

$$\begin{aligned}\Omega_{\text{STAR}} &= 3\sqrt{3}n(n-1)+\frac{9}{4}n(n-2) \\ &\quad + 12\sum_{j=2}^{\frac{n-2}{2}}\sum_{i=1}^{j-1}\sqrt{9j^2+3i^2} \\ &\quad + 12\sum_{j=2}^{\frac{n}{2}}\sum_{i=1}^{j-1}\sqrt{9(j-\frac{1}{2})^2+3(i-\frac{1}{2})^2},\ \ n\text{: even}.\end{aligned} \tag{6.24}$$

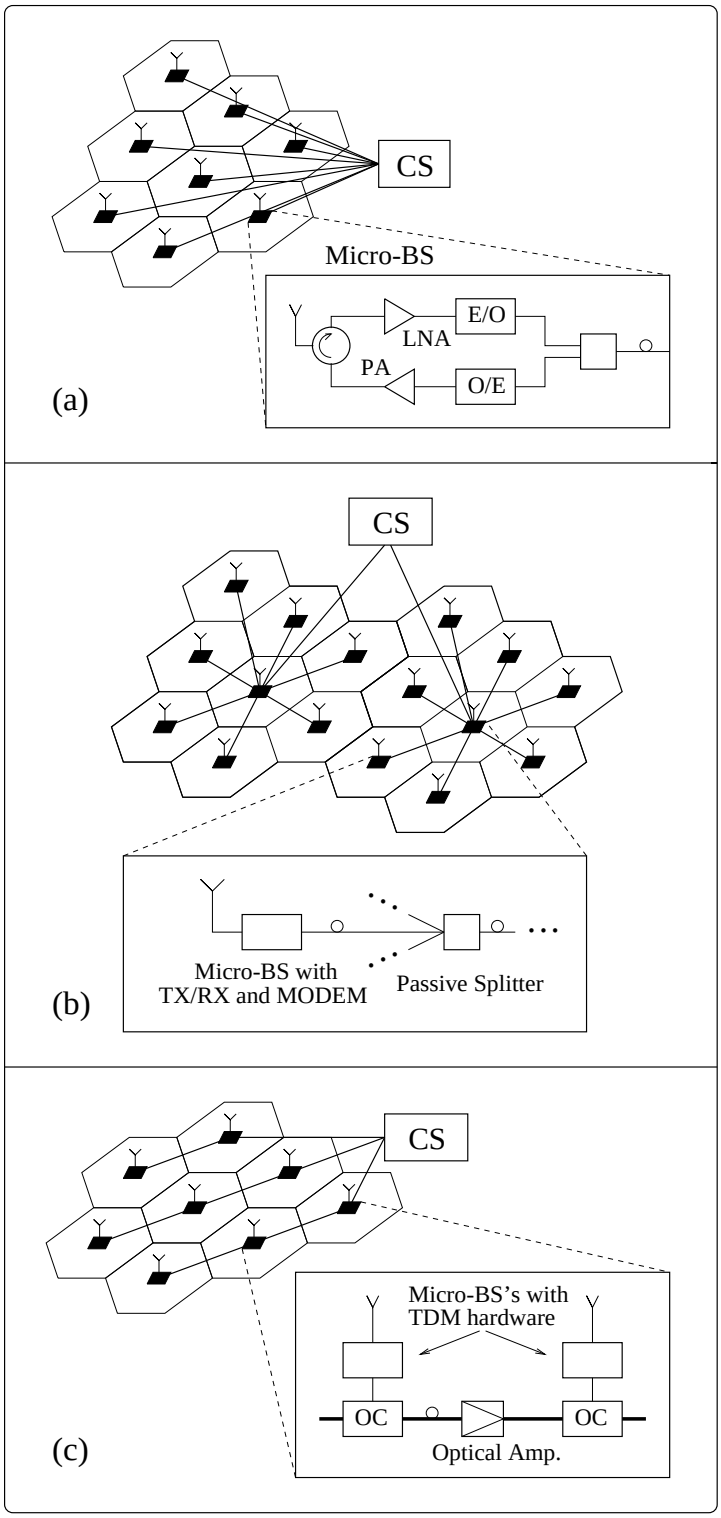


Figure 6.1: WAN's using optical fiber. (a) SCM links (logical star topology). (b) Double-star links (logical bus topology). (c) TDM links (logical bus topology).

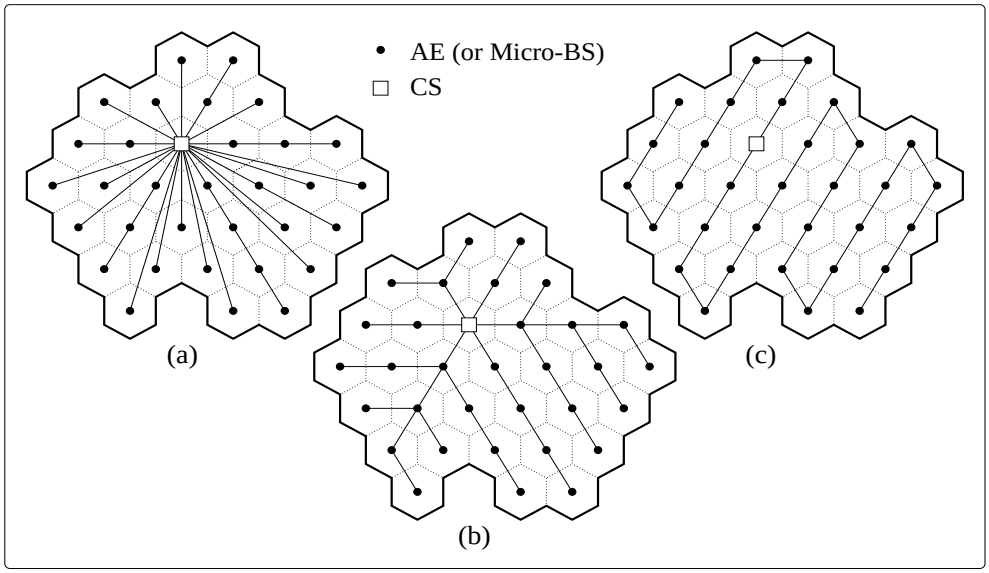


Figure 6.2: (a) Star, and (b)–(c) MST architectures in hexagonal layout.

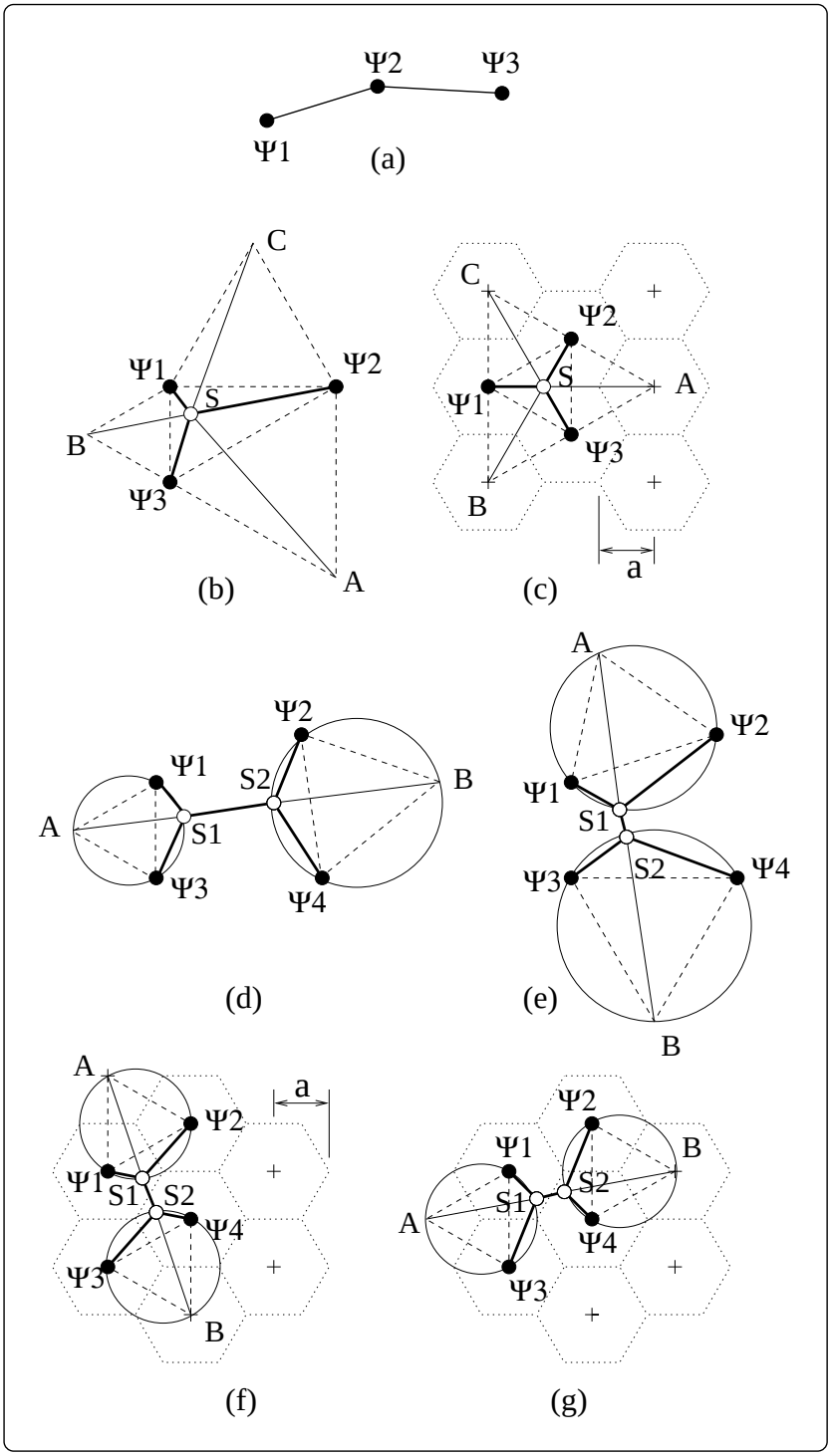


Figure 6.3: SMT construction: (a) $L=3$, general case, $\triangle\Psi_1\Psi_2\Psi_3$ has an angle $\geq 120°$. (b) $L=3$, general case, $\triangle\Psi_1\Psi_2\Psi_3$ has no angles $\geq 120°$. (c) $L=3$, the special case of hexagonal layout. (d) $L=4$, general case. (e) $L=4$, general case, an ST (not an SMT). (f) and (g) $L=4$, the special case of hexagonal layout.

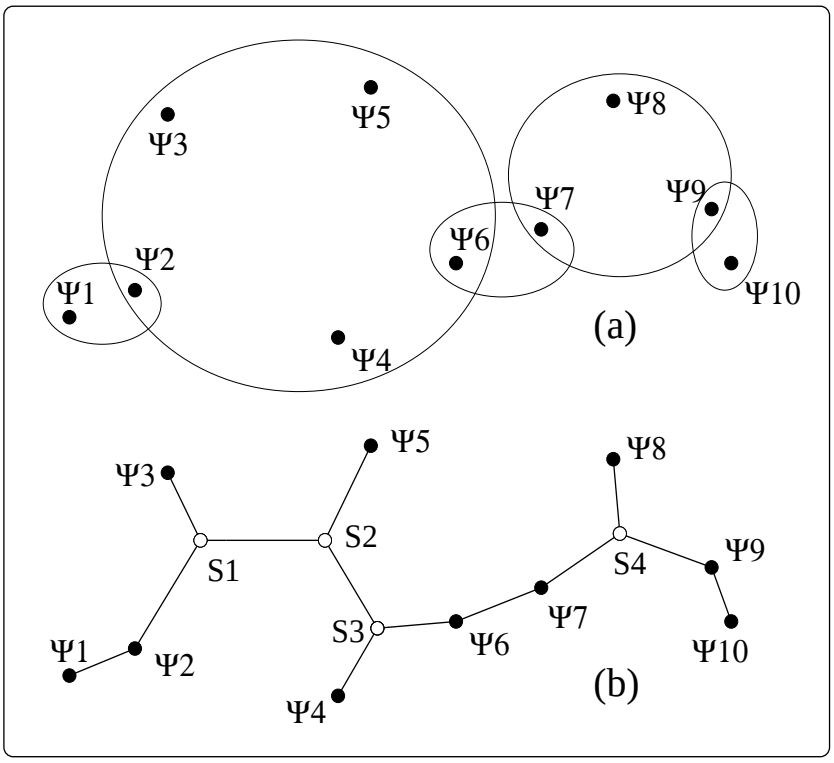


Figure 6.4: SMT construction for a case of $L=10$. (a) Decomposition. (b) Yielding SMT.

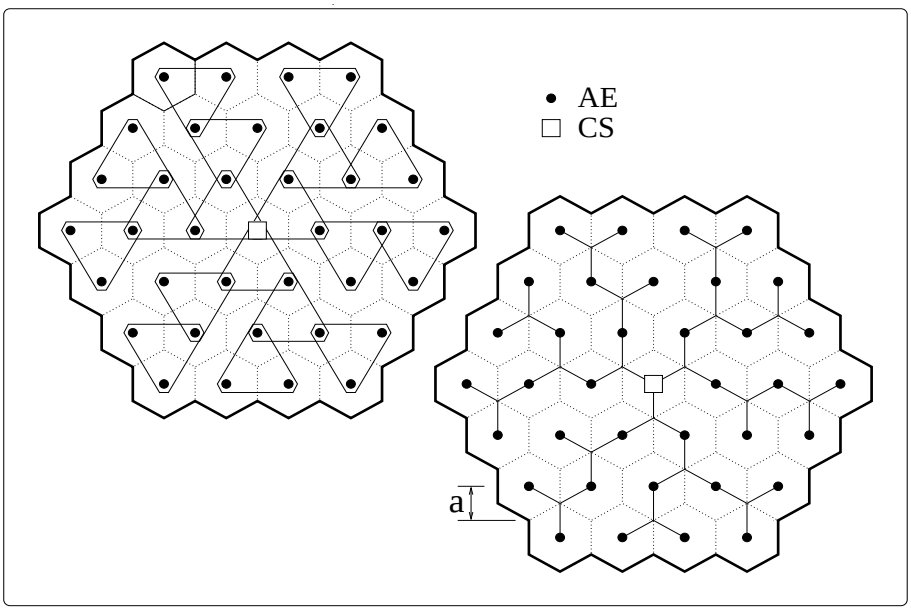


Figure 6.5: SMT construction in hexagonal layout: decomposition and the resultant SMT.

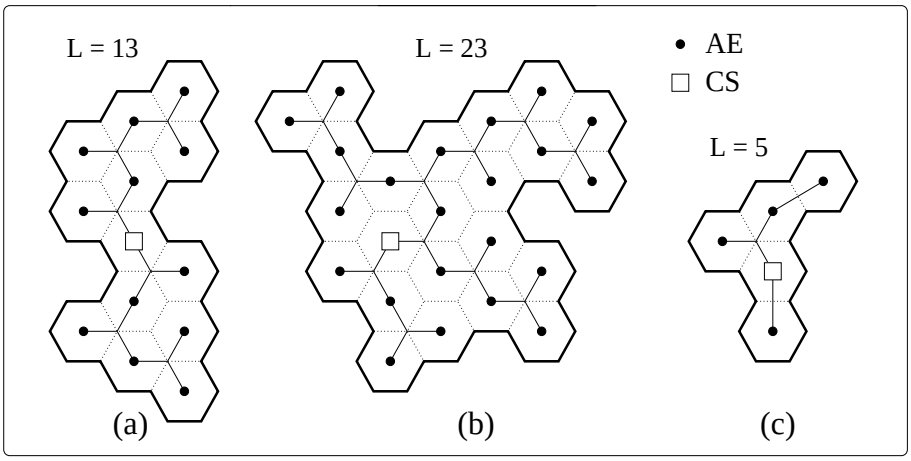


Figure 6.6: SMT's for general cell shapes in a hexagonal layout. (a) $L=13$, (b) $L=23$, (c) $L=5$.

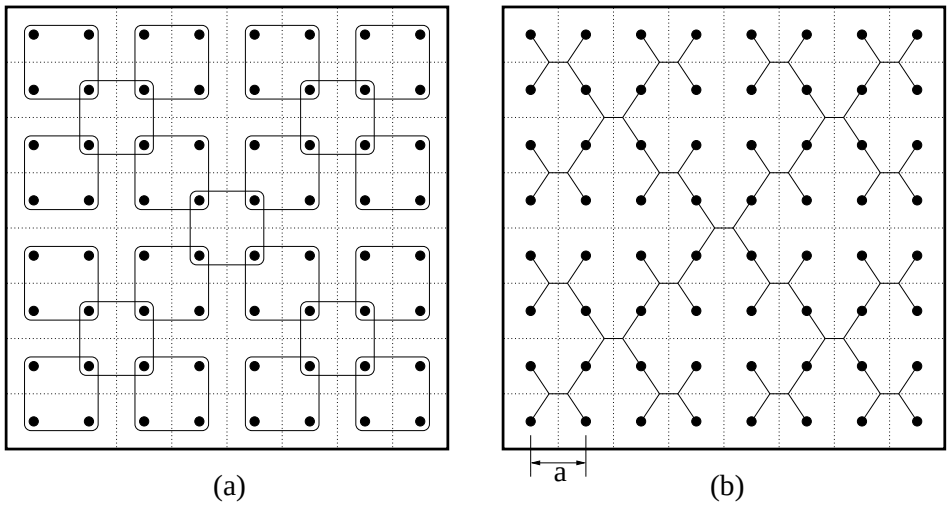


Figure 6.7: SMT construction in a square layout for the special case of a square service region with $n=8$. (a) Decomposition. (b) Yielding SMT.

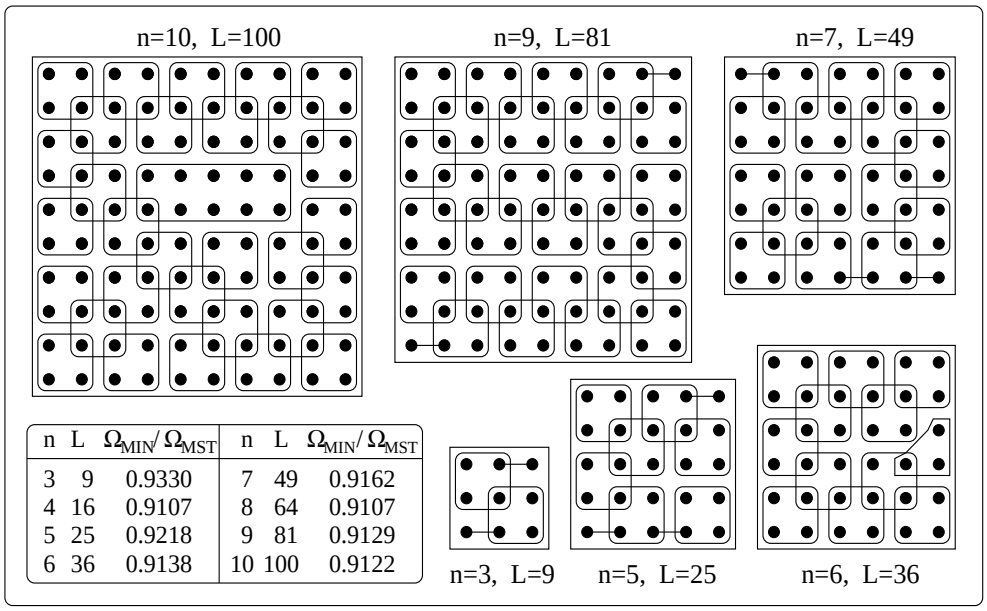


| n | L | $\Omega_{MIN}/\Omega_{MST}$ | n | L | $\Omega_{MIN}/\Omega_{MST}$ |
|---|---|---|---|---|---|
| 3 | 9 | 0.9330 | 7 | 49 | 0.9162 |
| 4 | 16 | 0.9107 | 8 | 64 | 0.9107 |
| 5 | 25 | 0.9218 | 9 | 81 | 0.9129 |
| 6 | 36 | 0.9138 | 10 | 100 | 0.9122 |

Figure 6.8: Decomposition strategies for square service region in square layout.

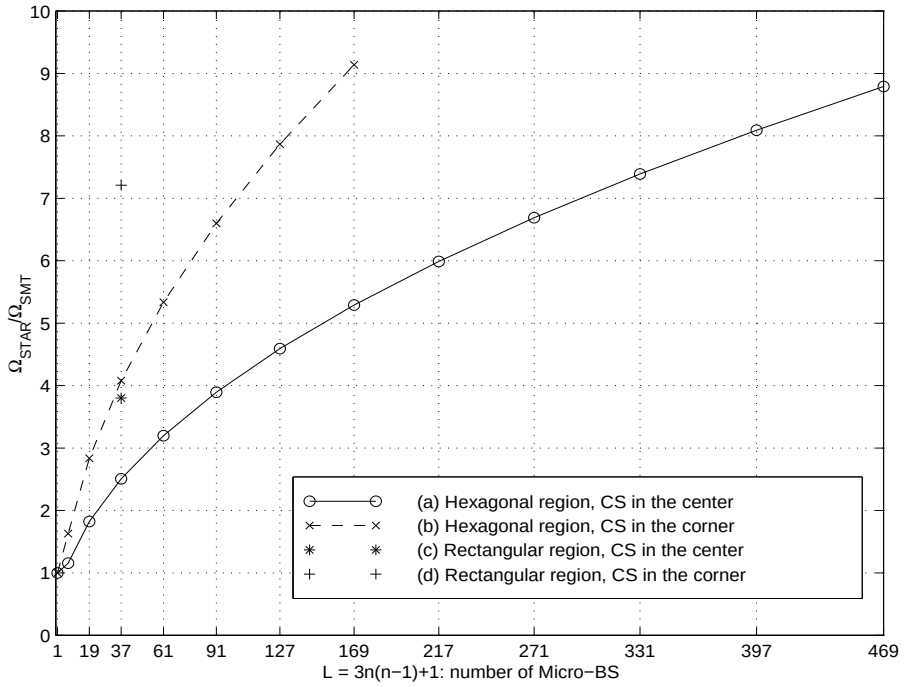


Figure 6.9: Conduit length comparisons between star and SMT architectures.

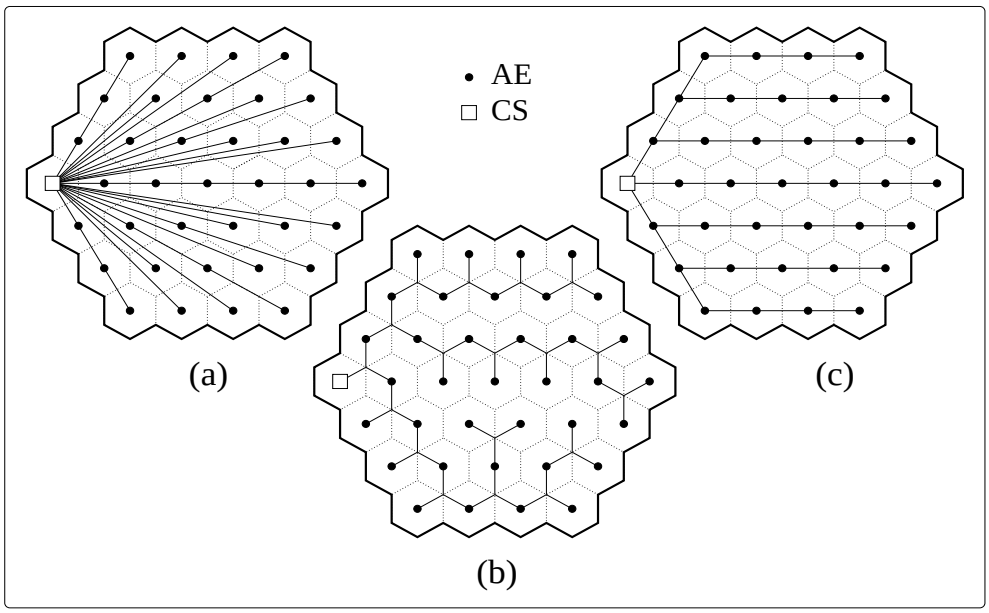


Figure 6.10: (a) Star, (b) SMT and (c) MST architectures for the case where the CS is in the corner of the cell.

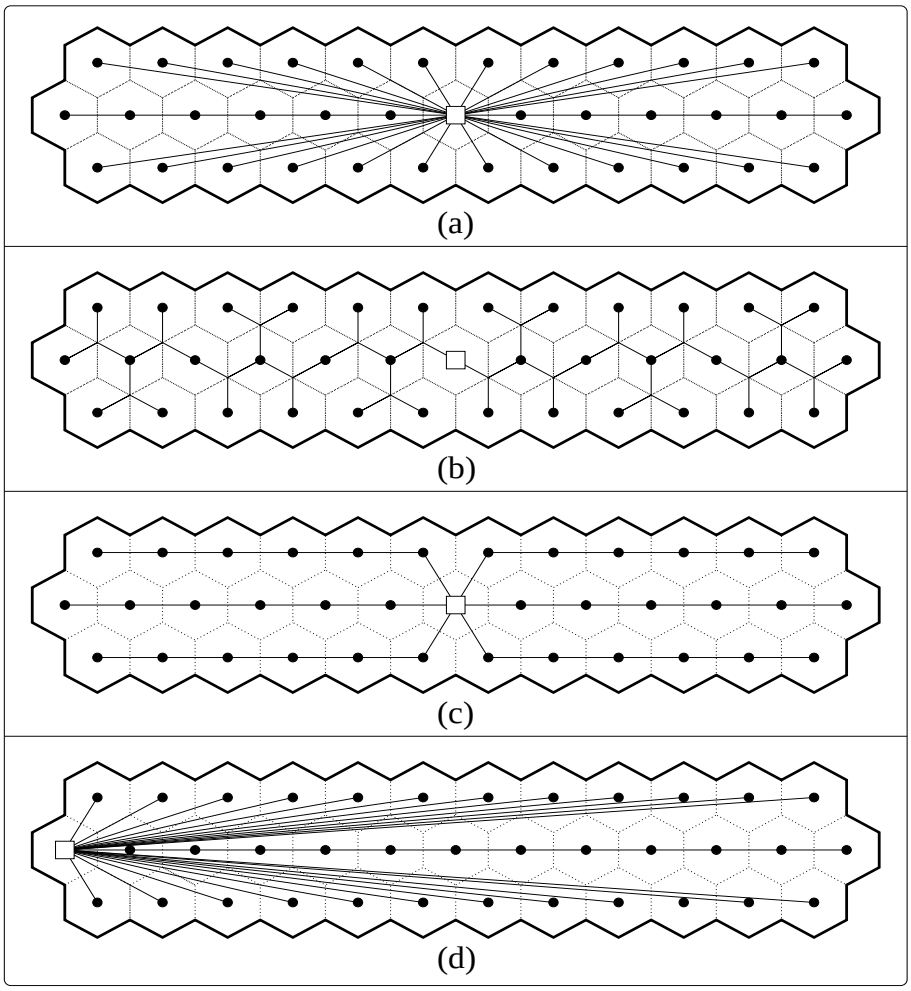


Figure 6.11: Rectangular cells in hexagonal layout with $L = 37$ AE's: (a) Star, (b) SMT, and (c) MST architectures with the CS in the center. (d) Star architecture with the CS in the corner.

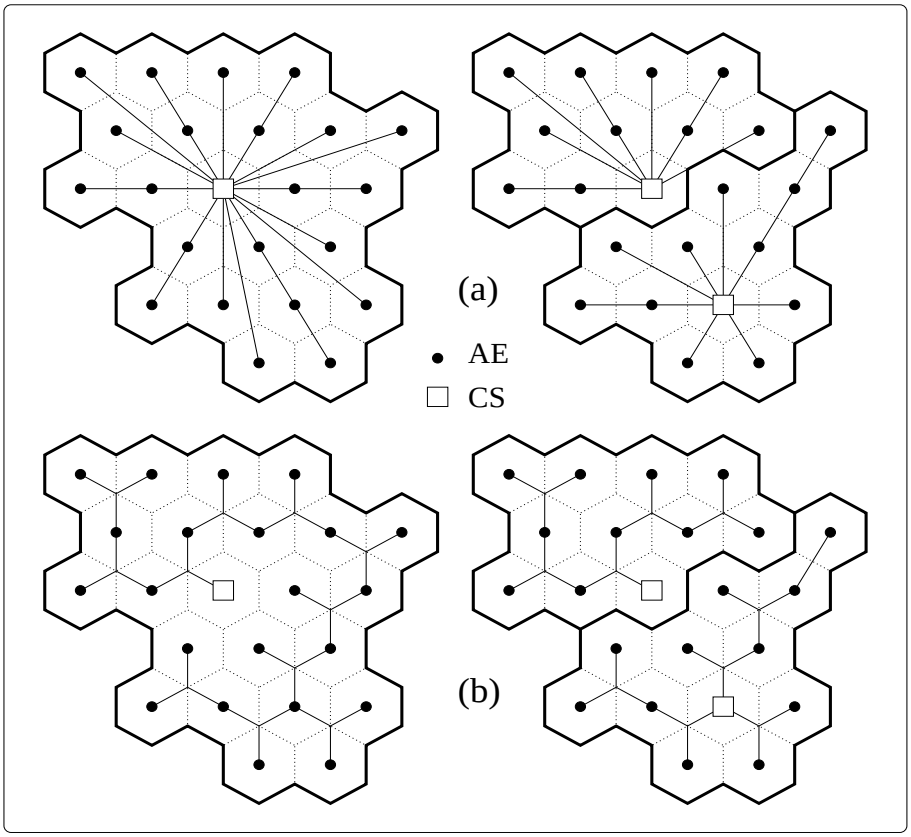


Figure 6.12: Cell splitting for SMT architecture.

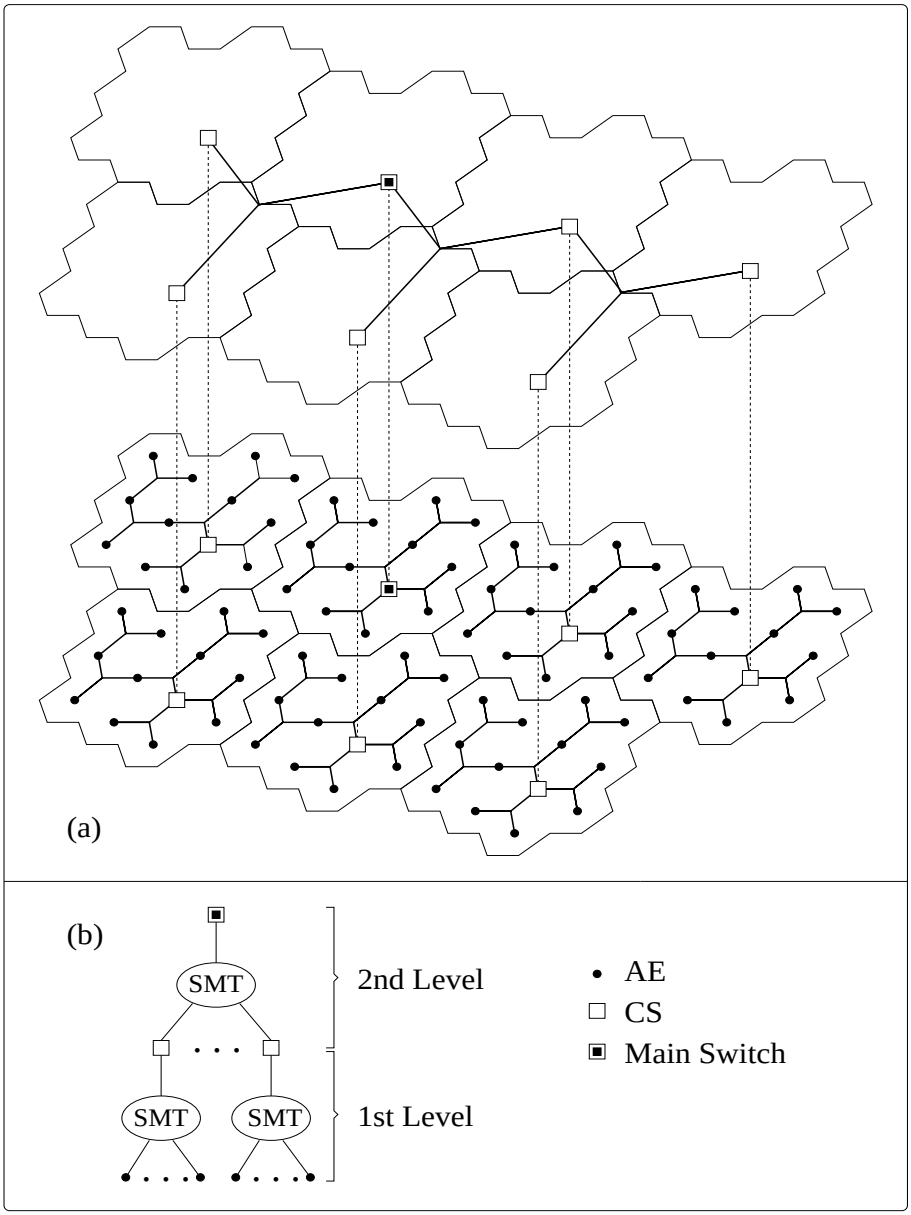


Figure 6.13: *Double-SMT* architecture for interconnecting CS's in hexagonal layout. (a) Details of the architecture. (b) Two-level tree representation.

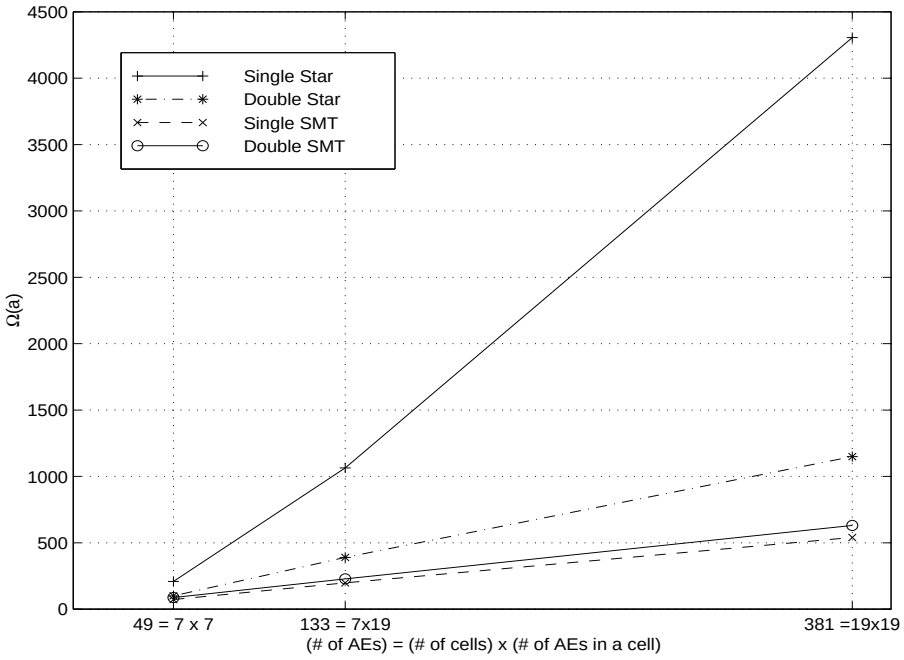


Figure 6.14: Conduit length comparisons for single and double-layer architectures.

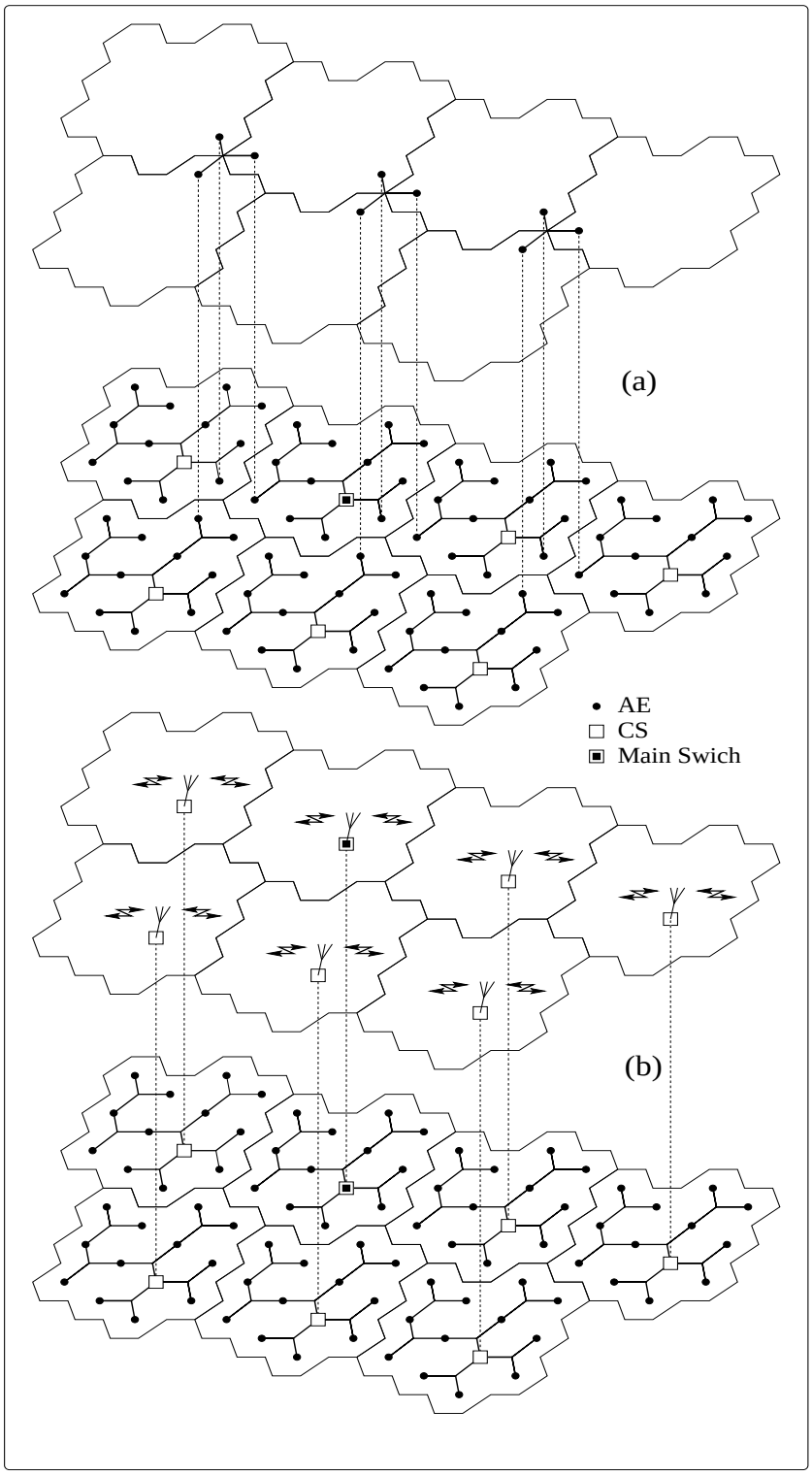


Figure 6.15: (a) *Extended-SMT* and (b) *single-layer SMT* architectures for interconnecting cells in hexagonal layout.

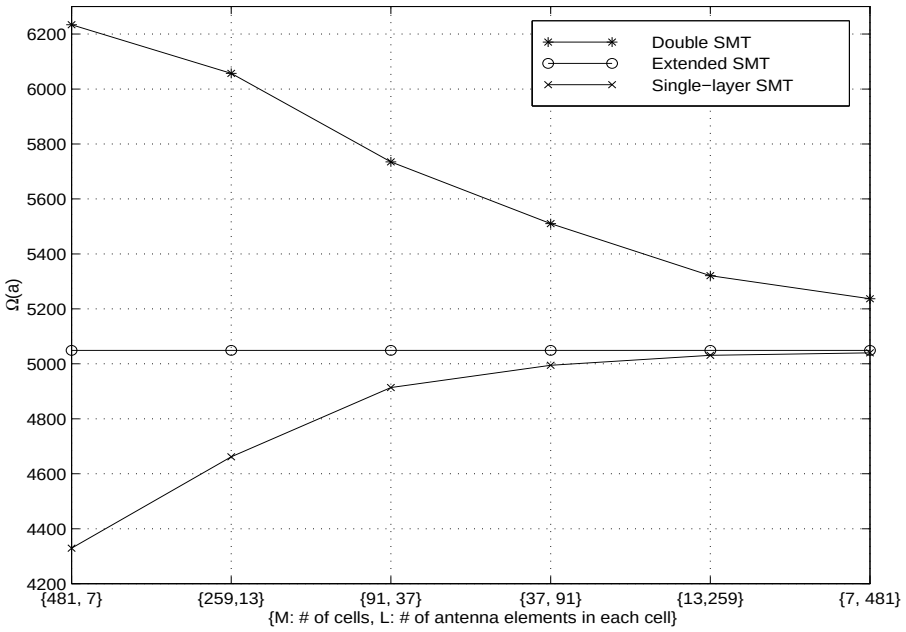


Figure 6.16: Conduit length comparisons for various interconnection strategies, with $ML = 3367$.

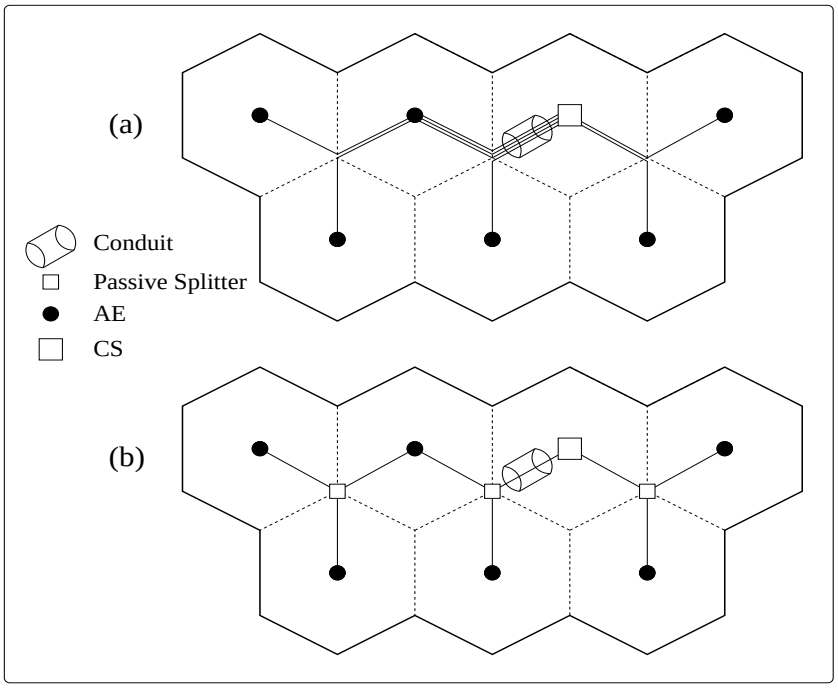


Figure 6.17: SMT conduit architecture for an access network which has (a) logical star, (b) logical bus topology.

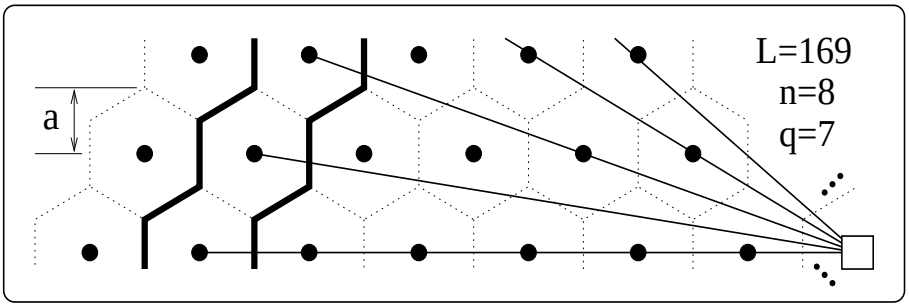


Figure 6.18: Concentric rings of Micro-BS's around the CS.

# Chapter 7

## Summary and Concluding Remarks

Interference management is of utmost importance in CDMA systems, since any reduction in interference translates into a direct increase in capacity. To this end, the main objective of this thesis is to utilize multi-antennas to achieve performance benefits at the system level through spatial interference management.

It is well known that CDMA distributed antenna (DA) systems provide coverage and diversity. We analyze the impact of these features on the power control process, and demonstrate that even with few antenna elements (AE's), the power control dynamic range can be reduced significantly. This reduction is achieved through the elimination of the occasional requirements for transmission at impractically high power levels (necessary to attain perfect power control); this in turn yields a notable reduction in the outage.

The DA system simulates a hypothetical optimal CA system, where signal fluctuations can be compensated for, in all fading conditions, by a perfect power control scheme. Consequently, even though the capacity of a DA system may be considerably higher than that of a CA type, the capacity is still low per AE (due to the multiple access interference accumulating in the common feeder). In order to overcome this shortcoming, we present a new antenna architecture, called sectorized distributed antenna (SDA), where each AE is connected to a separate feeder.

The power control algorithms developed for the conventional CA systems do not perform satisfactorily in the macrodiversity environment of the SDA types. Therefore, we suggest a novel nonlinear power control algorithm which balances the SIR in SDA systems, and also present an iterative solution for this algorithm that always converges. The convergence characteristics of this algorithm are investigated, and suitable termination criteria are given. Following this, the relation between the number of iterations and the yielding error statistics are analyzed.

We demonstrate analytically and through simulations that in a CDMA SDA system with $L$ AE's, the reverse link SIR (or, equivalently, capacity or transmission rate) increases by approximately a factor of $L$.

The SDA system offers more returns compared to the conventional macrodiversity and soft-handoff schemes addressed in the literature; because, in those schemes, post-detection combining is employed, which is mainly based on selection combining or on application of majority-logic. In the SDA system, on the other hand, by the placement of more AE's, more signal, or energy (which is already in the air), is collected, and by jointly decoding the collected signals at the CS, all of this energy is utilized.

The conventional diversity schemes mitigate only against fading; however, in the SDA scheme, there is also a gain over the MAI. The total interference experienced at the CS is reduced approximately by the number of AE's (due to the existence of a separate connection for each AE). Therefore, the capacity of an $L$-element SDA scheme is comparable to that of a $L$-cell cluster serving the same region, which is far more than the capacity of an $L$-branch diversity. This gain of the SDA system over the conventional diversity schemes is achieved through the exploitation of the space dimension (i.e., through the distributed nature of the AE's).

In fact, an SDA system with $L$ AE's still has two main advantages over a cellular cluster with $L$ CA's, due to the joint decoding (enhanced macrodiversity) capability of the SDA system, and also to the effective power control algorithm used. The linear capacity increase in the reverse link of an SDA system is valid (unlike in a cellular type), even if (a) the antenna patterns of the AE's overlap, and (b) the users are not distributed homogeneously throughout the service area (non-uniform traffic). Therefore, sectorization in the context of DA is more efficient than cell-splitting in the conventional cellular systems.

In order to achieve maximal performance from the SDA architecture, the interference picked up by an AE for a user should be uncorrelated with those picked up by other AE's. Therefore, the existance of many AE's, and thus, a combiner with many branches, does not automatically guarantee an enhanced performance; we must ensure that the corresponding interference components are uncorrelated (or only slightly correlated so that its effect is insignificant). To this end, the correlated interference analysis is performed; the conditions, under which the correlation occurs, are evaluated, and the effects of the system parameters on the correlation are investigated.

The correlated interference analysis presented in this thesis is an important step towards a comprehensive understanding of the relationship between the number of AE's and the yielding capacity in CDMA multi-antenna systems. It is hoped that such an understanding may lead to answering more fundamental questions on CDMA multi-antenna systems.

In an extensive network with thousands of AE's and numerous processors/switches, it may be crucial to have a strategy or algorithm to achieve the interconnection in an efficient manner, since even modest improvements in the design of the wireless access network would result in significant savings. To this end, antenna interconnection strategies are studied in order to determine cost-

efficient as well as robust and flexible interconnection architectures, by using results from the theory of minimal networks, especially those on Steiner trees.

In order to illustrate some of the main results obtained in this thesis, we will present a reverse link capacity comparison between the SDA and conventional cellular systems.

## 7.1 Reverse Link Capacity Comparison: Case of Single-Cell with CA versus SDA System

In this section and the following one, we assume that an SIR threshold level, $\Gamma_o$, of

$$\Gamma_o = \frac{N}{K-1} \tag{7.1}$$

is required.

Let us first consider a single-cell system with a CA, and $K$ users [Fig. 7.1(a)]. If the PBPC

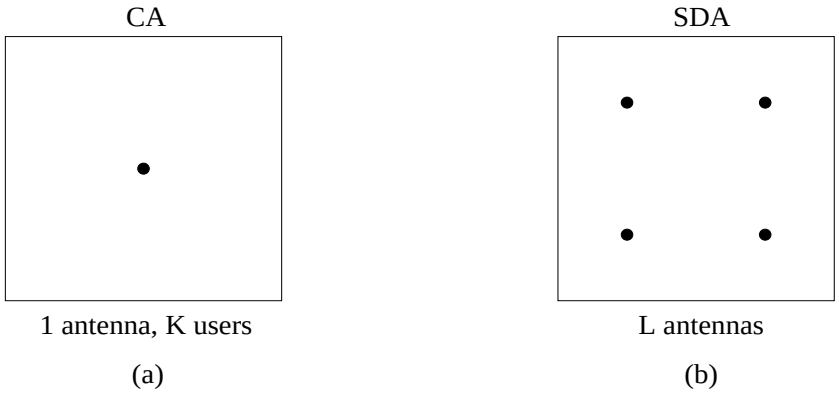


Figure 7.1: (a) Single cell with a CA, (b) SDA system with $L$ AE's.

algorithm is used[1], then the SIR for each user will be

$$\Gamma_{\mathrm{CA}} = \frac{N}{K-1}. \tag{7.2}$$

Since none of the users in the single-cell system has an SIR value below the threshold level given in Eqn. 7.1, the system capacity, $C$, is

$$C_{\mathrm{CA}} = K. \tag{7.3}$$

Next, we consider an SDA system with $L$ AE's (which employs SBMPC) serving the same region, as shown in Fig. 7.1(b). It would be interesting to investigate whether the SDA system can actually support $LK$ users with the threshold constraint given in Eqn. 7.1. In an SDA system with $LK$ users, the range of SIR can be computed using Eqn.s 3.7 and 3.8 as

$$\frac{NL}{LK-1} \leq \Gamma_{\mathrm{SDA}} \leq \frac{NL}{LK-L} = \frac{N}{K-1}. \tag{7.4}$$

[1]Note that for a single-cell system with CA, power-balancing is equivalent to SIR-balancing.

Obviously, the lower limit in the above range is less than $\Gamma_o$. One can easily show that, in order to maintain the threshold SIR, the system capacity should be in the following range:

$$LK - L + 1 \leq C_{\text{SDA}} \leq LK. \tag{7.5}$$

For instance, in a system with $L=4$ and $K=25$, $97 \leq C_{\text{SDA}} \leq 100$.

We conclude from this comparison that by replacing a CA system with an $L$-element SDA type, an approximately $L$-fold capacity increase is achieved, in the reverse link.

## 7.2 Reverse Link Capacity Comparison: Case of Conventional Cellular System versus SDA System

### 7.2.1 Conventional Cellular Systems

Now, we consider a conventional CDMA cellular system with $L$ cells, where macrodiversity is not used. We start by considering an *ideal* scenario, and then we will investigate a more realistic

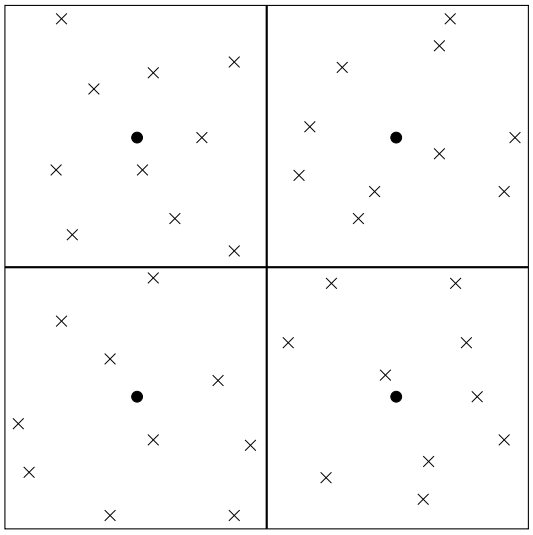

Figure 7.2: An ideal cellular system with perfect electromagnetic isolation between cells (shown by thick lines), and with equal numbers of users in each cell.

*non-ideal* scenario.

**A. Ideal Scenario:**

This scenario is referred to as ideal because of the two unrealistic assumptions made:

a) Antenna radiation patterns do not overlap; that is, the cells are perfectly isolated, and therefore, intercell interference does not exist.

b) Users are homogeneously distributed throughout the service area; that is, there are equal numbers of users in each cell.

Such a system is illustrated in Fig. 7.2. This system is composed of $L$ non-interacting single-cell systems discussed in Sec. 7.1. Therefore, the system capacity is, simply,

$$C_{\text{Cellular,ideal}} = LK. \tag{7.6}$$

**B. Non-Ideal Scenario:**

Now, we will remove the above two assumptions. The removal of assumption a) results in intercell interference effect. The severity of intercell interference will depend on the position of

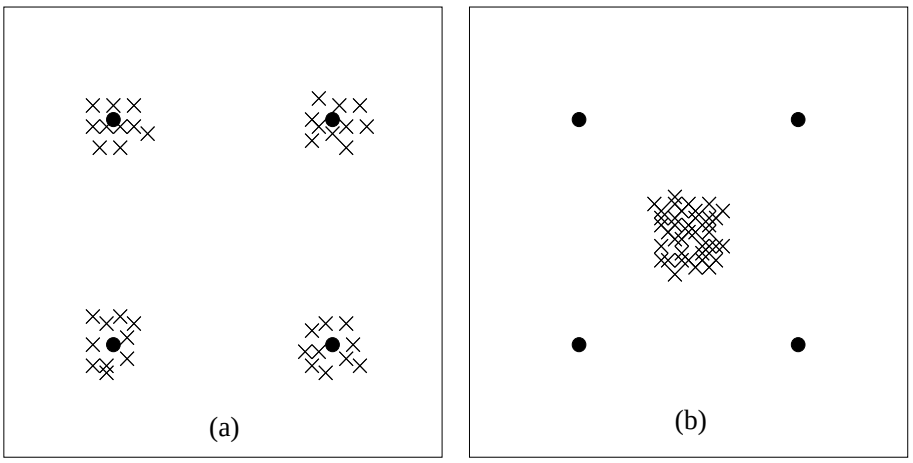


Figure 7.3: User distributions that correspond to (a) best, and (b) worst cases, from SIR point of view.

users in the system. Similar to the analysis in Sec. 3.2, we can find the upper and lower limits of SIR, $\Gamma_{\text{Cellular,UL}}$ and $\Gamma_{\text{Cellular,LL}}$, respectively. In any case, due to the required threshold level, the number of users that a cell can support cannot exceed $K$.

The best situation occurs if all the users in each cell are close to the corresponding CA, as shown in Fig. 7.3(a). In such a case, intercell interference would be insignificant; therefore, each cell can, indeed, support $K$ users. So, the system capacity will be almost equal to that of the ideal case given in Eqn. 7.6:

$$C_{\text{Cellular,UL}} = LK. \tag{7.7}$$

The best situation occurs, on the other hand, if all the users in the system are together at the center of the service region, as shown in Fig. 7.3(b). In this case, due to the severe intercell interference, each cell can support only a fraction of the potential $K$ users; since, if there were $K$

users in each cell, then

$$\Gamma_{\text{Cellular,LL}} = \frac{N}{(K-1)+(L-1)K} = \frac{N}{LK-1}, \tag{7.8}$$

which is much less than the threshold SIR given in Eqn. 7.1. One can easily show that, in order to satisfy the threshold constraint, none of the cells should have more than $K/L$ users. Therefore,

$$C_{\text{Cellular,LL}} = K, \tag{7.9}$$

which is only $(1/L)$th of the potential users that could ultimately be supported.

Next, we remove assumption b); in other words, we allow non-homogeneous user distribution

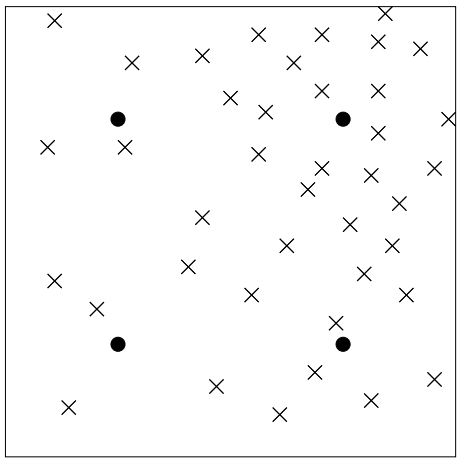

Figure 7.4: Non-homogeneous user distribution in a cellular system.

in the system, as shown in Fig. 7.4. In such a case, some of the users in the overcrowded cells will be blocked. This will yield low efficiency and poor utilization of resources.

Combining the two effects (overlapping antenna patterns and uneven user distribution), we conclude that

$$C_{\text{Cellular}} = \frac{LK}{\varphi}, \tag{7.10}$$

where $1 < \varphi < L$, with $\varphi$ values around 2 being not uncommon in practical systems.

### 7.2.2 SDA Systems

In the same service area, if an SDA system, which employs SBMPC with $L$ AE's, is used instead, then the range of the system capacity can be computed (using a similar set of steps followed in Sec. 7.1) as

$$LK-L+1 \;\leq\; C_{\text{SDA}} \;\leq\; LK. \tag{7.11}$$

We conclude that through the use of multi-antenna reception (joint decoding) with an SIR-balanced power control algorithm, the system capacity is increased approximately to the level

of an ideal cellular system, despite the overlapping antenna patterns and non-homogeneous user distribution (non-uniform traffic).

In the reverse link capacity comparisons given in this chapter, the possible effects of the correlated interference (discussed in Ch. 5) are not taken into account. The results from Ch. 5 indicate that, for reasonably high chip rates (wideband CDMA) and for service areas which are not very small, the effect of correlated interference is mild when the number of AE's is relatively low. However, we still need to be cautious: if the user distribution is significantly non-homogeneous, thereby yielding situations where many users are very close to each other, then the correlation effects may no longer be non-significant. It should be emphasized that the results presented in Ch. 3, on the reverse link capacity of the SDA systems, correspond to upper bounds; the actual returns are expected to be more modest due to the effects of the correlated interference. Further investigation is required to determine the tightness of these bounds.

# Bibliography


[1] S. V. Hanly, "Capacity and power control in spread spectrum macrodiversity radio networks," *IEEE Trans. Commun.*, pp. 247–256, February 1996.

[2] S. Chia, "The universal mobile telecommunication system," *IEEE Commun. Mag.*, pp. 54–62, December 1992.

[3] R. Steele, "The evolution of personal communications," *IEEE Personal Commun. Mag.*, pp. 6–11, 2nd Quarter 1994.

[4] D. C. Cox, "Wireless personal communications: What is it?," *IEEE Personal Commun. Mag.*, pp. 20–35, April 1994.

[5] A. J. Viterbi, "The evolution of digital wireless technology from space exploration to personal communication services," *IEEE Trans. Veh. Technol.*, vol. 43, pp. 638–644, August 1994.

[6] W. C. Y. Lee, "Future vision for wireless communications," *Proc. IEEE 7th Int. Symp. Personal, Indoor, and Mobile Radio Commun. (PIMRC'96)*, vol. 1, pp. 1–4, 1996. Taipei, Taiwan, R.O.C.

[7] W. C. Y. Lee, *Mobile Cellular Telecommunications: Analog and Digital Systems.* McGraw-Hill, 2nd ed., 1995.

[8] J. D. Gibson, *The Mobile Communications Handbook.* CRC Press, 1996.

[9] T. S. Rappaport, *Wireless Communications: Principles and Practice.* Prentice Hall PTR, 1996.

[10] W. C. Y. Lee, *Mobile Communications Engineering: Theory and Applications.* McGraw-Hill, 2nd ed., 1998.

[11] A. J. Viterbi, *CDMA: Principles of Spread Spectrum Communications.* Addison-Wesley, 1995.

[12] R. Prasad, *CDMA for Wireless Personal Communications.* Artech House, 1996.

[13] S. Glisic and B. Vucetic, *Spread Spectrum CDMA Systems for Wireless Communications.* Artech House, 1997.

[14] L. J. Greenstein, N. Amitay, T.-S. Chu, L. J. Cimini, Jr., G. J. Foschini, M. J. Gans, C.-L. I, A. J. Rustako, Jr., R. A. Valenzuela, and G. Vanucci, "Microcells in personal communications systems," *IEEE Commun. Mag.*, pp. 76–88, December 1992.

[15] J. Sarnecki, C. Vinodrai, A. Javed, P. O'Kelly, and K. Dick, "Microcell design principles," *IEEE Commun. Mag.*, pp. 76–82, April 1993.

[16] A. F. Naguib, A. Paulraj, and T. Kailath, "Capacity improvement with base-station antenna arrays in cellular CDMA," *IEEE Trans. Veh. Technol.*, vol. 43, pp. 691–698, August 1994.

[17] J. S. Thompson, P. M. Grant, and B. Mulgrew, "Smart antenna arrays for CDMA systems," *IEEE Personal Commun. Mag.*, pp. 16–25, October 1996.

[18] L. C. Godara, "Applications of antenna arrays to mobile communications, part I: performance improvement, feasibility, and system considerations," *Proc. IEEE*, vol. 85, pp. 1031–1060, July 1997.

[19] P. Delogne, *Leaky Feeders and Subsurface Radio Communications.* Teregrinus, 1982.

[20] P. Delogne, "EM propagation in tunnels," *IEEE Trans. Antennas Propagat.*, vol. 39, pp. 401–406, March 1991.

[21] M. Nakamura, H. Tsunomachi, and R. Fukui, "Road vehicle communication system for vehicle control using leaky coaxial cable," *IEEE Commun. Mag.*, pp. 84–89, October 1996.

[22] J. Harrington and D. Geller, "Re-radiation of signals employing guided antenna systems operating in tandem with two-way signal booster amplifier," *Proc. IEEE 38th Vehicular Technol. Conf. (VTC'88)*, pp. 312–320, 1988.

[23] R. A. Isberg and W. C. Y. Lee, "Performance tests of a low power cellular enhancer in a parking garage," *Proc. IEEE 39th Vehicular Technol. Conf. (VTC'89)*, vol. 2, pp. 542–546, 1989.

[24] R. A. Isberg and M. Pristupa, "Multichannel VHF, UHF and 800 MHz subway radio communications tests in Toronto," *Proc. IEEE 39th Vehicular Technol. Conf. (VTC'89)*, vol. 2, pp. 839–845, 1989.

[25] B. J. Leff, "Application engineering considerations for cellular repeaters," *Proc. IEEE 39th Vehicular Technol. Conf. (VTC'89)*, vol. 2, pp. 532–534, 1989.

[26] F. A. Thatcher, "Design of a subsurface radio communications system using several types of distributed radiators," *Proc. IEEE 40th Vehicular Technol. Conf. (VTC'90)*, vol. 1, pp. 152–155, 1990.

[27] R. A. Isberg and T. E. Herold, "Tests of distributed antenna system along a railway test track," *Proc. IEEE 42nd Vehicular Technol. Conf. (VTC'92)*, vol. 1, pp. 196–201, 1992.

[28] M. A. Franklin, "Radio communications in the channel tunnel," *IEE 7th European Conf. on Mobile Personal Commun.*, pp. 120–124, December 13-15, 1993.

[29] R. J. Jakubowski, "Results of distributed antenna and leaky feeder systems tests at 800 MHz in the Washington D.C. metro system tunnels," *Proc. IEEE 44st Vehicular Technol. Conf. (VTC'94)*, pp. 1113–1116, 1994.

[30] A. A. M. Saleh, A. J. Rustako, Jr., and R. S. Roman, "Distributed antennas for indoor radio communications," *IEEE Trans. Commun.*, vol. COM-35, pp. 1245–1251, December 1987.

[31] T. S. Chu and M. J. Gans, "Fiber optic microcellular radio," *Proc. IEEE 41st Vehicular Technol. Conf. (VTC'91)*, pp. 339–344, 1991.

[32] P. Chow, A. Karim, V. Fung, and C. Dietrich, "Performance advantages of distributed antennas in indoor wireless communication systems," *Proc. IEEE 44st Vehicular Technol. Conf. (VTC'94)*, pp. 1522–1526, 1994.

[33] R. W. Donaldson and A. S. Beasley, "Wireless CATV network access for personal communications using simulcasting," *IEEE Trans. Veh. Technol.*, vol. 43, pp. 666–671, August 1994.

[34] K. J. Kerpez, "A radio access system with distributed antennas," *IEEE Trans. Veh. Technol.*, vol. 45, pp. 265–275, May 1996.

[35] A. Salmasi and K. Gilhousen, "On the system design aspect of code division multiple access (CDMA) applied to digital cellular and personal communications networks," *Proc. IEEE 41st Vehicular Technol. Conf. (VTC'91)*, pp. 57–62, 1991.

[36] S. G. Gopani, J. H. Thompson, and R. Dean, "GHz SAW delay line for direct sequence spread spectrum, CDMA in-door communication system," *IEEE Ultrasonics Symp.*, vol. 1, pp. 89–93, 1993.

[37] H. Yanikomeroglu and E. S. Sousa, "CDMA distributed antenna system for indoor wireless communications," *Proc. IEEE 2nd Int. Conf. Universal Personal Commun. (ICUPC'93)*, vol. 2, 12-15 October, 1993. Ottawa, Canada.

[38] J. Yang, "Analysis and simulation of a CDMA PCS indoor system with distributed antennae," *Proc. IEEE 6th Int. Symp. Personal, Indoor, and Mobile Radio Commun. (PIMRC'95)*, vol. 3, pp. 1123–1127, 1995. Toronto, Canada.

[39] G.-H. Chen, C.-M. Yu, and C.-C. Huang, "A simulation study of a distributed antenna-based CDMA," *Proc. IEEE 7th Int. Symp. Personal, Indoor, and Mobile Radio Commun. (PIMRC'96)*, vol. 2, pp. 517–521, 1996.

[40] E. S. Sousa, "Antenna architectures for CDMA integrated wireless access networks," *Proc. IEEE 6th Int. Symp. Personal, Indoor, and Mobile Radio Commun. (PIMRC'95)*, vol. 3, pp. 921–925, 1995. Toronto, Canada.

[41] A. J. Viterbi and R. Padovani, "Implications of mobile cellular CDMA," *IEEE Commun. Mag.*, pp. 38–41, December 1992.

[42] H. H. Xia, A. Herrera, S. Kim, F. Rico, and B. Bettencourt, "Measurements and modeling of CDMA PCS in-building system with distributed antenna," *Proc. IEEE 44st Vehicular Technol. Conf. (VTC'94)*, pp. 733–737, 1994.

[43] H. Yanikomeroglu and E. S. Sousa, "Interconnection strategies for wireless access network architectures," *Proc. 3rd Int. Workshop on Mobile Multimedia Commun. (MoMuc'96)*, p. A.1.1.3, September 25-27, 1996. Princeton, NJ, USA.

[44] H. Yanikomeroglu and E. S. Sousa, "Steiner minimal tree architectures for the interconnection of wireless access networks," *Proc. 5th Canadian Workshop on Information Theory*, pp. 113–116, June 3-6, 1997. Toronto, Canada.

[45] H. Yanikomeroglu and E. S. Sousa, "Interconnection strategies for wireless access networks," *Proc. IEEE 8th Int. Symp. Personal, Indoor, and Mobile Radio Commun. (PIMRC'97)*, vol. 3, pp. 882–886, September 1997. Helsinki, Finland.

[46] H. Yanikomeroglu and E. S. Sousa, "Antenna interconnection strategies for personal communication systems," *IEEE J. Select. Areas Commun.*, vol. 15/7, pp. 1327–1336, September 1997.

[47] H. Yanikomeroglu and E. S. Sousa, "On the power control and number of antenna elements in CDMA distributed antenna systems," *Proc. IEEE Int. Conf. Commun. (ICC'98)*, pp. 1040–1045, June 7-11, 1998. Atlanta, GA, USA.

[48] H. Yanikomeroglu and E. S. Sousa, "CDMA sectorized distributed antenna system," *to appear in Proc. IEEE Int. Symp. Spread Spectrum Techniques and Applications (ISSSTA'98)*, September 2-4, 1998. Sun City, South Africa.

[49] H. Yanikomeroglu and E. S. Sousa, "SIR-balanced macro power control for CDMA sectorized distributed antenna systems," *to appear in Proc. IEEE 9th Int. Symp. Personal, Indoor and Mobile Radio Commun. (PIMRC'98)*, September 8-11, 1998. Boston, MA, USA.

[50] B. Hashem and E. S. Sousa, "On the capacity of a cellular DS/CDMA system under slow multipath fading and fixed step power control," *Proc. IEEE 6th Int. Conf. Universal Personal Commun. (ICUPC'97)*, pp. 352–355, 1997.

[51] J. M. Aein, "Power balancing in systems employing frequency reuse," *COMSAT Tech. Rev.*, vol. 3, no. 2, Fall 1973.

[52] R. W. Nettleton, "Traffic theory and interference management for a spread spectrum cellular mobile radio system," *Proc. IEEE Int. Conf. Commun. (ICC'80)*, pp. 24.5.1–24.5.5, 1980.

[53] H. Alavi and R. W. Nettleton, "Downstream power control for a spread spectrum cellular mobile radio system," *Proc. IEEE Globecom*, pp. 84–88, 1982.

[54] R. W. Nettleton and H. Alavi, "Power control for spread-spectrum cellular mobile radio system," *Proc. IEEE Veh. Technol. Conf. (VTC'83)*, pp. 242–246, 1983.

[55] J. Zander, "Performance of optimum transmitter power control in cellular radio systems," *IEEE Trans. Veh. Technol.*, vol. 41, pp. 57–62, February 1992.

[56] J. Zander, "Distributed cochannel interference control in cellular radio systems," *IEEE Trans. Veh. Technol.*, vol. 41, pp. 305–311, August 1992.

[57] S. A. Grandhi, R. Vijayan, D. J. Goodman, and J. Zander, "Centralized power control in cellular radio systems," *IEEE Trans. Veh. Technol.*, vol. 42, pp. 466–468, November 1993.

[58] R. A. Silverman, *Calculus with Analytic Geometry.* Englewood Cliffs, NJ: Prentice-Hall, 1985.

[59] M. Shibutani, T. Kanai, W. Domon, K. Emura, and J. Namiki, "Optical fiber feeder for microcellular mobile communication system (H-015)," *IEEE J. Select. Areas Commun.*, vol. 11, September 1993.

[60] D. Tang, "Fiber-optic antenna remoting for multisector cellular cell sites," *Proc. IEEE Int. Conf. Commun. (ICC'92)*, vol. 1, pp. 76–81, 1992.

[61] K. Morita and H. Ohtsuka, "The new generation of wireless communications based on fiber-radio technologies," *IEICE Trans. Commun.*, vol. E76-B, pp. 1061–1068, September 1993.

[62] H. Jung and O. K. Tonguz, "Access network for PCS," *Proc. IEEE 7th Int. Symp. Personal, Indoor, and Mobile Radio Commun. (PIMRC'96)*, vol. 3, pp. 1267–1271, 1996. Taipei, Taiwan, R.O.C.

[63] J. C. Fan, C. L. Lu, R. F. Kalman, and L. G. Kazovsky, "Design and analysis of a novel fiber-based PCS optical network," *Proc. IEEE Int. Conf. Commun. (ICC'95)*, vol. 1, pp. 601–605, 1995.

[64] O. K. Tonguz and H. Jung, "Personal communications access networks using subcarrier multiplexed optical links," *J. Lightwave Technol.*, vol. 14, pp. 1400–1409, June 1996.

[65] W. I. Way, "Optical fiber-based microcellular systems: An overview," *IEICE Trans. Commun.*, vol. E76-B, pp. 1091–1102, September 1993.

[66] K. Kumozaki, "A fiber-optic passive double star network for microcellular radio communication systems applications," *IEICE Trans. Commun.*, vol. E76-B, pp. 1122–1127, September 1993.

[67] H. Harada, S. Kajiya, K. Tsukamoto, S. Komaki, and N. Morinaga, "TDM intercell connection fiber-optic bus link for personal radio communication systems," *IEICE Trans. Commun.*, vol. E78-B, pp. 1287–1294, September 1995.

[68] D. W. Tcha and M. G. Yoon, "Conduit and cable installation for a centralized network with logical star-star topology," *IEEE Trans. Commun.*, vol. 43, February/March/April 1995.

[69] K. H. Rosen, *Discrete Mathematics and Its Application.* New York: McGraw-Hill, 3rd ed., 1995.

[70] A. O. Ivanov and A. A. Tuzhilin, *Minimal Networks: The Steiner Problem and Its Generalization.* Boca Raton, FL: CRC Press, 1994.

[71] F. K. Hwang and D. S. Richards, "Steiner tree problems," *Networks*, vol. 22, pp. 55–89, 1992.

[72] F. K. Hwang and J. F. Weng, "Hexagonal coordinate systems and Steiner minimal trees," *Discrete Mathematics*, vol. 62, pp. 49–57, 1986.

[73] Z. A. Melzak, *Companion to Concrete Mathematics*. New York: John Wiley, 1973.

[74] H. O. Pollak, "Some remarks on the Steiner problem," *J. Combinatorial Theory*, pp. 278–295, 1978. Series A 24.

[75] Z. A. Melzak, "On the problem of Steiner," *Canadian Mathematical Bulletin*, vol. 4/2, pp. 143–148, May 1961.

[76] F. Chung and R. Graham, "Steiner trees for ladders," *Annals of Discrete Mathematics 2*, pp. 173–200, 1978.

[77] M. R. Garey, L. R. Graham, and D. S. Johnson, "The complexity of computing Steiner minimal trees," *SIAM J. Applied Mathematics*, vol. 32, pp. 835–859, 1977.

[78] F. K. Hwang and D. Z. Du, "Steiner minimal trees on Chinese checkerboards," *Mathematics Magazine*, vol. 64, pp. 332–339, December 1991.

[79] F. Chung, M. Gardner, and R. Graham, "Steiner trees on a checkerboard," *Mathematics Magazine*, vol. 62/2, pp. 83–96, April 1989.

[80] K. A. Falcone and O. K. Tonguz, "Practical constraints in growth of lightwave networks," *IEEE Trans. Commun.*, vol. 44, pp. 348–355, March 1996.

[81] J. Bannister, M. Gerla, and M. Kovacevic, "An all-optical multifiber tree network," *J. Lightwave Technol.*, vol. 11, pp. 997–1008, May/June 1993.